MAX-PLANCK-INSTITUT
FÜR METEOROLOGIE

The Volcanic Impact on Moisture Fluxes into the Stratosphere

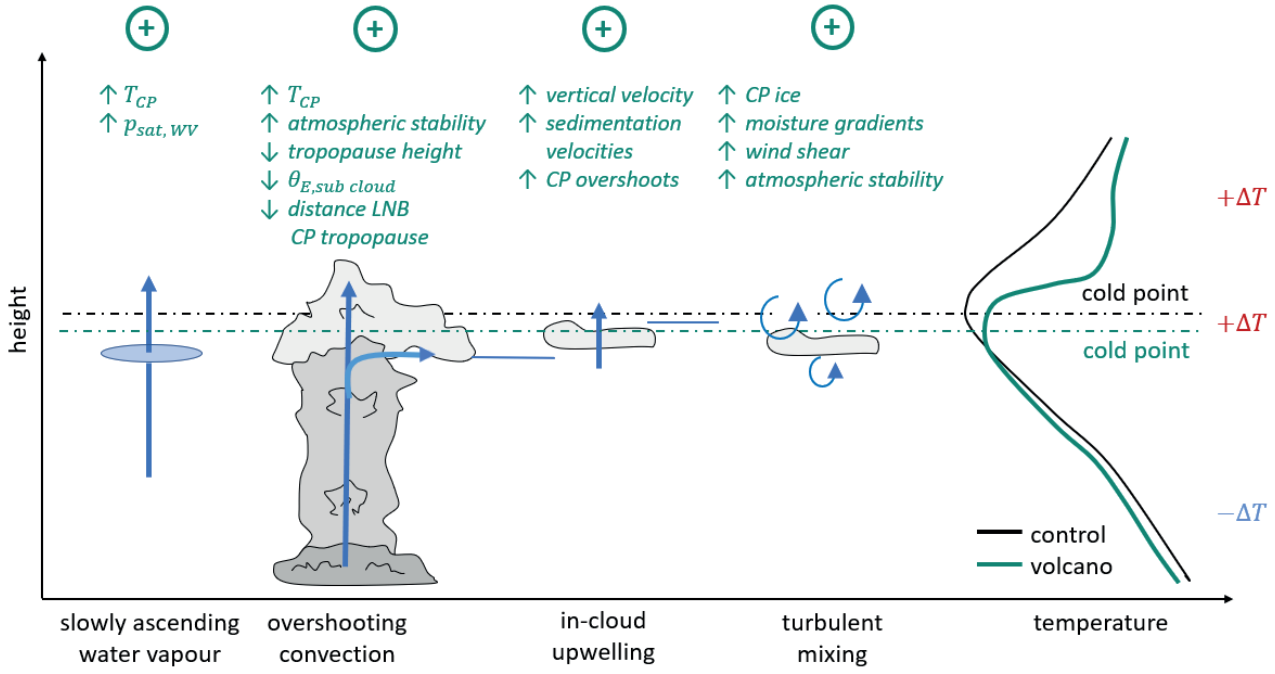

Clarissa Alicia Kroll

Hamburg 2023

Berichte zur Erdsystemforschung
Reports on Earth System Science

262
2023

Hinweis

Die Berichte zur Erdsystemforschung werden vom Max-Planck-Institut für Meteorologie in Hamburg in unregelmäßiger Abfolge herausgegeben.

Sie enthalten wissenschaftliche und technische Beiträge, inklusive Dissertationen.

Die Beiträge geben nicht notwendigerweise die Auffassung des Instituts wieder.

Die "Berichte zur Erdsystemforschung" führen die vorherigen Reihen "Reports" und "Examensarbeiten" weiter.

Anschrift / Address

Max-Planck-Institut für Meteorologie
Bundesstrasse 53
20146 Hamburg
Deutschland

Tel./Phone: +49 (0)40 4 11 73 - 0
Fax: +49 (0)40 4 11 73 - 298

name.surname@mpimet.mpg.de
www.mpimet.mpg.de

Notice

The Reports on Earth System Science are published by the Max Planck Institute for Meteorology in Hamburg. They appear in irregular intervals.

They contain scientific and technical contributions, including PhD theses.

The Reports do not necessarily reflect the opinion of the Institute.

The "Reports on Earth System Science" continue the former "Reports" and "Examensarbeiten" of the Max Planck Institute.

Layout

Bettina Diallo and Norbert P. Noreiks
Communication

Copyright

The Volcanic Impact on Moisture Fluxes into the Stratosphere

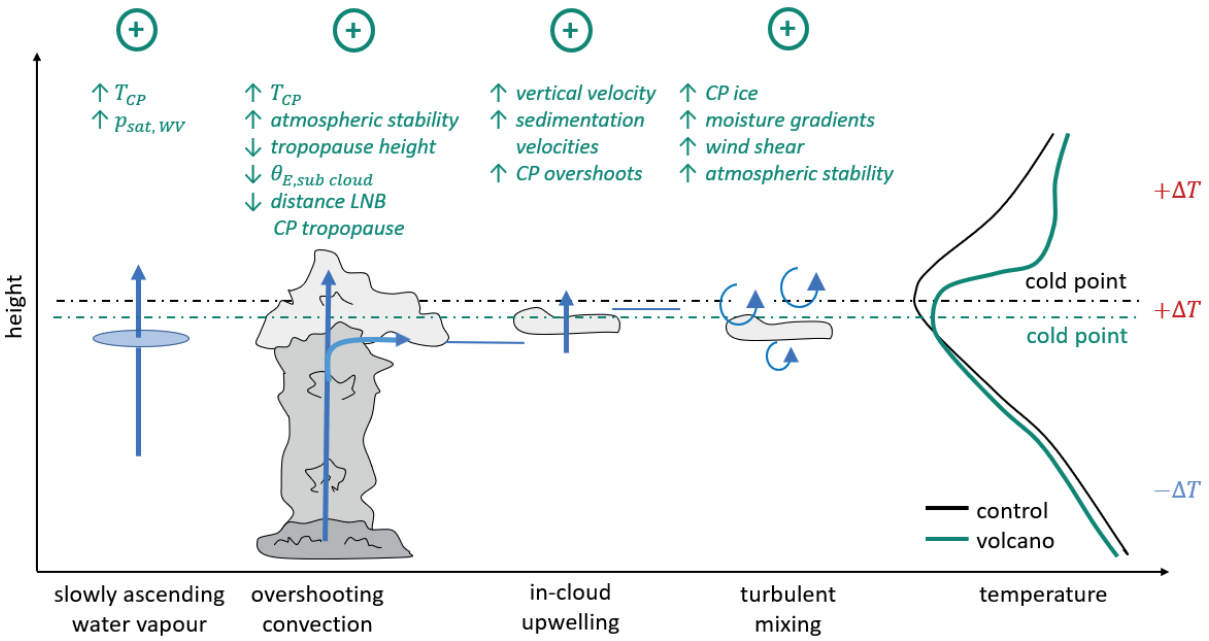

Clarissa Alicia Kroll

Hamburg 2023

Clarissa Alicia Kroll
aus München, Deutschland

Max-Planck-Institut für Meteorologie
The International Max Planck Research School on Earth System Modelling
(IMPRS-ESM)
Bundesstrasse 53
20146 Hamburg

Tag der Disputation: 16. Januar 2023

Folgende Gutachter empfehlen die Annahme der Dissertation:
Prof. Dr. Bjorn Stevens
Dr. Claudia Timmreck

Vorsitzender des Promotionsausschusses:
Prof. Dr. Hermann Held

Dekan der MIN-Fakultät:
Prof. Dr.-Ing. Norbert Ritter

Titelgrafik: Clarissa Kroll

ISSN 1614-1199 - doi: 10.17617/2.3489355

Clarissa Alicia Kroll

The Volcanic Impact on Moisture Fluxes into the Stratosphere

ABSTRACT

Moisture enters the tropical tropopause layer (TTL) and lower stratosphere via different pathways; be it as large-scale slowly ascending water vapor or by way of small-scale processes such as convective overshoots, in-cloud upwelling, or turbulent mixing. The partitioning between these different pathways is highly influenced by the TTL's character as a transition region between radiative-dynamically and convective-radiative-dynamically controlled atmospheric regions. Volcanic eruptions or geoengineering interventions based on stratospheric aerosol injection have the potential to disturb the heating balance by injecting sulfur compounds into the tropopause layer and stratosphere. The consecutively formed sulfate aerosol interacts with terrestrial and solar near infrared radiation, heating up its surroundings. In this work the impact of the corresponding temperature perturbation on the stratospheric water vapor budget in the tropics is investigated.

As sulfate aerosol often interferes with water vapor measurements and the last strong eruption occurred in a time with less observational data coverage in general, very little data on the changes of stratospheric water vapor (SWV) after volcanic eruptions exists. My first study therefore focuses on a direct quantification of changes in SWV based on a simulation set of 100 ensemble members for volcanic eruption magnitudes ranging from 2.5 Tg S to 40 Tg S. The huge number of different realizations allows for a deduction of those parameters which are important in determining the impact of the radiative forcing on the SWV levels. A comparison between the 100 ensemble member simulations for the Mt. Pinatubo eruption and 5 Tg S to 10 Tg S eruptions scenarios shows that the profile shape and height with respect to the tropopause are of crucial importance. This finding highlights the pitfalls of prescribing aerosol at fixed height levels in models differing with respect to their tropopause height. The study also identifies 10 Tg S as the volcanic eruption strength at which the volcanic signal dominates over internal variability of the SWV. At this eruption magnitude the SWV forcing counteracts up to 4 % of the aerosol forcing in the tropics. The dependence of important variables, such as the cold-point temperature and the radiative forcing of SWV, on aerosol optical depth values is determined via curve fitting.

In the second study the role of small-scale processes transporting frozen moisture into the stratosphere is investigated. Here I present the first budget analysis based on global convection resolving simulations for SWV changes after perturbations by sulfate aerosol in the TTL. A moisture flux analysis relying on online budget calculations reveals an exceptionally robust 80:20 partitioning of water vapor and frozen hydrometeor fluxes into the stratosphere - even under the substantial perturbations the aerosol heating entails, such as a 9 K warming of the cold-point temperatures and a downward shift of the tropopause by 1 km. The constant flux partitioning suggests that the Clausius Clapeyron scaling for the water vapor fluxes can be extended to the frozen fluxes as well. This greatly simplifies estimates of changes in moisture fluxes: The frozen moisture flux is easily determined by the partitioning ratio and the slope of the Clausius Clapeyron equation at the lowest cold-point temperatures.

The third, ongoing investigation concentrates on the question which moisture pathway - overshooting convection, in-cloud upwelling, or turbulent mixing - is responsible for the increases in frozen moisture fluxes after aerosol perturbations in the TTL. Although I show that both turbulent mixing and in-cloud upwelling increase, the main contributor to the flux and constant partitioning can be traced back to convective overshoots in the perturbed simulations.
In summary, this work enhances the understanding of the TTL and the stratospheric water vapor budget under external perturbations. After starting from specific case scenarios of volcanic eruptions, the work proceeds to set the focus on a conceptional understanding of governing processes.

ZUSAMMENFASSUNG

Feuchte kann über verschiedene Wege in die tropische Tropopause oder den unteren Teil der Stratosphäre gelangen; sei es als großskalig langsam aufsteigender Wasserdampf oder über kleinskalige Prozesse wie überschießende Konvektion, Aufsteigen innerhalb von Wolken, oder durch turbulentes Mischen. Die Aufteilung auf diese Transportwege ist stark durch den Charakter der Tropopause als Übergangsschicht zwischen Regionen, die durch Strahlung und Dynamik kontrolliert werden sowie Gebiete, die zusätzlich durch Konvektion bestimmt werden, geprägt. Vulkanausbrüche oder Geoengineeringinterventionen, die auf der Injektion von Schwefelderivaten basieren, haben das Potential die Balance zwischen diesen Prozessen zu stören, indem sie Schwefelderivate in die Tropopausenregion und die Stratosphäre injizieren. Das gebildetete Aerosol interagiert mit der terrestrischen und solaren Nahinfrarotstrahlung und führt zu einem Aufheizen der Umgebung. In dieser Arbeit werden die Auswirkungen der entsprechenden Temperaturperturbation auf das stratosphärische Wasserdampfbudget in den Tropen untersucht.
Es existieren nur wenige Observationsdatensätze zu Änderungen von stratosphärischem Wasserdampf (SW) nach großen Vulkaneruptionen, da Sulfataerosol viele Messungen von SW erschwert und bei der letzten starken Eruption allgemein wenige Messungen durchgeführt wurden. Die erste Studie dieser Arbeit liefert daher eine direkte Quantifizierung der Verändungen des SW basierend auf einem Simulationsset von je 100 Ensemblerealisierungen für Vulkaneruptionen zwischen 2.5 Tg S bis 40 Tg S. Die große Anzahl an verschiedenen Realisationen erlaubt es diejenigen Parameter zu bestimmen, welche wichtig für die Abschätzung der Auswirkungen des Strahlungsantriebs auf die SW-Niveaus sind. Durch einen Vergleich zwischen 100 Ensemblerealisierung für die Eruption von Pinatubo sowie den 5 Tg S und 10 Tg S Szenarien zeige ich, dass die Form und Höhe des Aerosolprofils in Bezug auf die Tropopause von entscheidender Bedeutung ist. Dies legt mögliche Probleme beim Vorschreiben von Aerosol auf festen Höhenniveaus in Modellen, die unterschiedliche Tropopausenhöhen besitzen, offen. Diese Studie weist auch nach, dass bei einer Eruption von 10 Tg S das Vulkansignal über die interne Variabilität des stratosphärischen Wasserdampfes dominiert und der Strahlungsantrieb durch den zusätzlichen SW bis zu 4 % des Aerosolstrahlungsantriebes in den Tropen entgegenwirkt. Um eine einfache Abschätzung der Auswirkung von Vulkaneruptionen auf den Wasserdampfgehalt zu ermöglichen, wird die Abhängigkeit wichtiger Variablen für SW von der optischen Dichte des Aerosol abgeleitet.
In der zweiten Studie wird neben dem Beitrag des großskalig langsam aufsteigenden Wasserdampfes nun auch explizit die Rolle kleinskaliger Prozesse, die gefrorener Hydrometeore beinhalten, für die SW-Werte untersucht. In dieser Arbeit präsentiere ich die Ergebnisse der ersten Budgetanalyse für SW Änderungen nach Perturbationen mit Sulfataerosol in der Tropopause, die auf globalen konvektionsauflösenden Simulationen basiert. Die Analyse des Feuchteflusses offenbart eine sehr robuste 80:20 Aufteilung des Feuchteflusses auf Wasserdampf und gefrorene Hydrometeore. Diese Aufteilung bleibt selbst unter erheblichen Perturbationen wie einer Erhöhung

der kältesten Temperaturen zwischen Troposphäre und Stratosphäre um 9 K und einem Absenken der Tropopause um 1 km bestehen. Dieses Ergebnis legt nahe, dass die Clausius Clapeyron Skalierung für die Wasserdampfflüsse auf Flüsse gefrorener Aggregatzustände erweitert werden kann. Diese Erkenntnis vereinfacht die Abschätzung von Änderungen in Feuchteflüssen erheblich: Der bisher unsichere, schwer zu bestimmende Beitrag der gefrorenen Hydrometeore kann durch Aufteilung der Feuchteflüsse in Wasserdampf und gefrorene Hydrometeore sowie die Steigung der Clausius Clapeyron Gleichung bei den niedrigsten Temperaturen in der Tropopausenregion bestimmt werden.
Die dritte, laufende Studie beschäftigt sich näher mit der Frage welcher Weg - überschießende Konvektion, Aufsteigen innerhalb von Wolken oder turbulentes Mischen - für den Anstieg in Flüssen gefrorener Hydrometeore nach Aerosolperturbationen in der Tropopausenregion verantwortlich ist. Obwohl ich zeige, dass turbulentes Mischen und Aufsteigen innerhalb von Wolken zunehmen, kommt der Hauptbeitrag zum Fluss durch eine Zunahme überschießender Konvektion zustande.
Diese Arbeit verbessert das Verständnis der Tropopausenregion und des SW Budget unter externen Perturbationen. Beginnend mit spezifischen Fallstudien für Vulkaneruptionen wird der Fokus darauf gesetzt das konzeptionelle Verständnis der bestimmenden Prozesse voranzutreiben.

PUBLICATIONS RELATED TO THIS DISSERTATION

Some ideas and figures have appeared previously in the following publications:

Kroll, C. A., Dacie, S., Azoulay, A., Schmidt, H., and Timmreck, C.: *The impact of volcanic eruptions of different magnitude on stratospheric water vapor in the tropics*, Atmospheric Chemistry Physics, 2021 6565–6591, https://doi.org/10.5194/acp-21-6565-2021.

Kroll, C. A., Fueglistaler, S., Schmidt, H., Kornblueh, L., Timmreck, C.: *The sensitivity of moisture flux partitioning in the tropical tropopause layer to external forcing*, submitted to Geophysical Research Letters, 2022.

Kroll, C. A., Fueglistaler, S., Schmidt, H., Kornblueh, L., Timmreck, C.: *The impact of volcanic aerosol heating on turbulent mixing, in-cloud upwelling, and convection in the tropical tropopause layer*, in preparation for Atmospheric Chemistry Physics, 2022.

During the PhD work was contributed to the following collaborative project:

Hohenegger, C., Korn, P., Linardakis, L., Redler, R., Schnur, R., Adamidis, P., Bao, J., Bastin, S., Behravesh, M., Bergemann, M., Biercamp, J., Bockelmann, H., Brokopf, R., Brüggemann, N., Casaroli, L., Chegini, F., Datseris, G., Esch, M., George, G., Giorgetta, M., Gutjahr, O., Haak, H., Hanke, M., Ilyina, T., Jahns, T., Jungclaus, J., Kern, M., Klocke1, D., Kluft, L., Kölling, T., Kornblueh, L., Kosukhin, S., **Kroll, C.**, Lee, J., Mauritsen, T., Mehlmann, C., Mieslinger, T., Naumann, A. K., Paccini, L., Peinado, A., Sri Praturi, D., Putrasahan, D., Rast, S., Riddick, T., Roeber, N., Schmidt, H., Schulzweida, U., Schütte, F., F., Hans Segura, H., Shevchenko, R., Singh, V., Specht, M., Stephan, C. C., von Storch, J-S., Vogel, R., Wengel, C., Winkler, M., Ziemen, F., Marotzke, J. and Stevens, B.: *ICON-Sapphire: simulating the components of the Earth System and their interactions at kilometer and subkilometer scales*, submitted to Geoscientific Model Development, 2022, https://doi.org/10.5194/gmd-2022-171.

ACKNOWLEDGEMENTS

First of all I want to thank my panel, Claudia Timmreck, Hauke Schmidt and Bjorn Stevens, for their continued support throughout my PhD thesis. I have been lucky to have a PhD supervisor in Claudia Timmreck who noticeably never lost her excitement for her research topic and shared her enthusiasm with her group. Even during stressful proposal writing seasons she always took her time for discussions with me finding just the right balance between encouragement and challenge. Also many thanks to Hauke Schmidt for consistently being critical in a constructive way and training me to defend my ideas. Bjorn Stevens has been a great panel chair surveying my project and providing critical support when needed.

Although not officially part of my panel, Stephan Fueglistaler of Princeton University played a significant role in my PhD research by collaborating with me on the second and third part of my project. Thanks for encouraging me to emerge myself in thorough and detailed analysis, but at the right moment step back to condense my findings in clear messages.

Science would not be science without discussions. Often the scientific working group is the first address for feedback. Thanks to all members of the *Stratospheric Forcing and Climate* group - Laurits Andreasen, Shi-Wei Fang, Henning Franke, Moritz Günther, Julia Kley, Ulrike Niemeier, Ilaria Quaglia and Claudia Timmreck - for creating a friendly and open space for discussion and leaving some space to laugh together. Additionally, I was very lucky to also have many colleagues at MPI who were always happy to discuss new ideas and results - even when communication was more complicated in the past two Covid years. Sally Dacie, Andrea Schneidereit, Alon Azoulay, Jiawei Bao, Thibaut Dauhut, Diego Jiménez-de-la-Cuesta-Otero, Paul Keil, Kirsten Krüger, and Dian Putrashan, you all enriched my scientific work. Also thanks to my "adoptive" group *Drivers of Tropical Circulation* - Clara Bayley, Hernan Campos, Theresa Lang, Jule Radke and Ann Kristin Naumann - for giving me a "more microphysical" perspective on my research.

The *sapphire* team has been an enormous support when I set up my high resolution simulations. My special thanks go to Luis Kornblueh for his advice and humorous optimistic approach when the model surprised me with unanticipated "features" and Sebastian Rast for thoroughly discussing model behaviour with me and providing sympathy when I went through the tougher phases in my ICON "relationship". Reiner Schnur has been a tremendous help in the quest of finding ICON bugs. Marco Giorgetta always generously shared his knowledge on ICON. Daniel Klocke, Lukas Kluft, Leonidas Linardakis, René Redler, Niklas Röber and Florian Ziemen discussed many different model aspects with me. Also a big cheer to the DKRZ support team for fixing all the problems on "our" supercomputers *mistral* and *levante* and thus removing many obstacles in our everyday workflow. I am also grateful for the exchange with Axel Seifert and Daniel Reinert from the Deutsche Wetterdienst (DWD), who shared their knowledge on the graupel microphyiscs and transport schemes in

ICON.

With the IMPRS-Office I knew I always had somebody to turn to throughout my PhD journey. Antje Weitz, Cornelia Kampmann and Michaela Born made me feel integrated and welcome at MPI from my first day on. The training within the IMPRS - from lecture courses to the annual retreat, often tailored to the students own needs - is something I would not want to miss at MPI.

Many thanks to my colleagues and friends who made me feel at home in Hamburg. Sally and Luca, my office mates, have been amazing sharing all the ups and downs of everyday PhD life. Without Almuth, Andrea, Ulrike and Luis the two year Covid era would have been a very lonely time - thanks for all the chats, weekend excursions, lunches and garden picnics. I was very happy to meet an old study friend in Clara at MPI. She and my buddy Laura introduced me to many of the other PhD students. I have greatly appreciated being part of the IMPRS crowd - meeting so many people from different cultures and scientific backgrounds was a very enriching experience for me. As I can't name all of you here, just as a pars pro toto: Diego, Henning, Moritz, Abisha, Laura, Lukas, John, Jule, Theresa L., Theresa M., *, I am happy I got to know you.

Last but not least a big thanks to my family for standing behind me - also during the PhD phase of my life. Specifically with respect to this time period: Mum, thanks for discussing various PhD "dramas". Dad, thanks for sharing your love for natural sciences with me and showing me one is never too old to be curious. Severina, without you my apartment in Hamburg would only be half as comfortable. Matthias, thanks for all the tips on how to speed up the computational analysis of my more bulky data and most importantly: patiently listening to everything you might never wanted to know about stratospheric water vapor.

CONTENTS

I UNIFYING ESSAY 1

1 INTRODUCTION 3
- 1.1 Importance of stratosphere and stratospheric water vapor . . . 3
- 1.2 Tropical stratospheric water vapor budget . . . 4
- 1.3 Stratospheric water vapor budget after volcanic eruptions . . . 5
- 1.4 Open scientific questions . . . 6
  - 1.4.1 Large-scale slowly ascending water vapor at the cold-point and changes under volcanic perturbations . . . 6
  - 1.4.2 The contribution of small-scale processes to the stratospheric moisture budget and changes under volcanic perturbations . . 8
- 1.5 Methodological approach to research questions . . . 10
  - 1.5.1 Addressing the changes in the large-scale slowly ascending water vapor after volcanic eruptions . . . 10
  - 1.5.2 Addressing the importance of small-scale processes and their changes after perturbations . . . 12

2 SYNTHESIS OF RESULTS 13
- 2.1 The impact of volcanic eruptions of different magnitude on stratospheric water vapor in the tropics . . . 13
- 2.2 The sensitivity of moisture flux partitioning in the tropical tropopause layer to external forcing . . . 19
- 2.3 The impact of volcanic aerosol heating on turbulent mixing, in-cloud upwelling and convection in the tropical tropopause layer . . . 23

3 CONCLUSION AND OUTLOOK 31
- 3.1 Answers to research questions . . . 31
- 3.2 Findings in scientific context and outlook . . . 33
- 3.3 Final remarks . . . 38

II APPENDIX 39

A THE IMPACT OF VOLCANIC ERUPTIONS OF DIFFERENT MAGNITUDE ON STRATOSPHERIC WATER VAPOR IN THE TROPICS 41
- A.1 Introduction . . . 42
- A.2 Methods . . . 45
  - A.2.1 The EVAens ensemble and the GE historical simulations . . . 45
  - A.2.2 Stratospherically adjusted clear sky forcing calculations . . . 47
- A.3 Results . . . 49
  - A.3.1 Effects on the time evolution of TOA radiative imbalance and surface temperature . . . 49
  - A.3.2 Effects on the cold point temperature . . . 50
  - A.3.3 Effects on the tape recorder signal . . . 53
  - A.3.4 Intra-ensemble variability . . . 57
  - A.3.5 Comparison to the MPI-GE historical simulations (Mt. Pinatubo) 58
  - A.3.6 Adjusted forcing caused by the SWV increases . . . 62

A.4 Discussion . . . 65
A.4.1 Magnitude of SWV increases due to indirect volcanic mechanism 65
A.4.2 Comparison to studies based on observations and reanalysis data 66
A.4.3 SWV contributions due to the indirect volcanic and direct volcanic injection . . . 68
A.4.4 SWV Forcing . . . 68
A.4.5 Predictability of responses . . . 70
A.5 Conclusion and Outlook . . . 70
A.6 Appendix A: Scaling of different physical parameters altered by the presence of volcanic aerosol . . . 73
A.7 Appendix B: Percental changes in the tape recorder signal . . . 76
A.8 Appendix C: Intra-ensemble variability in the entire tropics . . . 76
A.9 Appendix D: Aerosol extinction profiles - 550 nm solar waveband . . . 77
A.10 Appendix E: SWV forcing - SW component . . . 78
A.11 Appendix F: Global spread of the stratospheric water vapour . . . 79
B THE SENSITIVITY OF MOISTURE FLUX PARTITIONING IN THE COLD-POINT TROPOPAUSE TO EXTERNAL FORCING 81
B.1 Introduction . . . 83
B.2 Methods . . . 85
B.2.1 Model simulations . . . 85
B.2.2 Budget calculations . . . 85
B.2.3 Choice of reference height . . . 86
B.3 Results . . . 86
B.3.1 Quantifying the perturbation . . . 86
B.3.2 Water vapour distribution at the cold-point tropopause . . . 87
B.3.3 Change in flux partitioning . . . 88
B.4 Discussion . . . 88
C THE IMPACT OF VOLCANIC AEROSOL HEATING ON TURBULENT MIXING, IN-CLOUD UPWELLING AND CONVECTION IN THE TROPICAL TROPOPAUSE LAYER 91
C.1 Model setup . . . 92
C.2 Height dependent moisture distribution . . . 93
C.3 Height dependent moisture fluxes . . . 94
C.4 Convection in ICON . . . 95
C.5 Sublimation above the cold point tropopause . . . 96

BIBLIOGRAPHY 98

ACRONYMS

AOD Aerosol Optical Depth

BDC Brewer Dobson Circulation

CaVE Convection after Volcanic Eruptions (Simulations)

CP Cold Point

ENSO El Niño–Southern Oscillation

ERA ECMWF ReAnalysis

EVA Easy Volcanic Aerosol (Forcing Generator)

EVAens EVA ensemble (Simulations)

GCM General Circulation Model

ICON Icosahedral Nonhydrostatic (Weather and Climate Model)

LNB Level of Neutral Buoyancy

LR Lapse Rate

MPI-ESM-LR Max Planck Institute - Earth System Model in its Low Resolution

QBO Quasi-Biennial Oscillation

SST Sea Surface Temperature

SWV Stratospheric Water Vapor

TOA Top of the atmosphere

TTL Tropical tropopause layer

Part I

UNIFYING ESSAY

1 INTRODUCTION

This work investigates the relative importance of different pathways by which moisture enters the tropical stratosphere. A special focus is laid on the question of how moisture fluxes into the stratosphere are impacted by external forcing, such as volcanic aerosol heating, in the tropical tropopause layer.

1.1 IMPORTANCE OF STRATOSPHERE AND STRATOSPHERIC WATER VAPOR

The stratosphere - "sphere of layers".

The stratosphere, the so-called "sphere of layers", is the second lowest atmospheric region after the troposphere. It owes its name to the fact that it is stably stratified since temperature increases with height due to UV absorption by ozone. This characteristic is in stark contrast to the troposphere, the "sphere of change", where temperatures decrease with height. In the troposphere atmospheric conditions are not only controlled by dynamical and radiative processes - as in the stratosphere -, but also by convection, leading to more rapid changes. One should not be misled however by the etymology. Despite its "stratified" nature and elevated position in the atmosphere, the stratosphere influences tropospheric conditions. For example, winter surface weather on sub-seasonal to seasonal timescales (Domeisen et al., 2020a, Domeisen et al., 2020b) is influenced by stratospheric dynamics. With respect to radiative processes, the stratosphere is best known for the ozone layer which absorbs part of the incoming solar UV radiation. The depletion of this layer, protecting living organisms from harmful UV-C and UV-B, due to human activity led to international efforts to restore the ozone layer (compare Montreal Protocol, 1987). Stratospheric adjustments play an important role in the system response to external forcings, coining the definition of "stratospherically adjusted forcing" (Hansen et al., 2005). For example, the stratospheric temperature reduction due to elevating CO_2 levels (Manabe and Wetherald, 1975) will further increase the instantaneous CO_2 forcing as it additionally reduces outgoing longwave radiation. In the case of volcanic eruptions, sulfur injected into the stratosphere resides longer than in the troposphere where it, and its derivates, rain and sediment out within weeks. This longer residence time is the prerequisite for oxidizing the sulfur and forming an aerosol layer leading to a longer lasting forcing (e.g. Shindell, 2013).

SWV acts as a greenhouse gas, participates in ozone, sulfur, and methane chemistry, and can impact the circulation.

A distinct feature of the stratosphere is its extreme dryness with mean water vapor values only occuring in ppmv region (e.g. Seidel et al., 2001). This dryness is explained by the very low upper tropospheric temperatures which lead to strong freeze drying restricting the amount of moisture entering the stratosphere (Brewer, 1949). In spite of its low concentrations, stratospheric water vapor (SWV) is a vital player in a number of processes which impact both stratospheric and tropospheric conditions: First, SWV acts as a greenhouse gas (e.g. Forster and Shine, 2002, Solomon et al., 2010). Second, strong increases in stratospheric water vapor can lead to circulation changes, impacting the Brewer-Dobson circulation (BDC), the mean meridional circulation within the stratosphere, as well as jets and storm tracks (Maycock et al.,

2013). Third, SWV plays an important role in stratospheric chemistry since water vapor, as a source of HO_x, can promote ozone and methane depletion (Ko et al., 2013). Additionally, stratospheric water vapor levels are critical in reactions of the stratospheric sulfur chemistry after volcanic eruptions (Rosenlof, 2018), since water is a key ingredient both for the formation of H_2SO_4 and for the first step of SO_2 oxidation which requires OH. Therefore, the aerosol particle formation, aerosol effective radii, and development of the Aerosol Optical Depth (AOD) after a volcanic eruption all depend on the moisture content in the lower stratosphere (LeGrande et al., 2016, Clyne et al., 2021). Hence, volcanic aerosol forcing and its evolution are modulated by stratospheric moisture.

1.2 TROPICAL STRATOSPHERIC WATER VAPOR BUDGET

Large-scale and small-scale processes.

Water vapor can enter the tropical stratosphere from the troposphere via different pathways: on large scales by slowly ascending water vapor, and on small scales by convective overshoots, in-cloud upwelling, or turbulent mixing. All pathways are influenced by the characteristics of the tropical tropopause layer (TTL), the transition layer between radiative-convective-dynamically and radiative-dynamically controlled atmospheric regions and as such the gateway to the stratosphere (Fueglistaler et al., 2009).

Dominating large-scale process: "atmospheric tape recorder".

In the inner tropics, the large-scale slowly ascending water vapor dominates the moisture fluxes into the stratosphere (Brewer, 1949). As the temperature-dependent saturation specific humidity constrains the maximum amount of water vapor, the moisture entering the stratosphere strongly depends on the cold-point (CP) temperature, the coldest temperature between troposphere and stratosphere. The seasonal cold-point temperature variations influencing the water vapor amount entering the stratosphere give rise to the renowned "tape recorder" signal. The name is inspired by the CP temperature controlled alternating high and low water vapor values slowly propagating upwards in the stratosphere (Mote et al., 1996) within the BDC (compare Figure 1). Interannual variations in the cold-point temperatures and water vapor entering the stratosphere can be traced back to variability of e.g. the BDC, the El Niño–Southern Oscillation (ENSO)[1] and the quasi-biennial oscillation (QBO)[2] (e.g. Geller et al., 2002, Randel et al., 2004, Fueglistaler and Haynes, 2005, Randel et al., 2006).

Small-scale processes: needed to close the budget.

However, long-term water vapor trends can only be explained when also considering small-scale contributions (e.g. Fueglistaler et al., 2013, Dessler et al., 2016), which arise mainly from the transport of frozen water into the TTL and lower stratosphere. The first source of frozen water, convective overshoots, are convective towers with enough kinetic energy to reach the TTL and surpass the cold-point tropopause (Dauhut et al., 2015, Dauhut et al., 2018, Bolot and Fueglistaler, 2021, Dauhut and Hohenegger, 2022). A second, slower pathway, called in-cloud upwelling hereafter, is moisture transport within ice clouds. The interaction of ice crystals with radiation leads to local heating and an updraft within these ice clouds. This ascent may connect

1 El Niño–Southern Oscillation is a pattern of changes in sea surface temperatures and winds in the tropical Pacific ocean which affects rainfall patterns.

2 The QBO is an oscillation between equatorial easterly and westerly winds in the tropical stratosphere with an average period of 28 to 29 months.

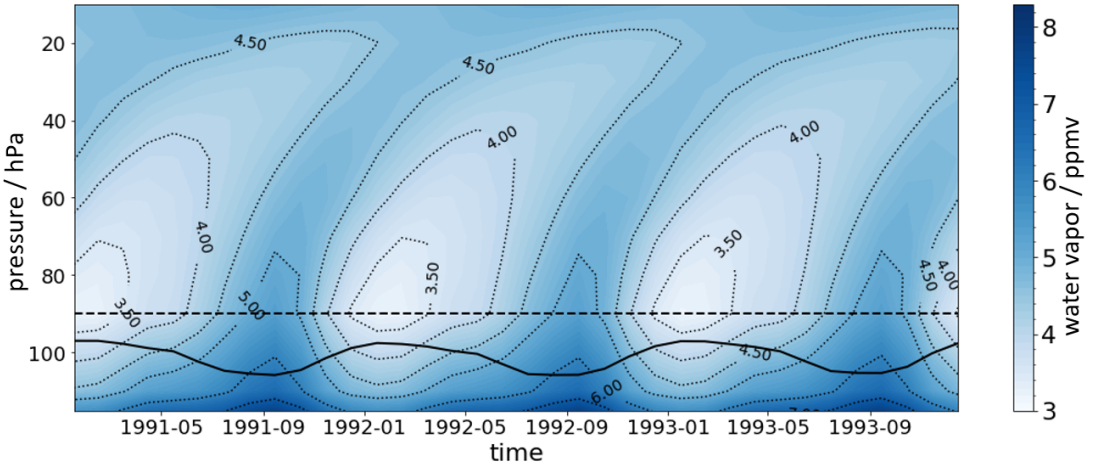

Figure 1: The atmospheric tape recorder: Temporal evolution of tropical water vapor above 115 hPa showing the seasonal variations of cold-point temperature imprinted on atmospheric humidity content as simulated in an idealized setup with the MPI-ESM (*EVAens* with 0 Tg S, see Section 1.5). The height of the lapse rate tropopause and cold-point tropopause are shown by a solid and dashed black line, respectively.

deep convective events with the main transporting circulation in the stratosphere, the BDC (e.g. Corti et al., 2006), continuing the upwards transport of moisture. The third pathway of moisture injection is turbulent mixing (e.g. Konopka et al., 2007, Bardeen et al., 2013, Podglajen et al., 2017), which can be triggered by atmospheric instabilities and vertical wind shear, if vertical moisture gradients are present. These gradients exist in the TTL as the stratosphere is extremely dry and the convective tops reaching up to the TTL carry with them considerable amounts of frozen hydrometeors.

Methane oxidation within the stratosphere.

Apart from upward transport from the troposphere, water vapor can also originate from methane oxidation occurring in the stratosphere itself (e.g. Le Texier et al., 1988, Rohs et al., 2006). This mechanism takes place in the middle stratosphere and leads to a moistening comparable to 5 % of the water vapor entering the stratosphere from below. It is also responsible for the increased moisture contents at higher altitudes visible in Figure 1.

1.3 STRATOSPHERIC WATER VAPOR BUDGET AFTER VOLCANIC ERUPTIONS

Volcanic eruptions can alter the stratospheric water vapor budget both directly, during the eruption event itself by injecting moisture from within the volcanic plume, and indirectly in the aftermath of the eruption as a result of the volcanic aerosol forcing in the TTL.

Direct injection of water vapor from within the volcanic plume.

The direct injection is a singular event with immediate effects. Since up to 81 % of the eruption volume is water (Coffey, 1996), eruptions with high explosivity and eruption volume could lead to a substantial moistening of the stratosphere directly after the eruption event. However, freeze drying and sedimentation normally remove around 90 % of the water vapor in the eruption column before it reaches the stratosphere (Glaze et al., 1997). In most cases, the direct injection will consequently only lead to highly localized water vapor increases which disappear in the background

noise within a couple of days to weeks (Murcray et al., 1981, Schwartz et al., 2013, Sioris et al., 2016a). An exception is the recent eruption of Hunga Tonga–Hunga Ha'apai in 2022, which led to a peak SWV increase by up to 10 % of the total stratospheric water vapor content (Xu et al., 2022, Millán et al., 2022). This amount is unprecedented in previous records and was favored as Hunga Tonga–Hunga Ha'apai is an undersea volcano, leading to a massive increase in the water entrained within the plume. Corresponding elevated water vapor levels persisted for months after the eruption (Schoeberl et al., 2022) and were detectable for at least ten months (Zhu et al., 2022), although with continuously decreasing impact. The final dissipation may require years (Hall and Waugh, 1997).

Indirect effects on water vapor in the aftermath of volcanic eruption.

In this work, the indirect effects of volcanic eruptions on the SWV are investigated which can be attributed to heating-induced alterations of the atmospheric temperature profile occurring over a much wider time span. These indirect effects include all changes in the large-scale slowly ascending water vapor as well as small-scale contributions of convective overshooting, in-cloud upwelling, and turbulent mixing. From these four processes only the slowly ascending water vapor has been studied prior in the context of volcanic eruptions.

1.4 OPEN SCIENTIFIC QUESTIONS

The *status quo* of the research field on stratospheric water vapor changes after volcanic perturbations prior to this work is described in this section. In this general survey open questions are identified which will be addressed within this dissertation.

1.4.1 *Large-scale slowly ascending water vapor at the cold-point and changes under volcanic perturbations*

The physical mechanism for changes in slowly ascending water vapor after volcanic eruptions is understood: the longwave and near IR heating by the volcanic aerosol leads to elevated cold-point temperatures which translate into an increased saturation specific humidity and thus more water vapor entering the stratosphere (e.g. Considine et al., 2001, Joshi and Shine, 2003).

Scarcity of reliable observational records.

Despite the well-established knowledge of this mechanism, a direct quantification of its impact on the SWV is complicated for a number of reasons. First, the measurement accuracy required to determine SWV levels is comparatively high as values normally lie in the ppmv range. Data coverage for the upper troposphere and lower stratosphere is still not sufficient and often individual data sets disagree (Müller et al., 2016, Khosrawi et al., 2018). Second, the number of volcanic eruptions injecting large amounts of sulfur into the stratosphere to investigate is limited. The main candidate, Mt. Pinatubo erupted in 1991, over 30 years ago. Third, for the small number of relevant volcanic eruptions on record, internal variability often obscures the signal and observations are incomplete. In addition stronger events can lead to device outages and disagreements between individual observational products.

Scarcity of reliable observational records - the example of Mt. Pinatubo.

The eruptions of Mt. Pinatubo is the most relevant event for stratospheric water vapor changes. During this period satellite based stratospheric water vapor measurements were performed with SAGE II[3](Thomason et al., 2004), UARS HALOE[4](Russell III et al., 1993) and UARS MLS[5] (Livesey et al., 2003). Additionally, the Boulder balloon data (e.g. Vömel et al., 1995) and measurements from three short term ATMOS missions[6] (Michelsen et al., 2000), which are spatially and/or temporally limited, exist. Both SAGE II and HALOE retrievals failed or are biased due to the large aerosol amount in the TTL region and can not be used without precautions (e.g. Hegglin et al., 2014, Fueglistaler, 2012, Fueglistaler et al., 2013). Data from MLS is not flagged as unreliable, but the record starts during the outage of SAGE II and HALOE, after the eruption of Mt. Pinatubo, and only lasts until 1993 (Davis et al., 2016). Taken together, these measurements do not form a good basis for the most relevant volcanic eruption within the last century.

SWV reanalysis products not suitable for scientific analysis.

As reanalysis data builds upon observations, this lack of data is also reflected in their output. In addition, the stratosphere is typically not the main focus of assimilation. The representation of SWV therefore is based on model physics rather than actual observational data. As is, stratospheric moisture fields are consequently often tuned to represent the average climatology, which reduces interannual variability considerably. Even in untuned situations however, volcanic forcing is still often omitted (Diallo et al., 2017). This leads to problems when comparing simulations to reanalysis data in which the volcano was not explicitly accounted for (e.g. Löffler et al., 2016) and inconsistencies between different reanalysis products describing the same eruption (e.g. Tao et al., 2019). Some authors including those of the SPARC 2022[7] report therefore discourage the usage of SWV fields from reanalysis in general (Davis et al., 2017, Khosrawi et al., 2018, Fujiwara et al., 2022).

Reanalysis often not accounting for volcanic eruptions.

Problems with indirect quantifications.

Additional complications can arise as the volcanic aerosol perturbs multiple physical processes which can alter the SWV content such as temperature and the BDC. Consequently, their contribution can not be disentangled in some of the commonly used regression methods (e.g. Dessler et al., 2014). Given all these complications it remains unclear how large an eruption must be to lead to an easily detectable stratospheric water vapor increase, which other parameters are important to determine the SWV increase, and how SWV increases can be best estimated for a given eruption.

Lack of information on the magnitude of radiative forcing originating from SWV entering the stratosphere via the indirect pathways after volcanic eruptions.

Many studies on stratospheric water vapor after volcanic eruptions are motivated by the importance of SWV as a greenhouse gas. However, there is no study rigorously investigating the temporal evolution of the SWV forcing in relationship to the volcanic aerosol forcing. Joshi and Shine, 2003, calculate one global estimate for the forcing by the additional SWV, but without information on either its temporal evolution or the scaling for different eruption strengths. In a subsequent study Joshi and

3 SAGE II stands for "Stratospheric Aerosol and Gas Experiment II". Measurements were performed between Oct. 1984 and Aug. 2005.

4 UARS HALOE stands for "Upper Atmospheric Research Satellite Halogen Occultation Experiment". Measurements were performed in the time frame between Oct. 1991 and Nov. 2005.

5 UARS MLS stands for "Upper Atmosphere Research Satellite Microwave Limb Sounder". Measurements were performed in the time frame between Oct. 1991 and Oct. 1999.

6 ATMOS stands for "Atmospheric Trace Molecule Spectroscopy" and describes solar occultation measurements with a Fourier transform infrared spectrometer. The instrument was taken on three short term missions on a space shuttle in 1992, 1993 and 1994.

7 SPARC is short for "Stratosphere-troposphere Processes And their Role in Climate".

Jones, 2009, indirectly quantify the longwave forcing component for directly injected water vapor, without analyzing the indirect pathway. Similarly, Krishnamohan et al., 2019, used SWV to explain their top-of-atmosphere energy imbalance in a geoengineering study, without directly quantifying the SWV forcing or separating it from the volcanic aerosol forcing itself. This rather diffuse knowledge base complicates the assessment of its importance for an accurate representation of forcing changes after volcanic eruption.

In summary, the first part of this thesis pursues the following questions:

- *What is the critical magnitude for a volcanic eruption to have a significant impact on the stratospheric water vapor content by dominating over internal variability?*
- *By how much does stratospheric water vapor increase for different eruption magnitudes if directly quantified, i.e. not from the residuum?*
- *Which parameters are critical for a determining the SWV increase?*
- *What is the contribution of the SWV forcing to the overall radiation budget?*
- *Can cold-point temperature warming and SWV forcing be estimated based on eruption magnitude or AOD? Is there an easy approximation for SWV increases?*

The findings are outlined in Section 2.1 and summarized in Section 3.1.

1.4.2 *The contribution of small-scale processes to the stratospheric moisture budget and changes under volcanic perturbations*

Parametrizations and tunings impede a reliable budget analysis.

Even in the absence of volcanic eruptions, the composition of the stratospheric water vapor budget is still a highly debated subject. Especially, the contribution of convection (e.g. Schoeberl et al., 2018, Bolot and Fueglistaler, 2021, Dauhut and Hohenegger, 2022) and turbulent mixing (e.g. Wilson, 2004, Konopka et al., 2007, Riese et al., 2012, Podglajen et al., 2017) to the fluxes into the stratosphere remains unclear. The core of the problem lies in the limitations and inaccuracies that currently used convective parametrization schemes bring with them (e.g. Arakawa, 2004, Jones and Randall, 2011, Sherwood et al., 2014). To compensate for an imperfect representation of overshooting, regions like the TTL are also often tuned to match observational records. Additionally some shortcomings of parametrization schemes are not immediately apparent as often errors in process representation compensate for each other (Hardiman et al., 2015). This may lead to problems when studying the sensitivity of the climate system to external perturbations, as tuning and compensating processes can lead to bias corrections for wrong reasons.

The emerging convection-resolving simulations circumvent this problem.

The emerging convection-resolving simulations offer the unique possibility to study moisture fluxes into the stratosphere without the impediments of convective parametrizations (e.g. Stevens et al., 2020). However, they bring with them their own set of problems. Computation costs often require a reduction of the investigated domain. Smaller domains restrict the study to small-scale processes, while the large-scale contributions to the moisture budget need to be estimated. Sometimes the analysis of a single convective event is extrapolated to the entire stratospheric water vapor budget (e.g. Dauhut et al., 2015) in order to generate estimates for the frozen moisture

contribution. Despite this extrapolation procedure being based on statistics of observational records for deep convection, it still leads to inaccuracies as convective injections differ depending on their region of origin (Wright et al., 2011) and not all overshoots are hydrating (Dauhut et al., 2018).
In summary, both most commonly used approaches, coarse simulations with convective parametrizations and single case studies with convection-resolving simulations, compromise either on the inaccuracies introduced by convective parametrizations or on those from estimating the moisture budget based on a single convective event. Both problems can be overcome by relying on global convection-permitting simulations with global extent. However, as this approach is computationally quite expensive, only one study using this approach exists (Dauhut and Hohenegger, 2022).

Volcanic aerosol heating: an unprecedented sensitivity experiment for the TTL.

The knowledge base on the sensitivity of frozen moisture fluxes in the TTL under external perturbations is even more limited. Up till now, the sensitivity of overshooting convection, in-cloud upwelling, and turbulent mixing to volcanic aerosol heating in the TTL has not been studied within a complete budget analysis relying on global convection-resolving simulations. Consequently, it is even unclear if the contribution of frozen hydrometeors to the total budget will increase or decrease and must be examined.

Overarching effect: changes in the temperature field.

In the following the different mechanisms which could influence the changes in overshooting convection, in-cloud upwelling, and turbulent mixing are analyzed. All three processes are influenced by changes in the large-scale temperature field. In the upper troposphere and TTL the aerosol heating will lead to increased temperatures which will directly translate into the saturation specific humidity. In saturated ascending air parcels the condensation, and with it the frozen moisture content, will be influenced by the saturation specific humidity of the air parcels and the slope of the Clausius Clapeyron equation. This would suggest increased condensation per Kelvin decrease in temperature at slightly elevated temperatures.

Overshooting convection: increased stability versus lower lying tropopause.

For overshooting convection, the change in atmospheric stability will be an additional determining factor. The heating leads to an increase in atmospheric stability which suggests that convection would not reach as high in a volcanically perturbed scenario. On the other hand, the tropopause itself is shifted downward due to the heating. In an unperturbed scenario deep convection would tie the temperature profile to the moist adiabat which is very steep in the temperature range of the TTL, thus essentially pushing the TTL upwards. If the kinetic energy of the convective events does not change as drastically as the tropopause height, this lower lying tropopause might - in contrast to the stability argument - allow for more convective overshoots as the convection is working on reestablishing the original balance of moisture flux partitioning.

In-cloud upwelling: more ice, increased upwelling and sedimentation, changed convective conditions.

In-cloud upwelling could increase, both because of an increase in the vertical velocities resulting from the additional heating in the TTL, and because of increased amounts of cloud ice due to larger relative changes in the ice content per Kelvin cooling of the atmospheric temperatures. However, if overshooting were to be reduced in the aftermath of volcanic eruptions this might also lead to a reduction in the cloud formation and to a corresponding decrease of in-cloud upwelling. Similarly, if the increased ice formation in the TTL led to larger ice particles which sediment out faster, in-cloud upwelling would be reduced.

Turbulent mixing: (moisture gradients) tied to overshoots and in-cloud upwelling.

Depending on whether overshooting convection and in-cloud upwelling is increas-

ing or decreasing, the moisture gradients, and with them conditions for turbulent mixing, would be altered. Here it is especially interesting which of the triggers for turbulent mixing - atmospheric instabilities or wind shear - will dominate the picture as both are known to change after volcanic eruptions.

In summary, in the second part of my work I address the following questions:

- *Does the overall dependence of stratospheric water vapor on tropical cold-point temperature change in the convection-resolving simulations compared to simulations relying on convective parametrizations?*
- *What is the relative importance of water vapor versus frozen hydrometeors for the TTL moisture fluxes?*
- *How do the respective moisture fluxes and their relative partitioning change under external forcing such as volcanic aerosol heating?*
- *Do the individual contributions to frozen moisture fluxes and their relative importance change under volcanic aerosol forcing and if so why? Specifically: What are the changes in convection, in-cloud upwelling, and turbulent mixing?*

The questions for this project on small-scale processes are answered in two steps: First, the overall picture and partitioning between non-frozen and frozen moisture is investigated for both a perturbed and unperturbed scenario (Section 2.2). Second, first results of the analysis of the frozen moisture flux composition, focusing on the contribution of overshooting convection, in-cloud upwelling, and turbulent mixing are presented (Section 2.3). A summary can be found in Section 3.1.

1.5 METHODOLOGICAL APPROACH TO RESEARCH QUESTIONS

The two main identified research areas demand individual modelling strategies.

Depending on the research question and aim addressed within the respective subproject, models suited best for the respective purpose are chosen. The research questions developed above have two distinct overarching themes:

1. Changes in the large-scale slowly ascending water vapor after volcanic eruptions and their forcing impact: Directly quantifying SWV changes after volcanic eruptions of different magnitude.
2. Importance of small-processes such as convection, in-cloud upwelling, and turbulent mixing for the SWV budget: Understanding the sensitivity of flux partitioning of frozen and non-frozen moisture into the TTL to external perturbations and explaining possible changes.

This work therefore employs a two-fold strategy combining the benefits of coarse and high resolution simulations. The following shows how the investigation requirements determined the model selection.

1.5.1 *Addressing the changes in the large-scale slowly ascending water vapor after volcanic eruptions*

Coarse resolution ensemble simulations to investigate the large-scale picture.

The study on the changes of the large-scale slowly ascending water vapor after volcanic eruptions addresses the magnitude of SWV changes as well as the forcing con-

sequences of increased SWV levels after volcanic eruptions. To study the large-scale picture, a range of different volcanic eruptions has to be simulated with many ensemble members for each scenario. Large ensemble simulations offer the possibility to study variability, whereas different eruption magnitudes allow the identification of possible nonlinearities and empirical formulas to estimate the effect of an increased aerosol optical depth (AOD) on SWV.
Coarse resolution simulations are the best model choice because they allow for longer simulations with different eruptions scenarios while still capturing the essential physical processes. The analysis relies on two different ensembles relying on different aerosol input data:

Experiment descriptions MPI-GE historical simulations, and EVAens.

- The *MPI-GE historical simulations* (Maher et al., 2019) consists of 100 ensemble member runs using volcanic aerosol data based on historical observations, the so called Pinatubo aerosol data set (PADS, Stenchikov et al. (1998), Driscoll et al. (2012), Schmidt et al. (2013)). Each member of the 100 ensemble set starts from its individual initial conditions. For this study the period from 1991 to 1993 is investigated, which covers the eruption of Mt. Pinatubo in June 1991.
- The *EVAens* (Azoulay et al., 2020), where 100 ensemble member runs were conducted for five different, idealized tropical eruptions ([2.5,5,10,20,40] Tg of injected sulfur) and an unperturbed control. The volcanic aerosol data sets were calculated offline with the EVA forcing generator (Toohey et al., 2016). These simulations where branched off from the *MPI-GE historical simulations* in January 1991.

Model description for MPI-ESM-LR.

Both ensemble simulations were performed with the coupled, coarse resolution climate model **MPI-ESM-LR**[8]. The coupled model with 200 km horizontal resolution includes the atmosphere component ECHAM (version echam-6.3.01p3, Stevens et al. (2013)), the land component JSBACH (version jsbach-3.00, Reick et al. (2013), Schneck et al. (2013)), the ocean component MPIOM (version mpiom-1.6.1p1, Marsland et al. (2003), Jungclaus et al. (2013)), and the biogeochemistry component HAMOCC (HAMOCC5.2, Ilyina et al. (2013)). The simulation of convective processes relies on parametrizations which also describe overshooting convection (Möbis and Stevens, 2012). The overshooting mass flux is fully detrained in the two levels above the level of neutral buoyancy. The overshooting fraction is hard-coded. Aerosol is prescribed based on its optical properties.

Model description for konrad.

The 1-D radiative convective equilibrium model **konrad** (Kluft et al., 2019, Dacie et al., 2019) is used for radiative forcing calculations. This model is tuned to represent the tropical atmosphere. The radiation is based on the Rapid Radiative Transfer Model for General Circulation Models (RRTMG) (Mlawer et al., 1997). Tropospheric temperatures are determined by convective adjustment to a moist adiabat, while stratospheric temperatures are calculated assuming radiative-dynamical equilibrium.

1.5.2 *Addressing the importance of small-scale processes and their changes after perturbations*

Convection-resolving simulations for a combined investigation of large-scale and small-scale processes.

For a study of small-scale processes such as convection and in-cloud upwelling it is necessary to explicitly resolve convection in high resolution simulations. Because computational constraints allow only for a short simulated time frame, it is essential to generate a clear strong signal to gain insight into physical processes. Hence, a realistic representation of a volcanic eruption is not the intention. The focus lies on an idealized setup. This means, seasonal variations and influence of SST changes have to be suppressed. The magnitude of the simulated eruption is chosen based on the knowledge gained in the large-scale study, which identified the eruption magnitude creating a signal stronger than internal variability.

Experiment description: CaVE.

For the *CaVE*[9] simulations, which were conducted exclusively for this work, two scenarios are integrated: a scenario with 0 Tg S (Control) and a scenario with a tropical eruption of 20 Tg S (Perturbed). As in the *EVAens*, aerosol is prescribed based on its optical properties as calculated offline with the EVA forcing generator (Toohey et al., 2016). In order to extract a clear signal without seasonal variations, the simulations are performed in perpetual January mode. This also means that the aerosol layer does not evolve over time but is set constant to the month with peak near IR extinction in order to maximize the heating effect in the TTL. As the focus of this study lies exclusively on the effect of a heating source in the TTL, the SSTs of Perturbed are set to the Control SSTs, which are kept constant over time. For both scenarios 60 model days after a 150 day spin-up are are analyzed. In order to manage computational and storage resources, a horizontal resolution of 10 km is chosen which has been shown to realistically simulate overshooting convection (Hohenegger et al., 2020).

Model description: ICON-A.

CaVE employs high resolution, convection-resolving simulations with **ICON-A**[10] (Crueger et al., 2018, Giorgetta et al., 2018). ICON-A is an atmosphere-only model. Within the sapphire setup configuration (Hohenegger et al., 2022), a one-moment microphysics scheme (Baldauf et al., 2011) and the Total Turbulent Energy (TTE) scheme (e.g Louis, 1979, Brinkop and Roeckner, 1995, Mauritsen et al., 2007, Angevine et al., 2010, Pithan, 2014, Zilitinkevich et al., 2009) are used. The aerosol is described by its optical properties.

Method to obtain a water vapor budget.

Analyzing the contribution of frozen and non-frozen hydrometeors to the total moisture flux entering the stratosphere makes a budget analysis necessary. Special focus is laid on ensuring mass conservation within the analysis to obtain reliable and reproducible results. Additional output streams for the moisture fluxes are added to ICON to avoid errors arising from offline calculations. Damping triggered by violations of the Courant-Friedrichs-Lewy criterion (Courant, 1928) is minimized by restricting the model time step to a quarter of the time recommended for the used resolution. All flux analyses are additionally performed on the native output grid as mass closure can only be guaranteed on the original terrain-following coordinates.

8 short for: "Max Planck Institute - Earth System Model in its Low Resolution"

9 The simulation set was named "CaVE" as an acronym for "Convection after Volcanic Eruptions" inspired by the famous pre 79 AD mosaic in Pompeii at the valley of the Vesuvius stating "Cave canem" - beware of the dog - in strange irony as greater threats were slumbering nearby.

10 short for: "Icosahedral Nonhydrostatic Weather and Climate Model - Atmosphere"

2 SYNTHESIS OF RESULTS

2.1 THE IMPACT OF VOLCANIC ERUPTIONS OF DIFFERENT MAGNITUDE ON STRATOSPHERIC WATER VAPOR IN THE TROPICS

Related research questions: *What is the critical magnitude for a volcanic eruption to have a significant impact on the stratospheric water vapor content? That is, when do its effects dominate over internal variability? By how much does stratospheric water vapor increase for different eruption magnitudes if directly quantified, i.e. not from the residuum? Which parameters are critical for determining the SWV increase? What is the contribution of the SWV forcing to the overall radiation budget? Can cold point temperature warming and SWV forcing be estimated based on eruption magnitude or AOD? Is there an easy approximation for SWV increases?*

The first project (Kroll et al., 2021) investigates the impact of tropical volcanic eruptions of different magnitudes on the large-scale slowly ascending water vapor. As described in Section 1.5 the analysis is based on the *EVAens* with eruption strengths of 2.5, 5, 10, 20, and 40 Tg S and the *MPI-GE historical simulations* featuring the Mt. Pinatubo eruption (1991-1993). The Mt. Pinatubo eruption with 7 Tg S (best estimate, Timmreck et al., 2018) is best described by the (5 - 10) Tg S *EVAens* simulations. Table 1 lists three additional historical volcanic eruptions to bring the magnitude of the *EVAens* eruptions into context.

At 10 Tg S: SWV signal exceeds 2 σ spread of control.

In order to determine the eruption magnitude leading to a significant impact on the stratospheric water vapor content, the variability of the cold-point temperature and stratospheric water vapor content in an unperturbed scenario (0 Tg S) has to be quantified. Figure 2 visualizes the tropical seasonal means (September-October-November) in cold-point temperature and SWV content. Each point denotes a single ensemble member. In my eruption set, the 10 Tg S eruption marks the critical magnitude at which 99 % of the ensemble members of the eruption event create SWV values which does not show any overlap with the 2 σ range of the control simulations in the year of the eruption. Comparable events should be detectable without additional postprocessing in observational records as well. This finding is consistent with observational evidence as records of Mt. Pinatubo's effect on stratospheric water vapor exist. For example, SWV values even slightly larger than those of the 10 Tg S simulations were recorded in the Boulder balloon data (Oltmans et al., 2000). Also the cold point warming of around 1.8 K fits observational records (e.g. Angell, 1997, Santer et al., 2003).

Approximation: +12 % SWV per Kelvin increase in cold-point temperature.

The overall agreement between the Clausius Clapeyron saturation specific humidity (orange dashed line) and the water vapor values from the model suggest a very good description of the water vapor values in the stratosphere by the large-scale slowly ascending water vapor. Together with the even simpler approximation of a 12 %/ K water vapor increase (grey dashed line), the Clausius Clapeyron relation offers a first estimate of the water vapor increases after volcanic eruptions when

the temperature increase is known. The good predictability of SWV increase based on the mean cold-point temperatures in the tropics is surprising as it are often the spatial minima of cold-point temperatures which determine the mean SWV entry (e.g. Oman et al., 2008). Because of this inconsistency, the correlation between mean cold-point humidity and mean cold-point temperature found in the *MPI-ESM* simulations with parameterized convection will be compared to the findings based on convection-resolving simulations in the second part of this work.

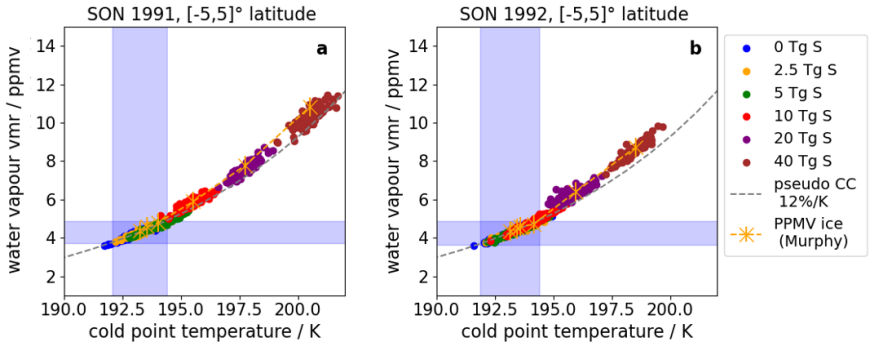

Figure 2: Seasonal averages of water vapor at the cold point as a function of cold-point temperature for September-October-November 1991 (a) and 1992 (b). Values for each individual ensemble member are shown as dots for the inner tropics. An approximation for the Clausius Clapeyron equation at this temperature range with an 12 % increase of water vapor per K is shown with a dashed grey line. The exact solution for the Clausius Clapeyron Equation over ice by Murphy and Koop (2005) is calculated for the average ensemble cold-point temperatures and pressure and is shown with a dashed orange line. The 2 σ range for the cold-point temperature and water vapor of the 0 Tg S ensemble is shaded in light blue.

SWV increases in relation to other natural sources of SWV variability.

The large number of ensemble members in the *EVAens* makes it possible to overcome the problem that internal variability of the tape recorder signal obscures the signal caused by the volcanic eruptions smaller than 10 Tg S. In the ensemble mean, increases in the SWV content are detectable for all eruptions strengths - even at 2.5 Tg of injected sulphur as shown in the top panel of Figure 3. As the values for SWV increases may seem relatively abstract, Table 1 lists some examples for real physical events leading to comparable SWV increases as observed for the various volcanic eruptions. Increases range everywhere between the SWV changes attributed to the QBO (Dessler et al., 2013) for the 2.5 Tg S ensemble to the summer time SWV background in the TTL for the 40 Tg S ensemble.

Differences in SWV response between 10 Tg S and Pinatubo simulation.

A direct comparison of the *EVAens* simulations and the *MPI-ESM historical simulations* can be made when comparing the 10 Tg S ensemble mean to the simulations employing the observational based PADS in Figure 3. The most prominent difference between both scenarios is the amplification of the SWV entry in the second post eruption summer in the PADS simulations. This feature is not present in any of the *EVAens* simulations, where the SWV signal already starts to decrease one year after the eruption.

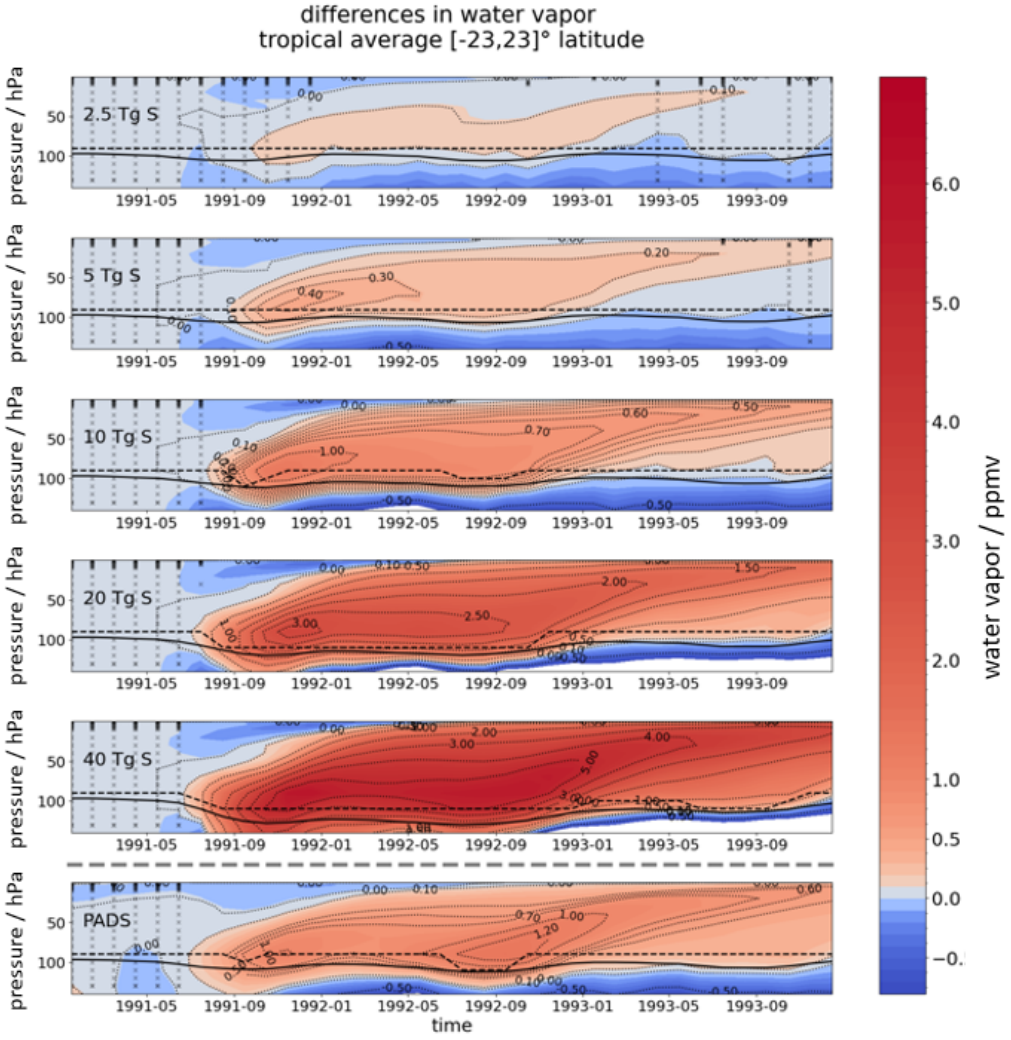

Figure 3: Tropical average in [-23, 23]° latitude of WV anomalies (volcanically perturbed - control simulation) above 140 hPa for the sulfur injections of 2.5 Tg S, 5 Tg S, 10 Tg S, 20 Tg S and 40 Tg S, as well as the PADS with a best estimate of 7 Tg S. The lowermost panel shows the MPI-GE historical simulations for Mt. Pinatubo. The lapse rate tropopause pressure is indicated by a black line and the cold-point pressure is shown as black dashed line. In regions not covered by black crosses, statistically significant differences between water vapor values of the perturbed and unperturbed runs (t-test at p=0.05) were found.

Important parameter: profile shape and height.

This difference in the respective signals can be explained by the differing shape of the aerosol profiles and their relative proximity to the tropopause. Whereas the EVA forcing data sets create an idealized extinction profile of Gaussian shape, keeping the peak height constant, the PADS shows variations in the shapes of the aerosol profiles. Figure 4 shows the temporal evolution of the aerosol extinction in the strongest IR waveband at the peak extinction and in the cold-point region. The peak extinction of the Mt. Pinatubo simulation (PADS) with an estimated ejection of 7 Tg S mostly lies between the 5 Tg S and 10 Tg S extinction values of the *EVAens* data. However, in contrast to the EVA forcing data sets, the extinction remains at a relatively constant level, ultimately even exceeding the 10 Tg S extinction by the end of the second post eruption year. In the second post eruption summer a downward shift of parts of the aerosol profile is taken into account as the sulphate particles slowly descend and fall out. These differences lead to an enhanced longwave and near IR heating in the cold-point region in the historical simulations based on the PADS, which is not present in the *EVAens*. PADS based extinction values in the cold-point region thus are higher than those of the 10 Tg S simulation. An immediate consequence of these differences in aerosol profile shape is the different timing of the peak SWV enhancement.

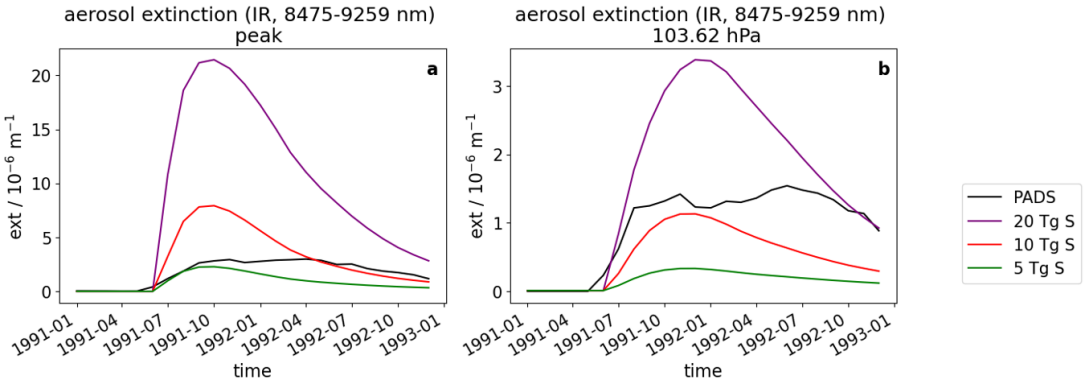

Figure 4: Temporal evolution of the aerosol extinction at the profile peak (a) and the cold-point region (b) for the 8475-9259 nm IR waveband.

Additional SWV forcing counterbalances up to 4 % of aerosol forcing in the tropics.

Finally, the radiative forcing due to the SWV originating from the indirect pathway after the volcanic eruption has to be quantified. The stratospherically adjusted forcing is determined by importing the tropical moisture fields into *konrad* and calculating the radiative fluxes there. For the 10 Tg S ensemble, a comparison of the SWV forcing with the aerosol forcing reveals that the SWV forcing counteracts up to 4 % of the aerosol forcing in the tropics for the 10 Tg S eruption scenario. For the 20 Tg S and 40 Tg S eruptions, the global TOA imbalance in the third eruption year even becomes positive. Part of this can be attributed to the SWV forcing slowly gaining in relative importance globally, as the aerosol falls out while the elevated water vapor levels are still present. An additional calculation for the 10 Tg S scenario, taking into account clouds when determining the forcing, shows an increase in the SWV forcing by around 0.1 $W\,m^{-2}$ as the additional SWV leads to absorption of shortwave radiation which would otherwise have been reflected by the cloud layer.

Table 1: List of tropical *EVAens* eruptions and physical phenomena leading to similar SWV increases and stratospherically adjusted forcings (F_a). References: a - Timmreck et al., 2018, b - Marshall et al., 2018, c - Dessler et al., 2013 , d - Wang et al., 2020 - radiative forcing caused by SWV changes in a 2xCO2 experiment, e - Davis et al., 2017, f -Myhre et al., 2013 - radiative forcing of emitted compounds over Industrial Era (as analyzed in 2013)

Tg S	comp. eruption [Tg S]	Δ SWV [ppmv]	comp. event	$F_{a,SWV}$ [W m^{-2}]	comp. event [W m^{-2}]
2.5		+0.1	< QBO (0.16– 0.32)[c]		
5	El Chichón (3.5)[a]	+0.4	> CO_2 caused increases (0.2-0.4)[d]		
	Agung (3.5)[a]				
10	Pinatubo (7)[a]	+1.1	≈ annual cycle amplitude (1.0-1.3)[e]	+0.1	<N_2O (+0.18)[f]
			> BDC (0.65)[c]		
20		+3.0	≈ SWV background winter	+0.3	
40	Tambora (30)[b]	+5.0	≈ SWV background summer	+0.6	> CH_4 (0.48)[f]
					≈ 1/3 CO_2 (1.82)[f]

AOD-based estimations of cold-point warming and SWV forcing are possible.

Both cold-point warming and SWV forcing can be estimated based on AOD values. Figure 5 shows a fit to the yearly tropical averages of the adjusted forcings due to the additional SWV in all *EVAens* ensemble means as a function of AOD. For every year, a power law is determined which can be used to estimate the yearly average forcing for comparable eruptions[1]. As for the SWV increases, Table 1 lists the SWV forcing and data from real events as references. For example, in the case of the 40 Tg S eruptions, the tropical SWV forcing would exceed the forcing by methane and amount to one third of the present[2] CO_2 forcing (Myhre et al., 2013). As the SWV increase is a consequence of the aerosol forcing, the SWV forcing reaches its peak after the aerosol forcing. The delay of maximum forcing is additionally amplified due to the slow transport of air masses within the BDC. At an average upwelling velocity in the order of mm s^{-1} (Fujiwara et al., 2022), the water vapor levels will be prevalent in the tropical stratosphere for months and the forcing will reflect the total SWV column.

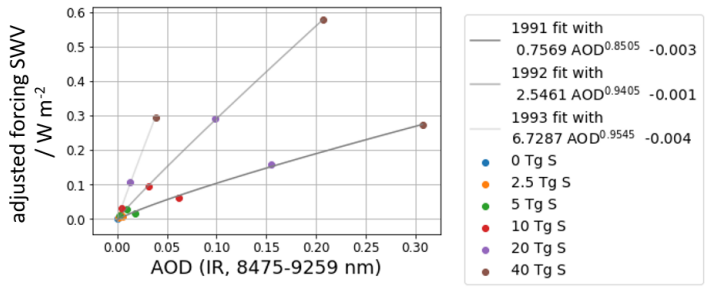

Figure 5: Yearly tropical averages of adjusted radiative forcing due to the additional SWV as a function of AOD (IR, 8475-9259 nm) for the three years after the eruption (1991-1993). A power function fit for each year with corresponding equation is shown.

1 A similar fit is obtained for the cold-point temperatures in the corresponding paper but not shown here.

2 According to an analysis in the year 2013.

2.2 THE SENSITIVITY OF MOISTURE FLUX PARTITIONING IN THE TROPICAL TROPOPAUSE LAYER TO EXTERNAL FORCING

Related research questions: *Does the overall dependence of stratospheric water vapor on tropical cold-point temperature change in the convection-resolving simulations compared to simulations relying on convective parametrizations? What is the relative importance of water vapor versus frozen hydrometeors for the TTL moisture fluxes? How do the respective moisture fluxes and their relative partitioning change under external forcing such as volcanic aerosol heating?*

The first part of this work (Section 2.1) reveals that a tropical eruption of 10 Tg S would be the first eruption size in the investigated eruption set of [2.5, 5, 10, 20, 40] Tg S which leads to a SWV signal stronger than the internal variability of the 0 Tg S ensemble. Therefore, to ensure that the water vapor signal should be detectable even if the simulated time frame was shortened to cut computational costs, a 20 Tg S eruption was chosen for the follow-up case study on moisture flux partitioning.

EVAens: mean CP temperature determines mean CP water vapor.

The *EVAens* simulations have shown a direct relation between the mean cold-point temperatures and mean water vapor at the cold point (compare Figure 2). Since the *CaVE* simulations have a twenty times higher horizontal resolution and do not rely on convective parametrization, it is prudent to re-examine this relationship in the *CaVE* simulations in order to see how both models compare with respect to their description of the large-scale stratospheric moisture budget.

CaVE: lowest 10^{th} percentile of CP temperature determines mean CP water vapor.

Figure 6 shows the respective mean and 10^{th} percentile cold-point temperature as well as the mean water vapor at the cold point for the 0 Tg S (blue) and 20 Tg S (red) simulation of *CaVE*. Solid lines indicate the Clausius Clapeyron Curve for the two atmospheric states. It is clear from Figure 6 that to get an accurate description of the CP water vapor in *CaVE* Control and Perturbed, not the mean CP temperatures, but the 10^{th} percentile of the inner tropical CP temperatures has to be used. In the case of Perturbed, the 10^{th} percentile approximation lies slightly above the simulated water vapor values. This difference to Control is caused by an increase in horizontal winds and, as analyzed within the next project (Section 2.3), by overshooting convection which leads to an increased modulation of the CP temperatures.

Concept of the "point of last saturation".

The theory of the last point of saturation (e.g. Sherwood, 1996) explains the correlation of the cold-point water vapor with the large-scale temperature field: For every distance traveled vertically, air parcels will travel a multiple of this distance horizontally since horizontal motions exceed the average upwelling velocities by far. Consequently, the air parcels will encounter a multitude of different temperatures, the coldest of which will set its saturation water vapor. In the theory of the "point of last saturation" frozen moisture is discarded immediately after formation. Although in reality this does not have to be the case and sublimation and evaporation can occur, some imprint of the horizontal temperature field remains. Correspondingly, the water vapor at the CP is often best estimated by using a lower percentile of the CP temperature range (e.g. Fueglistaler and Haynes, 2005).

Differences between EVAens and CaVE simulations.

The signature of the coldest temperature percentiles is not found in the *EVAens* simulations (compare Fig. 2) for three reasons. First, the horizontal resolution employed in the *EVAens* is much coarser leading to less variability over the same distance of horizontal travel. Second, although a rudimentary description of overshooting con-

vection is included in the *EVAens* (Möbis and Stevens, 2012), the explicitly resolved convection in the *CaVE* simulations represents convective cooling in the CP region more accurately than the *EVAens*, leading to additionally increased variation in the CP temperatures. Third, the explicitly resolved convection within the *CaVE* allows for a more accurate representation of cloud fields. This will most likely lead to a better description of dehydration events caused by air parcels passing thin cirrus clouds located above anvils. Due to the screening of surface temperatures by the anvils, the cirrus clouds above will lead to a radiative cooling of the passing air masses, especially above the Western Pacific in Northern Hemispheric winter (Holton and Gettelman, 2001, Hartmann and Larson, 2002), an area where indeed elevated frozen moisture content is found in the *CaVE* simulations.

Lowest temperatures as equivalent frost point temperature of the TTL.

This first assessment of the relationship between cold-point temperatures and specific moisture already demonstrates that the *CaVE* simulations render a physical representation of the water vapor levels in the TTL which is closer to the long known dependence of the water vapor levels on the lowest, and not mean, cold-point temperatures within the tropics (Newell and Gould-Stewart, 1981). These lowest temperatures - here given by the 10^{th} percentile of cold-point temperatures in the inner tropics - can then be interpreted as the equivalent frost point temperature based on which the average water vapor at the cold point in the inner tropics can be estimated.

To analyze the partitioning of moisture fluxes into large-scale slowly ascending wa-

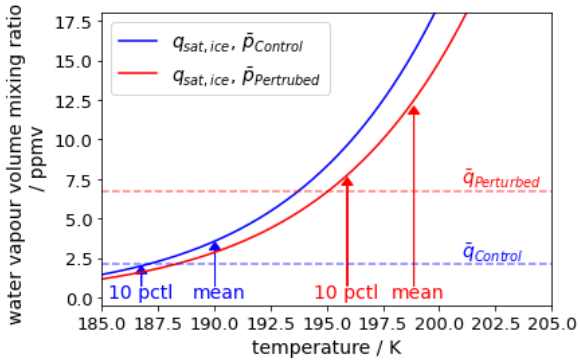

Figure 6: Two-months average water vapor at the mean cold-point height for Perturbed (red) and Control (blue) in the area [-5,5]°N, marked by horizontal dashed lines. The average water vapor values are compared against the expected saturation specific humidities at the mean cold-point temperature and the cold-point temperature at the 10^{th} percentile for Perturbed and Control, marked with arrows. The saturation water vapor above ice as implemented in ICON (COSMO, Doms and Förstner, 2021) is calculated for Perturbed and Control respectively at the average cold-point pressure $\bar{p}$ (solid line curves).

Control: Large-scale slowly ascending water vapor dominates budget with ≈ 80 % contribution.

ter vapor and small-scale frozen contributions, two months of moisture fluxes entering the stratosphere through the average cold-point tropopause are analyzed for the [-30,30]° N region, the suggested boundaries of the TTL (Fueglistaler et al., 2009). Figure 7 displays corresponding results, Control is depicted in blue, Perturbed in red. The water vapor flux is the dominating source of moisture amounting up to around 80 % of the moisture entering the stratosphere in Control, whereas frozen hydrometeors make up around 20 % of the moisture.

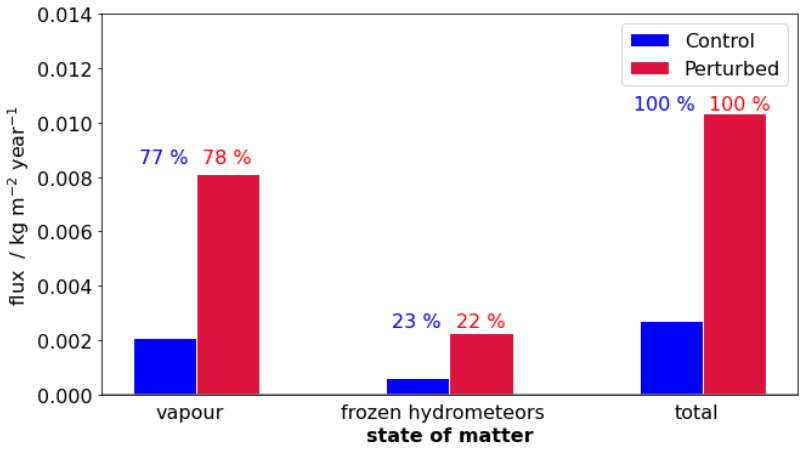

Figure 7: Average net moisture flux through the cold-point tropopause due to water vapor and frozen states of matter relevant for the TTL, as well as their total, between [-30,30]° N. Control is shown in blue, the corresponding fluxes for Perturbed simulation in red.

Comparison to observational based estimate and trajectory studies.

This analysis result is in good agreement with a study of the contributions to the stratospheric moisture budget by Bolot and Fueglistaler, 2021, which is based on observations, but larger than those found by most trajectory studies. Reported values from trajectory studies include Schoeberl et al., 2018, with 2 %, Ueyama et al., 2015, with 14 %, Ueyama et al., 2018, with 15 % and Smith et al., 2022, with 26 - 32 %. However, trajectory studies are known to be biased towards lower frozen moisture values as they are driven by coarse resolution wind fields which do not capture some of the essential features of overshooting convection (Dauhut et al., 2018) and often only quantify the frozen moisture flux indirectly.

Comparison to a convection-resolving study.

Dauhut and Hohenegger, 2022, analyzed the moisture changes in the stratosphere in the convection-resolving DYAMOND simulation of ICON (Stevens et al., 2019) finding a frozen contribution of 11 %. They restricted their analysis to an OLR threshold selecting only the deepest convective events. Without this threshold the contribution of frozen hydrometeors would be 29.3 %. Their result is not be directly comparable to the result of this study as they relied on a different physics package. Additionally, they also performed an offline calculation based on horizontally remapped moisture tendencies, in contrast to the work presented here, which relies on the online calculation of moisture fluxes on the native grid. Based on the experience gained when performing the flux analysis, these differences in the analysis procedure could easily lead to the discrepancy between the 20 % in this work and their 11 %. As the budget is only closed on original model levels any remapping will not only smooth out convective peaks but also lead to small inconsistencies which - in the dry region of the cold-point tropopause - gain in relative magnitude. Moisture tendencies will additionally obscure the overall picture as they offer no information on the background flow through the atmospheric columns.

In summary, inconsistencies between different methods and models remain. Whereas some biases, as in the case of trajectory models, are known others may remain to be found. The estimate of convective contribution to the total moisture flux in this study is in the higher range of reported values but agrees with estimates derived from observational records (e.g. Bolot and Fueglistaler, 2021).

TTL perturbation: All fluxes enhanced, partitioning remains unchanged.

When comparing the TTL moisture flux partitioning in Control and Perturbed (Figure 7), its resilience becomes evident. Even under the strong perturbation, which leads to a considerable TTL warming of around 9 K, the partitioning is conserved. As the stability in the TTL is increasing, the found flux increase of frozen hydrometeors seems counterintuitive at first thought, since fluxes of frozen hydrometeors originate from overshoots and in-cloud upwelling in their surroundings and are normally associated with regions of reduced atmospheric stability. For example, the cooling of the tropical upper tropospheric region is used to explain the associated enhancement of convective overshoots in the case of sudden stratospheric warmings (e.g. Kodera et al., 2015).

Convection influences the tropopause height.

It has to be considered though that the height of the TTL itself is set based on a balance between radiative-dynamically induced temperature changes in the higher lying regions and temperature changes due to convective-radiative-dynamical process from below (e.g. Fueglistaler et al., 2009). As such the tropopause temperature depends on the interplay of a set of different parameters like CO_2 and ozone concentrations, the QBO phase, the strength of the Brewer Dobson circulation, and convection (Manabe and Möller, 1961; Dobson et al., 1946; Gowan and Dobson, 1947; Thuburn and Craig, 2002; Johnson and Kriete, 1982; Fueglistaler et al., 2009; Dacie, 2020). Consequently, the tropopause (height) is also coupled to the convection and can not be seen as an independent parameter (Kuang and Bretherton, 2004, Hu et al., 2021). The temperature increase induced by aerosol heating leads to a downward shift of the tropopause in a region where convection would normally be more prevalent. At the top of convective events in the TTL, convection will lead to cooling (i.e. Johnson and Kriete, 1982, Holloway and Neelin, 2007, Paulik and Birner, 2012) and consequently push the tropopause upwards. Given that entrainment and sub-cloud moist static energy do not change as drastically as the tropopause temperatures, more convective events will reach the lower lying tropopause, counteracting part of the heating effects and moving the tropopause upwards in height until a new balance is found. In this simulation the balance mirrors the original partitioning of the moisture sources. When considering convection overshooting the CP tropopause as primary source of frozen moisture two mechanisms might lead to the increased moisture flux: a higher frequency of overshoots or overshoots transporting more frozen moisture due to the elevated background temperatures and higher ice formations per unit decrease in temperature.

Constant flux partitioning in climate change study.

The found constant partitioning may surprise at first, but is also supported by the results of a Lagrangian study (Smith et al., 2022) in which a near constant contribution of convection to the stratospheric moisture budget in $2xCO_2$ and $4xCO_4$ experiments was found. Their convective contribution of 21 % - 35 % ranges within the largest estimates known to the author and shows a large spread in results.

Results suggest season-independent flux partitioning.

Apart from perturbations due to external forcing, seasonal variations could also alter the moisture partitioning. Based on the exceptional robustness of the flux partitioning revealed even under the strong perturbation in the cold-point region as employed in this study, there is reason to expect the stable partitioning to hold also under seasonal variations with minor modulations due to e.g. monsoons or ENSO. Before it has been hypothesized that the differences in estimates for the partitioning of moisture fluxes into large-scale and small-scale processes originates from differences in the seasons investigated (e.g. Dauhut and Hohenegger, 2022). The corresponding rea-

soning was based on studies showing the seasonal variation of mass transported in the solid phase into the TTL which shows maxima in Northern Hemispheric spring and autumn and minima in Northern Hemispheric winter (e.g. Liu and Zipser, 2005), potentially indicating a varying contribution of convection to the total moisture budget. Inferring the share of convective events to the total moisture budget based on the transported share of ice mass with respect to its yearly total is however not as easy because the transported water vapor also varies with season in form of the tape recorder signal (Mote et al., 1996).

Constant partitioning over different seasons in observational and model based studies.

Additionally not all observation-based studies support the notion of season-dependent moisture flux partitioning. A season-independent partitioning is indicated by observational studies for MLS and HALOE data (Liu et al., 2010, Fueglistaler et al., 2013). Furthermore two modelling studies (Ueyama et al., 2015; Ueyama et al., 2018) support the notion of constant partitioning. They found an almost preserved partitioning of the moisture fluxes in the winter and summer season with 14 % resp. 15 % convective contribution.

Clausius Clapeyron scaling for water vapor and ice flux.

Knowledge of a constant partitioning has the potential to substantially simplify the estimation of changes in the stratospheric moisture budget under various perturbations since it can be only realised when both the non-frozen and frozen moisture follow Clausius Clapeyron scaling. The moisture budget can thus be described as the saturation specific humidity at the equivalent frost point temperature, e.g. the average of lowest temperatures within the TTL, plus an additional temperature offset ΔT which describes the contribution of the frozen moisture content according to the constant partitioning ratio. This Δ T can be determined by using e.g. the 12 % increase specific humidity per Kelvin increase in equivalent frost point temperature found in this work for temperatures between 190 K and 200 K. In the follow-up project (Section 2.3) changes in the contributions of the small-scale processes leading to fluxes of frozen hydrometers in the stratosphere will be discussed consecutively.

2.3 THE IMPACT OF VOLCANIC AEROSOL HEATING ON TURBULENT MIXING, IN-CLOUD UPWELLING AND CONVECTION IN THE TROPICAL TROPOPAUSE LAYER

Related research questions: *Do the individual contributions to frozen moisture fluxes and their relative importance change under volcanic aerosol forcing and if so why? Specifically: What are the changes in convection, in-cloud upwelling, and turbulent mixing?*

Study investigates processes contributing to increased frozen moisture flux at cold-point.

The second study (see Section 2.2) already showed that the flux of frozen hydrometeors into the TTL increases in consequence of an aerosol perturbation (see Figure 7). As frozen hydrometeors can originate from various small-scale processes a more detailed analysis on their origin and distribution is needed. The following section gives an overview over the ongoing investigations.

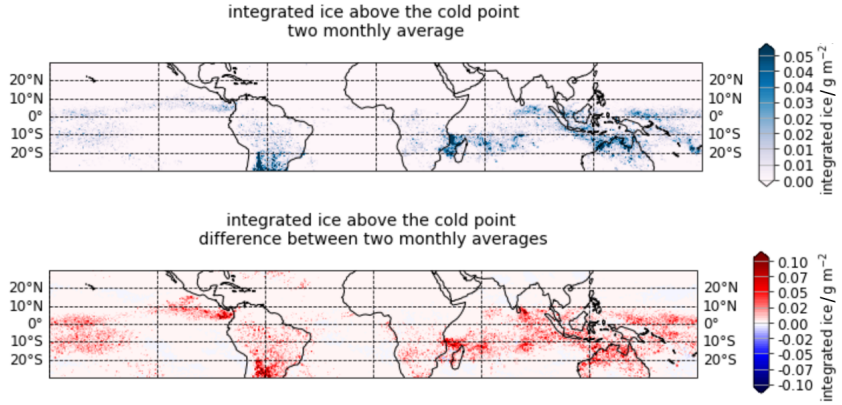

Figure 8: Upper panel: Two-months average of vertically integrated ice above the cold point in Control. Lower panel: Difference between the two-months averages of integrated ice above the cold point in Perturbed and Control (Perturbed-Control).

TTL ice and ice increases located in main convective areas.

The location of the frozen hydrometeors offers some insight on their origin. Figure 8 shows the cloud ice integrated above the cold point in a two-months average for Control and the difference between Perturbed and Control. The locations of cloud ice above the cold point shows strong, but not exact, correspondence with observational based studies on deep convection in the Northern Hemisphere winter season (e.g. Liu and Zipser, 2005, Kim et al., 2018). The Maritime Continent East Asia and South America comformably show especially pronounced ice levels, whereas the levels over Africa are not as prominent and shifted towards Madagascar. The disagreement over Africa may result from my analysis using the cold-point height as reference, since it offers a clear physical characteristic essential for the moisture flux, whereas in observational based studies other references, such as a reference height of 14 km, are used. The occurrence of ice in the convective areas suggests a connection to convective events and subsequent processes such as in-cloud upwelling or turbulent mixing at the cloud top. Additionally, convection induced gravity waves (e.g. Prasad et al., 2019, Atlas and Bretherton, 2022) may be creating some cloud ice in the areas around convective events. In Perturbed the ice fraction above the cold point increases by 60 %. The main areas of increase are located in the regions where ice was already present in Control. This suggests that the main driving processes remain the same and are merely amplified.

$\theta_{e,surf}$, LNB and entrainment as critical parameters for convective height.

Based on this finding, convection will be investigated first, because it seems to dominate the large-scale ice distribution, whereas in-cloud upwelling and turbulent mixing are secondary processes following convection. The analysis is based on estimators for the convective height after Fueglistaler et al., 2009: the equivalent potential temperature at the surface ($\theta_{e,surf}$), the air parcel's level of neutral buoyancy (LNB), and entrainment during the convection itself.

$\theta_{e,surf}$ reduced in Perturbed.

The first estimator is $\theta_{e,surf}$. In Perturbed he mean $\theta_{e,surf}$ of 348.0 K is only reduced by around 1 K compared to Control $\theta_{e,surf}$ of 348.8 K in the region between [-30,30]° N. This reduction in $\theta_{e,surf}$ is anticipated since the sulfate aerosol scatters the incoming solar radiation, reducing the energy input into the earth system, even-

Table 2: Summary of the results of the LNB calculations for the 2 m s^{-1} and 5 m s^{-1} vertical velocity thresholds. Total number of analyzed events, number of potential CP tropopause overshoots, and percentage of potential CP tropopause overshoots for Perturbed and Control selected over two months in perpetual January mode.

	total events		overshoots		overshoot percentages	
	2 m s^{-1}	5 m s^{-1}	2 m s^{-1}	5 m s^{-1}	2 m s^{-1}	5 m s^{-1}
Control	643080	87961	4026	833	0.63 %	0.95 %
Perturbed	587739	71769	5555	862	0.95 %	1.2 %

tually leading to a surface cooling, which in turn reduces the maximum convective height. As this idealized study focuses on the effect of possible heating in the TTL, the SSTs are kept constant so that only land temperatures can adapt. The reduction in $\theta_{e,surf}$ may be consequently amplified in a non-idealized setup. The setup also leads to an increased land-sea contrast, potentially causing a spatial redistribution of convection which is not representative of a volcanic or geoengineering scenario with longer lasting forcing. However, the spatial distribution of above CP cloud ice shows that areas over land still exhibit increases and not decreases in CP cloud ice.

Distance between LNB and tropopause decreases in Perturbed.

The second estimator for the convective height is the buoyancy of air parcels. Potential changes in the LNB and its relative distance to the CP tropopause are estimated for two months of data in the region between [-30,30]° N both for Control and Perturbed. In the algorithm, the convective cells are selected based on their vertical velocity at a height of 10 km. Thereafter their extent is determined recursively, and then their average temperature profile and that of their surroundings computed. These two average temperature profiles are used to estimate the LNB. This calculation is based on snapshots of ongoing convective events. For each height and air parcel the density based current buoyancy is estimated. Beneath the LNB all air parcels have to be buoyant. Since the future development is not considered, neither further latent heat release during the continued updraft nor possible entrainment are calculated. The selection of events at 10 km in height restricts the analysis to convective events with the immediate potential to reach the tropopause in the simulation's time step and minimizes biases due to latent heat release or entrainment which could lead to an under- or overestimation of the LNB. The results for Control and Perturbed are listed in Table 2 for two velocity thresholds. In Perturbed the frequency of high velocity events decreases. The reduction amounts to -9 % for the 2 m s^{-1} threshold and -18 % for the 5 m s^{-1}. The decreased percentage share at the 5 m s^{-1} threshold also might suggest a decrease in the vigorousness of events. Despite the decrease in frequency of events, the absolute number of LNBs above the CP tropopause is higher in Perturbed than in Control. The percentage share of CP overshoots approximately increases by 0.3 % for velocity thresholds of 2 m s^{-1} and 5 m s^{-1}.

Addressing the study limitations: latent heat release and entrainment.

The LNB calculation was only based on a snapshot of current atmospheric conditions. It did not include entrainment, which could reduce the height of convective tops nor did it consider future latent heat release which could increase the LNB. A solid estimation of changes in the third factor, entrainment, and an inclusion of the latent heat release would require a budget analysis of changes in moist static energy

(e.g. Zhang et al., 2016), which is beyond of the scope of this work. Consequently, as an alternative, the resulting final balance of parameters impacting the potential convective activity is determined by directly investigating the convective changes via moisture distributions in moisture space and velocity dependent cumulative mass transport. Both will be discussed below.

Increased mass transported by CP overshoots visible in moisture space.

Figure 9 shows the specific total frozen and liquid condensate as a function of height binned according to percentiles of column integrated water vapor. Higher percentiles of water vapor are used as an indicator of very deep convective systems (e.g. Schulz and Stevens, 2018). In Perturbed the specific frozen moisture content above the LR (dashed black line) and CP tropopause (solid black line) is increased compared to Control. The increase in the higher percentiles indicates that the amount of frozen moisture transported by overshoots to the LR or CP tropopause is elevated in Perturbed. This is consistent with the increase in CP overshoots in the LNB calculations meaning that, even if entrainment increased, the convection is still reaching the TTL. As the increase in overshoot numbers amounts to circa 0.3 % at the CP tropopause, it is likely that the amount of frozen moisture transported within the overshoots also plays an important role. The higher absolute temperature in the perturbed TTL could lead to a higher absolute condensing mass per degree decrease in Kelvin in saturated environments. This mechanism is currently under investigation.

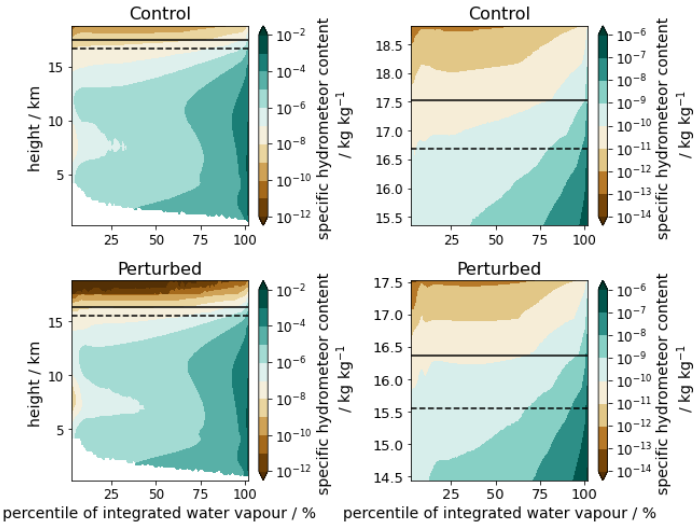

Figure 9: Left hand side: Specific hydrometeor content binned according to percentiles of integrated water vapor content in the area of [0,10]° N for two months of data. The average LR and CP tropopause are denoted with a dashed and continuous black line. Right hand side: Close-ups into the TTL for Control and Perturbed are shown.

Vertical velocities give insight into the processes by which moisture is transported.

In addition to the dominant convection processes discussed above, in-cloud upwelling can also be a way to bridge the vertical distance between convective outflows and the CP tropopause (Corti et al., 2006). The radiative heating within the clouds will lead to an updraft in the clouds transporting them further upwards. In ICON this process can be simulated as cloud ice is coupled to the radiation scheme. Disentangling deep convection and in-cloud upwelling is challenging though, as both tend to occur at the same locations with high convective activity and the three hourly output frequency does not allow for a trajectory analysis (e.g. Lang et al., 2022). However,

the distribution of the vertical moisture flux over the vertical velocities is an alternative way to get new insight into the relative importance of in-cloud upwelling and overshooting, as well as their changes under perturbations. In-cloud upwelling will only occur at velocities in the mm s^{-1} region (approximately [-4,4] mm s^{-1}). In contrast to this, overshooting convection will occur over a much wider velocity range - from mm s^{-1} for ceasing convective events to the m s^{-1} region for convection which did not reach its LNB and/or did not deplete its entire kinetic energy yet.

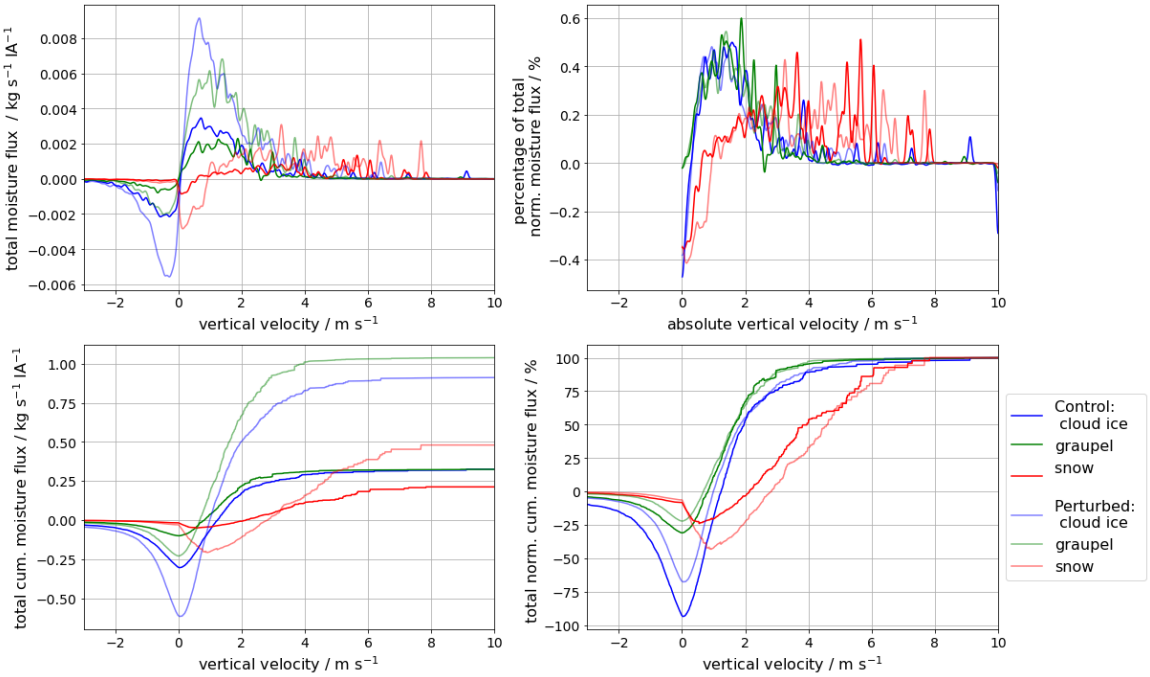

Figure 10: Analysis of CP moisture fluxes in the region between [-30,30]° N (= investigated area, IA). Upper panels: total moisture flux (left) and percentage of total absolute moisture flux (right) for cloud ice, graupel and snow binned according to vertical velocities (left) and absolute vertical velocity (right). For better visualization the data was smoothed with a 1D Gaussian Filter.
Lower panels: Total cumulative moisture flux for cloud ice, graupel and snow binned according to vertical velocities. The left panel shows the unnormalized flux values. The right panel shows the cumulative flux normalized to the total cumulative flux for each hydrometeor both for Control and Perturbed.

In-cloud upwelling counteracts part of the sedimentation but can not establish positive flux.

The upper panels in Figure 10 show the total vertical moisture flux at the cold point for cloud ice, graupel and snow binned according to the vertical velocity between [-30,30]° N. In Perturbed all moisture fluxes show in general the same behaviour as in Control and are merely amplified. Cloud ice is the only hydrometeor, next to water vapor, directly interacting with radiation and therefore capable of inducing in-cloud upwelling. At low absolute velocities cloud ice is the dominating flux and it seems to oscillate upwards and downwards. In order to estimate the net effect of the small velocities, the moisture flux is binned according to absolute velocity and normalized with respect to the total flux of cloud ice, graupel or snow (upper panel, right graph). Graupel is the only hydrometeor with positive fluxes near the 0 m s^{-1} absolute vertical velocity, indicating its prevalence in convective cores. In contrast, the contribu-

tion of the [-1,1] cm s^{-1} velocity bins of cloud ice to the total moisture flux is -0.7 % in Control and -0.4 % in Perturbed. The flux becomes only positive at velocities of 30 cm s^{-1}, which is outside the realm of in-cloud upwelling. Consequently, although in-cloud upwelling is causing part of the steep slope around zero vertical velocity, it and the ceasing convection is mostly counterbalancing the sedimenting cloud ice at negative velocities of the same magnitude. The analysis therefore suggests that in-cloud upwelling is very important to counterbalance part of the sedimentation in subsidence regions but can not establish a positive total flux.

Relatively constant importance of overshooting and in-cloud upwelling pathways.

The lower panels in Figure 10 show the corresponding cumulative total vertical moisture flux binned according to the vertical velocity between [-30,30]° N. The left panel, with the absolute fluxes, demonstrates that some frozen moisture in the form of graupel and ice is transported downwards in subsidence regions with negative vertical velocity. This negative moisture flux is only counterbalanced by upward transport of velocities between 0 m s^{-1} and 1 m s^{-1}. For Perturbed all cumulative fluxes in the individual categories are around three times larger than in Control. To compare the distribution of the moisture fluxes on the different velocities the right hand panel shows the cumulative fluxes for the hydrometeors normalized, each with respect to the their individual total cumulative flux. This comparison demonstrates that the distribution of moisture fluxes on different velocities is relatively constant for graupel and cloud ice considering the strong perturbation the TTL is undergoing. Some differences are visible though: The subsiding regions are less pronounced in Perturbed and the compensation of the downward flux occurs at lower positive velocities correspondingly. This is in accordance with increases in the vertical wind fields in the TTL and lower stratosphere found in these simulations and also reported elsewhere (e.g. Garcia et al., 2011, Diallo et al., 2017, Garfinkel et al., 2017). For snow changes are more pronounced. The Perturbed simulation exhibits a stronger snow sedimentation flux than the Control. This difference between cloud ice and graupel as well as snow is most likely attributable to the sensitivity of snow sedimentation velocities to temperature (Doms and Förstner, 2021).

Moisture gradients as prerequisite for turbulent mixing.

Turbulent mixing is the last contributor to the cross CP moisture flux. It takes place in areas with steep moisture gradients if triggered by atmospheric instabilities or wind shear. Table 3 lists the average and median of water vapor and ice gradients at the CP tropopause[3]. In Perturbed the moisture gradients are steeper than in Control. The increases are especially pronounced for cloud ice. These steeper moisture gradients in Perturbed can be explained by the increased number of and/or total mass transported by, deep convective events in Perturbed. As convective influence ceases in the TTL, the corresponding gradients will on average be negative, going from regions of high frozen moisture content at lower altitudes to lower frozen moisture content at higher altitudes. The reduced gradients for water vapor are linked to the more homogeneous water vapor fields.

Turbulent mixing increased but negligible at perturbed CP tropopause.

The increased moisture gradients in Perturbed should translate to an increase in turbulent mixing at the CP tropopause if the atmospheric background conditions are favourable with high wind shear or low atmospheric stability. Figure 11 shows the advective and sedimentation fluxes as well as the turbulent mixing fluxes at the CP tropopause. Two main observations can be made: First, the turbulent mixing is

3 Turbulent mixing is only applied to cloud water, cloud ice and water vapor in ICON, only the latter two are relevant in the TTL.

Table 3: Specific moisture gradients for water vapor and ice at the CP tropopause. Negative values denote decreasing moisture with height, positive values increasing moisture with height. All values are given in ppmm km^{-1}. Abbreviations: μ = mean, $\tilde{x}$ = median.

	Control		Perturbed	
	μ	$\tilde{x}$	μ	$\tilde{x}$
water vapor gradient	-0.007	-0.004	-0.326	-0.307
cloud ice gradient	-0.316	-0.001	-1.041	-0.005

stronger for cloud ice than for water vapor even though individual cloud crystals are heavier. This observation fits nicely to the stronger moisture gradients in the more inhomogeneous cloud ice field, triggering a stronger increase in turbulent mixing for cloud ice. Second, the influence of turbulent mixing is negligible compared to the advection and sedimentation terms. Also this finding is in accordance with expectations. The diffusivities in the TTL decline rapidly (Podglajen et al., 2017). The increasing scarcity of cloud ice with height will also reduce turbulent mixing.

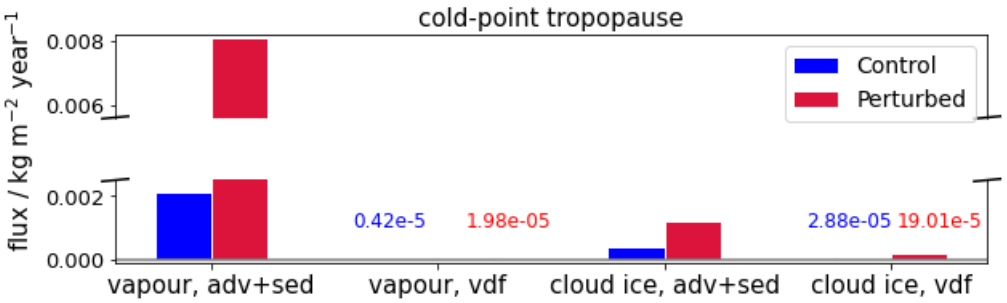

Figure 11: Moisture fluxes by combined advection and sedimentation (adv+sed) and turbulent mixing (vdf) through the cold-point tropopause due to water vapor and cloud ice between [-30,30]° N in a two month average. Control is shown in blue, the corresponding fluxes for Perturbed in red.

In summary, the explanation for the constant partitioning offered in the second study is supported by the in detail analysis of processes contributing to the frozen moisture flux. Convection is the driving mechanism to transport moisture in the TTL. A decreased distance between LNBs and downward shifted CP tropopause, and possibly a temperature caused increase in frozen moisture transported within the convective cores, dominate over a decrease in $\theta_{e,surf}$ in determining the final convective contribution to the stratospheric moisture budget. In-cloud upwelling and turbulent mixing slightly increase in Perturbed but have negligible importance at the CP tropopause. The relative importance of the different pathways is conserved in Perturbed to first order, although a slight decrease in subsidence can be denoted.

3 CONCLUSION AND OUTLOOK

3.1 ANSWERS TO RESEARCH QUESTIONS

The key findings to the governing questions of this work outlined in Section 1.4 are summarized below. The first set of answers addresses the large-scale slowly ascending water vapor and its changes after volcanic perturbations which were investigated with coarse resolution ensemble simulations:

1. *What is the critical magnitude for a volcanic eruption to have a significant impact on the stratospheric water vapor content by dominating over internal variability?*
   SWV and CP temperatures of single ensemble members up to an eruption magnitude of 10 Tg S are within the 2 σ range of the control. Starting from 10 Tg S scenario a detection of the volcanic signal longer than a couple of weeks post-eruption should be easier in observational records, even without additional analysis.

2. *By how much does stratospheric water vapor increase for different eruption magnitudes if directly quantified, i.e. not from the residuum?*
   A direct quantification of increases in the SWV content for tropical eruption magnitudes ranging between 2.5 Tg S to 40 Tg S reveals that, depending on the eruption volume, SWV increases between 0.1 ppmv to 5 ppmv can occur. This is comparable to SWV variations due to the influence of the QBO and tropical SWV background levels in NH summer time.

3. *Which parameters are critical for determining the SWV increase?*
   In order to estimate the SWV originating from the indirect pathway for a given eruption, knowledge of the AOD or eruption volume, time, and location does not suffice, since the aerosol altitude and profile shape also play a critical role.

4. *What is the contribution of the SWV forcing to the overall radiation budget?*
   The tropical stratospherically adjusted forcing due to the additional water vapor counterbalances a maximum of 4 % of the of total aerosol forcing in our experiment setup one year after the eruption. For the 20 Tg S and 40 Tg S scenarios the TOA radiative imbalance even turns positive within the third year after the eruption. The additional SWV forcing may contribute to this positive imbalance. The forcing due to the additional stratospheric water vapor reaches its peak forcing after the volcanic aerosol forcing because the increases in stratospheric moisture are a delayed consequence of the temperature increases caused by volcanic aerosol heating. Since the stratospheric water vapor accumulates over time, and is only slowly transported to the poles, it will also persist after the volcanic aerosol is no longer present in the stratosphere.

5. *Can cold-point temperature warming and SWV forcing be estimated based on eruption magnitude or AOD? Is there an easy approximation for SWV increases?*
   For an accurate prediction the location of the aerosol layer with respect to the tropopause is an additional necessary parameter. For tropical eruptions, with aerosol profiles at similar distance to the tropopause as those described in this work, a power function relationship of the form $aAOD^b + c$ between yearly averaged tropical cold-point warming and adjusted SWV forcing on IR-AOD can be deduced. Based on the water vapor at the cold point in an unperturbed case, a 12 % SWV increase per K increase in cold-point temperature is a good first estimate for eruption strengths up to 40 Tg S. This approximation closely follows the Clausius Clapeyron equation for the saturation water vapor pressure above ice in the cold-point temperature range.

The second set of answers addresses the importance of small-scale processes for moisture transport into the stratosphere and how they are affected by perturbations:

1. *Does the overall dependence of stratospheric water vapor on tropical cold-point temperature change in convection-resolving simulations compared to simulations relying on convective parametrizations?*
   The water vapor at the cold point is a function of the mean cold-point temperatures in the coarse resolution simulations (*MPI-GE historical simulations* and *EVAens*). In the convection-resolving simulations (*CaVE*) the specific humidity is set by the lowest cold-point temperatures which can be approximated by the 10^{th} percentile of inner tropical cold-point temperatures. The convection-resolving simulations are thus in better agreement with observations. The different equivalent frost point temperature arise due to increased variability in the calculated cold-point temperatures originating from a better representation of convective overshoots, higher spatial resolution, and better resolved cirrus cloud fields.

2. *What is the relative importance of water vapor versus frozen hydrometeors for the TTL moisture fluxes?*
   In the global convection-resolving simulations the water vapor flux amounts to around 80 % of the moisture entering the stratosphere, while frozen hydrometeors contribute 20 %. These values lie within the range reported in the literature for trajectory studies.

3. *How do the respective moisture fluxes and their relative partitioning change under external forcing such as volcanic aerosol heating?*
   Both the upward fluxes of water vapor and frozen hydrometeors into the tropical stratosphere exhibit increases due to the heating in the TTL. The partitioning of the fluxes into the frozen and non-frozen moisture states however remains constant, indicating a Clausius Clapeyron scaling both for the vapor and frozen moisture fluxes.

4. *Do the individual contributions to frozen moisture fluxes and their relative importance change under volcanic aerosol forcing and if so why?*
   Considering the strong perturbation in the TTL, the relative importance of overshooting convection, in-cloud upwelling and turbulent mixing is relatively well

conserved. Overshooting convection transports most of the moisture, followed by in-cloud upwelling and turbulent mixing. The importance of in-cloud upwelling is slightly enhanced and the importance of subsidence slightly extenuated in the perturbed scenario. Additionally, the increase in TTL temperatures favours sedimentation of snow in the low velocity range.

a) *What are the changes in overshooting convection?*
Different factors controlling the amount of overshooting convection are impacted in Perturbed: The equivalent potential temperature at the surface, $\theta_{e,surf}$, is reduced compared to the reference simulation and the stability in the tropopause region is increased. However, the number of levels of neutral buoyancy above the cold-point tropopause increases slightly, exhibiting a constant or slightly increased potential for CP overshooting events. The distribution of frozen hydrometeors in moisture space confirms that the increased frozen moisture flux is located in the areas of deep convection. An investigation of the distribution of the moisture flux binned according vertical velocities at the cold point backs up this finding. This demonstrates that the convection still influences the setting of the tropopause height and with it its moisture budget. Higher temperatures in the TTL might lead to a larger amount of frozen moisture created per Kelvin decrease in temperature, potentially leading convective events injecting more frozen mass per convective overshoot.

b) *What are the changes in in-cloud upwelling?*
Although the dominant fraction of mass is transported in the low velocity range an investigation of the mass flux distribution on vertical velocities demonstrates in-cloud upwelling can not compensate the sedimenting cloud ice. The net mass transport in the velocity range for in-cloud upwellng of [-4,4] mm s^{-1} is negative. In the perturbed simulation in-cloud upwelling is enhanced whereas subsidence is reduced. In-cloud upwelling increases in relative importance compared to Control.

c) *What are the changes in turbulent mixing?*
The reduced distance between the convective top height and TTL creates steeper humidity gradients in the TTL, which leads to more turbulent mixing into the TTL. As turbulent mixing depends on steep moisture gradients, its contribution decreases from the lapse rate to the cold-point tropopause, where it is of negligible importance.

3.2 FINDINGS IN SCIENTIFIC CONTEXT AND OUTLOOK

First study investigating all moisture pathways to enter the stratosphere in unperturbed conditions and their changes due to volcanic aerosol perturbations.

This work investigated moisture pathways into the TTL and stratosphere along with their potential changes after volcanic eruptions. Both large-scale slowly ascending water vapor and small-scale processes of overshooting convection, in-cloud upwelling, and turbulent mixing were considered. This goes beyond the scope of previous studies which focused solely on the effect of volcanic aerosol heating on the large-scale slowly ascending water vapor (e.g. Angell, 1997, Considine et al., 2001, Joshi and Shine, 2003, Dessler et al., 2014, Löffler et al., 2016, Tao et al., 2019). This work shows that volcanic eruptions lead to an amplification of all stratospheric mois-

ture fluxes originating from the troposphere while the partitioning between frozen and non-frozen moisture sources remains constant. The reasons for the increase are summarized in the overview Fig. 12, which shows the considered moisture pathways and how they are affected by (sulfate aerosol) heating in the TTL.

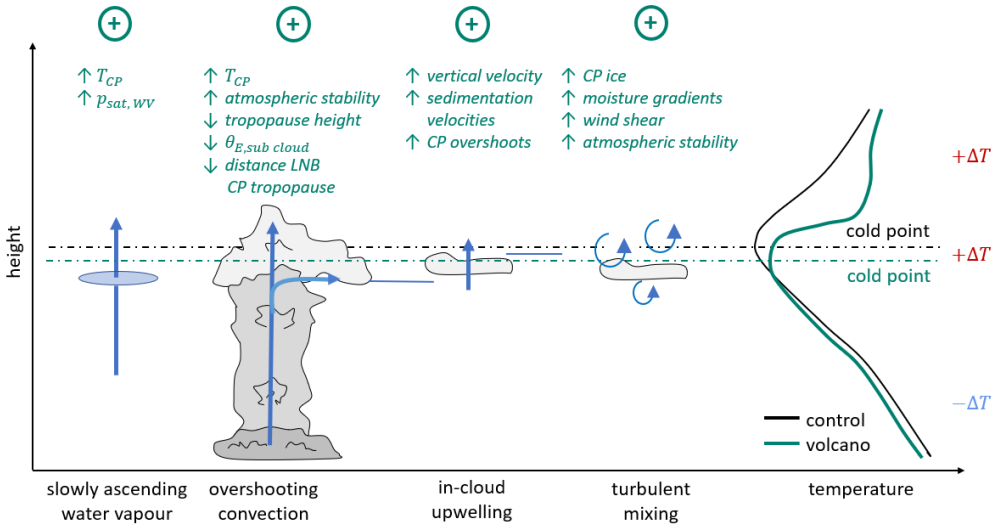

Figure 12: Overview of the different pathways for moisture to enter the TTL and lower stratosphere: slowly ascending water vapor, overshooting convection, in-cloud upwelling and turbulent mixing. The effects of the volcanic aerosol on each process are outlined with green writing. The overall effect is denoted with a plus resp. minus. Typical tropical temperature profiles as a function of height are shown on the right for Control (black) and Perturbed (green). The height of the CP tropopause is indicated with dashed horizontal lines.

Alleviating uncertainties caused by lack of observational data.

Observational data showing the volcanic impact on SWV is extremely scarce. Consequently, it was difficult to estimate which critical eruption magnitude first has a significant impact on SWV content, what the radiative consequences of the SWV increases are, and if there is a way to predict these effects. With my work I alleviate uncertainties caused by the current scarcity of observational data by analyzing an ensemble of realizations for various eruption magnitudes with varying background conditions at the eruption time. My first study, which focuses on the large-scale slowly ascending water vapor, offers a general model-based analysis on the changes in stratospheric water vapor after tropical volcanic eruptions of different magnitudes. The chosen approach of large ensemble simulations offers two main advantages over preexisting case studies.

Discriminating between effects of the volcanic aerosol heating and coincidental background conditions.

First, realisations with coincidentally strong background conditions, which dominate the stratospheric water vapor or counteract the effect of the volcanic forcing are equalized by other ensemble realisations. With the ensemble approach, a clear SWV signal for an eruption with an aerosol amount corresponding to the Mt. Pinatubo eruption could be found. Additionally, the spread in different initial background conditions allowed me to identify the first eruption magnitude creating an SWV signal which is easily detectable above background variability.

Providing a tool set to estimate SWV changes after similar tropical eruptions.

The second advantage of my model approach is that it offers the possibility to deduce and verify methods to estimate the impact of volcanic aerosol heating on pa-

rameters controlling the SWV entry and the corresponding forcing consequences. I have established a simple framework to estimate the changes in cold-point temperature, SWV levels, and SWV forcing for tropical eruptions between 2.5 Tg S and 40 Tg S with aerosol profile located at similar proximity to the tropopause as in my simulations. The resulting tool set, unlike other studies of individual past events, allows one to quickly perform a first situation assessment for future eruptions.

The importance of SWV induced forcing modifications.

My analysis shows that the tropical SWV forcing originating from the indirect pathway is of secondary importance compared with the aerosol forcing. Despite this I postulate that the changes in forcing due to SWV changes should be further investigated for three main reasons. First, as my analysis focuses solely on the indirect SWV entry while neglecting the direct SWV injection, it is a low estimate of the forcing. Second, the SWV forcing is higher in the polar region (e.g. Forster and Shine, 2002). The effect of the stronger forcing is amplified by the delayed transport of SWV to the polar regions in a time frame in which the influence of volcanic aerosol is already ceasing. This is also evident in my simulations, where the larger eruptions showed a positive TOA radiative imbalance in the third eruption year. Third, apart from the direct forcing effect, the additional water vapor will also impact stratospheric aerosol formation (i.e. LeGrande et al., 2016) and ozone chemistry (i.e. Tian et al., 2009, Rosenlof, 2018), indirectly modifying the forcing. This is especially important in the case of directly injected water vapor as it has an immediate effect on the aerosol formation process. For example, the handling of OH chemistry was identified to be responsible for some of the inter-model deviations in the VolMIP project (Clyne et al., 2021).

New suggestions of how to improve the method of prescribing aerosols.

I showed that the height of the aerosol profile with respect to the tropopause is critical for a realistic representation of the SWV increases after volcanic eruptions. This finding is also relevant for model intercomparison projects. The conventional approach to integrate the optical properties of volcanic aerosol in models is to import files with the aerosol characteristics set to a fixed height or pressure coordinates and not relative to the tropopause height. However, since the tropopause height varies within CMIP5 and CMIP6 models by up to 23 hPa (Wu and Reichler, 2020, Kim et al., 2013), this procedure can substantially alter results as the aerosol is introduced in physically different atmospheric regions. Based on my work, I therefore suggest to report the actual distance of peak extinction from the CP tropopause in order to improve comparability between models and yield a more realistic representation of the SWV changes caused by the volcanic eruption. Additionally, I propose to consider the short aerosol lifetime of days to weeks in the troposphere in *EVAens*. Currently, the *EVAens* aerosol layer extends far into the troposphere, leading to unphysical heating.

First convection-resolving study for moisture fluxes in the TTL under perturbations.

In my second project, I presented the first sensitivity study of TTL moisture fluxes to external forcing in a global convection-resolving model. The resolution of 10 km may be categorized by some high-resolution modelers as lying in the so-called "grey zone". For my specific research question however it is adequate because it represents deep convection realistically in ICON (Hohenegger et al., 2020). The paradigm to prefer parameterizations over resolved convection at resolutions coarser than 5 km has been shown not to be justified, as convection-resolving simulations perform equally or better at resolutions as coarse as 25 km (Vergara-Temprado et al., 2020). Increased resolution can still be employed after gaining first understanding, if needed.

Reliability of found constant partitioning.

I showed that both the control and the perturbed simulation exhibit a 80:20 partitioning of non-frozen and frozen moisture fluxes into the stratosphere. In perturbed the fluxes are only increased in absolute magnitude. While the percentage share might be model specific and requires further observational constraint, the constant partitioning can also be found in observational studies for different seasons (Liu et al., 2010, Fueglistaler et al., 2013) and a trajectory study for climate change scenarios (Smith et al., 2022), which increases the confidence in the result.

Relevance of constant partitioning: easy description of total moisture flux based on CC-scaling.

The constant partitioning found in my study is relevant for two reasons. First, as detailed in Section 2.2, the constant partitioning allows for a description of both the frozen and non-frozen moisture flux depending on the large scale temperature field. The non-frozen flux is given by the Clausius Clapeyron scaling based on the equivalent frost point temperature of the inner tropical TTL, whereas the frozen moisture flux is described by an additional ΔT offset determined by the 80:20 partitioning ratio and the slope of the Clausius Clapeyron curve. As the contribution of frozen moisture fluxes is considerably uncertain in the stratospheric moisture budget and challenging to determine accurately, this flux calculation substantially simplifies estimating potential changes in stratospheric moisture. In addition, my finding may be used to improve upon the parametrization of convective overshoots in general circulation models – if the parametrizations are able to capture the cold-point temperatures and their changes correctly. This constraint has to be investigated for every model individually as the spread in the current generation of CMIP6 models can be as large as 10 K (Garfinkel et al., 2021).

Relevance of constant partitioning: applicability to other perturbations.

Second, the constant partitioning found here does not seem to be exclusive to volcanic aerosol heating perturbations. It is also consistent with a season independent partitioning in observational based studies (Liu et al., 2010, Fueglistaler et al., 2013) which quantified the frozen moisture contribution from the residuum in their analysis, and a coarse resolution climate change study (Smith et al., 2022), which relied on trajectory tracking while explicitly considering the ice content of their air parcels. My convection-resolving simulations and direct quantification increase the confidence that the constant partitioning is not a product of parametrization biases or methodological approach.

Challenging the common perception of the TTL in volcanic eruption and geoengineering scenarios.

In the final part of my work (see Section 2.3) I am currently investigating the individual pathways for frozen moisture to enter the stratosphere with a special focus on the role of convection. My study showed that convection indeed plays the dominant role in transporting frozen moisture into the stratosphere - also after volcanic perturbations which increase the atmospheric stability in the TTL considerably. This finding challenges the common perception of the TTL after volcanic eruptions or geoengineering efforts. In the volcano and geoengineering community, a reduction of cloud cover (Kuebbeler et al., 2012, Visioni et al., 2018, Saint-Lu et al., 2022) and an increase in atmospheric stability have previously led to the assumption that the frozen moisture flux into the stratosphere is reduced as well. This common assertion is tied to the notion of a TTL which is fixed in height. On the contrary, however, the TTL is formed by the interplay of radiative, dynamical and convective processes and should be never considered as independent of convective influence (Kuang and Bretherton, 2004, Hu et al., 2021). However, under any perturbation, such as radiative heating, a new tropopause height, influenced by convective cooling counterbalancing part of the additional radiative heating, will be set. I could demonstrate that the distance

between LNB and CP tropopause slightly decreases in volcanically perturbed simulations. This suggests an increased or at least constant frequency of CP overshoots. Additionally favouring the frozen moisture transport could be the higher temperatures in the TTL which lead to a larger amount of frozen moisture generation per Kelvin decrease in temperature. This would increase the amount of frozen moisture per CP overshoot. A final analysis of the corresponding temperature and heating rates is currently ongoing.

Increased turbulent mixing in the context of measurement uncertainties.

The role of turbulent mixing for the stratospheric moisture budget is debated (e.g. Konopka et al., 2007, Podglajen et al., 2017, Bardeen et al., 2013, Pithan, 2014). In my simulations, these processes do not play a major role for the stratospheric moisture budget. However, during the model setup and analysis, I found a huge dependency of the turbulent mixing fluxes on the tuning parameters of the model. This problem is not exclusive to the TTE scheme in ICON. In the literature, there is considerable disagreement on the importance of turbulent mixing, spanning everywhere between less important than the mean tropical upwelling (Podglajen et al., 2017) to being the main transport mechanism from the convective outskirts to the lower branch of the BDC (Konopka et al., 2007). This is especially problematic as turbulent mixing in the TTL is not well constrained by observations (Wilson, 2004). As is, my unperturbed simulations capture the water vapor and cloud ice distribution as found in ERA5.1 reanalysis data, which increases the confidence in my results. However, considering the disagreement between individual studies, additional measurements of diffusivities would enhance our understanding of the importance of turbulent mixing and would help to optimize the description in models.

My estimate: indirect pathway more important than direct injection.

My thesis focused on the indirect pathway for moisture to enter the stratosphere after volcanic eruptions. As detailed in the introduction, water vapor may also be directly injected into the stratosphere from within the volcanic plume. To estimate the relative importance of both processes, I will compare the SWV increase due to Hunga Tonga, the strongest direct injection event recorded so far, with the SWV originating from the indirect pathway for a volcanic eruption causing an equivalent frost point temperature warming for the inner tropical CP region of 1 K. This 1 K warming would be smaller than the cold-point warming corresponding to the 10 Tg S eruption scenario (Kroll et al., 2021, Figure 16). Around 900 Tg of water vapor enters the stratosphere yearly from below (Sioris et al., 2016a). An increase of the equivalent frost point temperature of 1K and a 12 % per Kelvin increase in specific humidity (Kroll et al., 2021) would yield around 1008 Tg of water vapor. Taking into account that the partitioning between water vapor and frozen moisture is 80:20, this will result in a total moisture flux increase of 135 Tg, in the first year alone. This amount of water vapor injected indirectly is comparable to the Hunga Tonga values of 50 Tg (Vömel et al., 2022) to 146 Tg of water vapor (Millán et al., 2022). However, unlike the direct injection, the indirect pathway will be open for around 2.5 years and most direct injections are much weaker than the Hunga Tonga. I would therefore estimate the indirect injection to be more important than the direct one - if the volcano is not undersea, the aerosol reaches the stratosphere, and the cold point warming reaches values of and over 1 K.

3.3 FINAL REMARKS

In this work the sensitivity of moisture fluxes in the TTL to (volcanic aerosol) heating was investigated. All indirect pathways from large-scale slowly ascending water vapor to small-scale processes of overshooting convection, in-cloud upwelling, and turbulent mixing were investigated, finding an increase in the overall moisture transport. The study also showed once again that perturbing the earth system is a reliable method to gain insight into governing processes, which may promote our general understanding of the climate system.

Part II

APPENDIX

A

THE IMPACT OF VOLCANIC ERUPTIONS OF DIFFERENT MAGNITUDE ON STRATOSPHERIC WATER VAPOR IN THE TROPICS

The work in this appendix has been published as:

Kroll, C. A., Dacie, S., Azoulay, A., Schmidt, H., and Timmreck, C.: The impact of volcanic eruptions of different magnitude on stratospheric water vapor in the tropics, Atmos. Chem. Phys., 21, 6565–6591, https://doi.org/10.5194/acp-21-6565-2021, 2021.

The Impact of Volcanic Eruptions of Different Magnitude on Stratospheric Water Vapour in the Tropics

Clarissa Alicia Kroll[1,2], Sally Dacie[1,2], Alon Azoulay[1,3], Hauke Schmidt[1], Claudia Timmreck[1]

[1]Max Planck Institute for Meteorology, Hamburg, Germany
[2]International Max Planck Research School on Earth System Modelling (IMPRS-ESM), Hamburg, Germany
[3]now at: Remote Sensing Technology Institute (IMF), German Aerospace Center (DLR), Oberpfaffenhofen, Germany

ABSTRACT

Increasing the temperature of the tropical cold point region through heating by volcanic aerosol results in increases in the entry value of stratospheric water vapour (SWV) and subsequent changes in the atmospheric energy budget. We analyze tropical volcanic eruptions of different strengths with sulfur (S) injections ranging from 2.5 Tg S up to 40 Tg S using EVAens, the 100-member ensemble of the Max Planck Institute - Earth System Model in its low resolution configuration (MPI-ESM-LR) with artificial volcanic forcing generated by the Easy Volcanic Aerosol (EVA) tool. Significant increases in SWV are found for the mean over all ensemble members from 2.5 Tg S onward ranging between [5,160] %. However, for single ensemble members the standard deviation between the control run members (0 Tg S) is larger than SWV increase of single ensemble members for the eruption strengths up to 20 Tg S. A historical simulation using observation based forcing files of the Mt. Pinatubo eruption, which was estimated to have emitted (7.5 ± 2.5) Tg S, returns SWV increases slightly higher than the 10 Tg S EVAens simulations due to differences in the aerosol profile shape. An additional amplification of the tape recorder signal is also apparent, which is not present in the 10 Tg S run. These differences underline that it is not only the eruption volume, but also the aerosol layer shape and location with respect to the cold point that have to be considered for post-eruption SWV increases. The additional tropical clear sky SWV forcing for the different eruption strengths amounts to [0.02, 0.65] W m^{-2}, ranging between [2.5, 4] percent of the aerosol radiative forcing in the 10 Tg S scenario. The monthly cold point temperature increases leading to the SWV increase are not linear with respect to AOD nor is the corresponding SWV forcing, among others, due to hysteresis effects, seasonal dependencies, aerosol profile heights, and feedbacks. However, knowledge of the cold point temperature increase allows for an estimation of SWV increases of 12 % per Kelvin increase in mean cold point temperature. For yearly averages power functions are fitted to the cold point warming and SWV forcing with increasing AOD.

A.1 INTRODUCTION

It has been established that the entry of water vapour into the stratosphere is largely controlled by the temperature of the tropical tropopause (e.g, Brewer, 1949; Mote

et al., 1996; Fueglistaler et al., 2009; Dessler et al., 2014). Following up on the discussion of the long term increasing trend in stratospheric water vapor (SWV) observed during the 1980s and 1990s it was proposed that volcanic eruptions could be influencing the SWV budget (e.g, Rosenlof et al., 2001; Joshi and Shine, 2003). Mainly two processes are considered: the direct volcanic injection from the volcanic plume, and an indirect volcanic mechanism due to an increase of the tropopause temperature, referred to hereafter as the indirect volcanic pathway. The increased SWV levels may remain in the stratosphere for more than 5 years (Hall and Waugh, 1997), even though the volcanic aerosol sediments out of the stratosphere within 1 - 3 years (Robock, 2000). However, the magnitude of the SWV increase and the contribution from the different entry mechanisms are still unclear.

80 % of the eruption material is water vapour (Coffey, 1996), which could be directly injected into the stratosphere during an eruption event. But although the SWV originating form the direct injection can be detected shortly after the eruption event, it is a singular event. The corresponding elevated SWV levels are spread in the stratosphere and are not distinguishable from the background SWV anymore. Satellite evidence for the direct injection events exist. It is discussed briefly by Schwartz et al. (Schwartz et al. (2013)) and in depth by Sioris et al. (Sioris et al. (2016a), Sioris et al. (2016b)). Based on a model study Joshi and Jones, 2009, hypothesized that the environment surrounding the plume can also have a significant impact on the amount of SWV injected directly.

This study will focus on the indirect volcanic entry mechanism. In contrast to the direct entry, it can act for months or even years after volcanic eruptions since it depends on the heating caused by the aerosol layer in the stratosphere and not on the eruption event itself. This indirect volcanic entry is caused by the terrestrial long wave and near IR solar heating by the volcanic aerosol layer which leads to increased cold point temperatures. Consequently, the saturation water vapour pressure at the cold point is increased, thereby reducing the loss of WV due to ice formation and fallout. This mechanism enhances the entry of WV into the stratosphere.
In an early, idealized study, Joshi and Shine (2003), underlined the importance of the aerosol profile and corresponding heating in the tropopause region. Despite the mechanisms being known, its analysis is still complicated as internal variability and scarcity of observations has made it difficult to observe it in practice. Additionally, even if SWV increases are recorded, the data usage might be discouraged, as was the case for Mt. Pinatubo by SAGE II because discrepancies between different satellites could not be satisfactory explained (Fueglistaler et al., 2013).
The scarcity of observational data is also reflected in the quality of the available reanalysis products for SWV, the usage of which in general is discouraged in some papers (e.g, Davis et al., 2017) and which sometimes do not implicitly account for the volcanic forcing at all (Diallo et al. (2017), Tao et al. (2019)). The latter problem was also indicated by Löffler et al. (2016) when discussing SWV increases simulated for the eruption of Mt. Pinatubo. Nevertheless, by performing a regression analysis using a trajectory model fed by reanalysis data, Dessler et al. (2014) identified a SWV peak partially overlapping with the aerosol optical depth (AOD) signal of Mt. Pinatubo. As the SWV increase occurred before the eruption and AOD increase,

the question remained if the peak in the residual might instead be caused by another source of variability. Another possible issue in their analysis is that some of the effects modeled by the regressors are themselves influenced by volcanic eruptions, which may lead to the volcanic signal being attributed to a different source. An example are the increases of the Brewer Dobson circulation (BDC), which, in the case of a volcanic eruption, can be partially caused by the heating due to the aerosol layer. Tao et al. (2019) also undertook an indirect quantification of the SWV increase after volcanic eruptions via another regression analysis, explicitly accounting for volcanic source terms. They found a clear volcanic signal in the expected time frame, but the magnitude of the SWV increase differed strongly between the individual reanalysis data sources.

After entering the stratosphere, the additional SWV affects both stratospheric chemistry with respect to ozone loss (Robrecht et al. (2019), Rosenlof (2018), Tian et al. (2009)) and SO_2 oxidation (Bekki (1995), LeGrande et al. (2016)), as well as the radiative budget of the entire atmosphere (Solomon et al., 2010). Despite the forcing originating from the additional SWV often being mentioned as a motivation for studies, few studies exist on the forcing effect of the SWV increase after volcanic eruptions. Independent of volcanic eruptions, Forster and Shine (2002) analysed the forcing impact of SWV changes in an artificial SWV profile. In a study focusing on the Mt. Pinatubo eruption, Joshi and Shine (2003) calculated the additional global forcing originating from the post eruption SWV increase. As this was a side study of their paper, they did not investigate the temporal evolution nor the impact of different eruption strengths. In a study on the direct injection, Joshi and Jones (2009) quantified the long wave component of the SWV forcing indirectly, but their setup did not allow for a quantification of the additional contribution of the indirect volcanic pathway. Most recently Krishnamohan et al. (2019) attributed changes in their TOA imbalances for different geoengineering scenarios to a large influence of SWV. However, they did not separate the contributions of aerosol forcing and SWV.

So far, the questions remain open what the critical magnitude is for an eruption to have a significant impact on SWV content, what the radiative consequences of the SWV increase are, and if these effects can be predicted based on eruption magnitude or AOD. In this study we therefore investigate the changes in stratospheric water vapour originating from the indirect volcanic pathway using a large ensemble of coupled climate model simulations with 100 ensemble members each for five eruption strengths described by changing amount of stratospheric sulfur and a control run, called the EVAens (Azoulay et al., 2020). The idealized setup using forcing files generated with the Easy Volcanic Aerosol tool (EVA) offers the unique opportunity of a direct comparison between the different eruption strengths, since the date and location of the eruptions are identical and all ensembles have the same set of starting conditions. By comparing with the control run a direct quantification of the SWV increase is possible. The large ensemble size allows us to perform an analysis of the sensitivity of the increase in stratospheric water vapour to the eruption strength along with its statistical significance. The critical eruption strengths that cause stratospheric water vapour perturbations beyond the internal variability of the model are identified when analyzing the individual ensemble members.

A.2 METHODS

A.2.1 *The EVAens ensemble and the GE historical simulations*

This study is based on large ensemble simulations covering the time frame of January 1991 to December 1993 using two different volcanic forcing data sets: the EVAens (Azoulay et al., 2020) and a subset of the Max Planck Institute Grand Ensemble (MPI-GE) historical simulations (Maher et al., 2019).
Both ensemble simulations are performed with the Max Planck Institute - Earth System Model in its low resolution configuration (MPI-ESM-LR) (version, MPI-ESM 1.1.00p2). We apply an intermediate model version between the CMIP5 version (Giorgetta et al., 2013) and the CMIP6 version (Mauritsen et al. (2019)) of the MPI-ESM, with a behaviour closer to the CMIP6 version. The MPI-ESM itself is a coupled model including the atmosphere component ECHAM (version echam-6.3.01p3, Stevens et al. (2013)), the land component JSBACH (version jsbach-3.00, Reick et al. (2013), Schneck et al. (2013)), the ocean component MPIOM (version mpiom-1.6.1p1, Marsland et al. (2003), Jungclaus et al. (2013)), and the biogeochemistry component HAMOCC (HAMOCC5.2, Ilyina et al. (2013)).
In the model setup the atmosphere is run in a T63L47 configuration corresponding to a horizontal resolution of about 1.9 ° with 47 pressure levels up to 0.01 hPa. The influence of the sponge layer in the uppermost model layer reaches down to a height of 65 km with continuously decreasing impact. As the MPI-ESM-LR does not include interactive atmospheric chemistry or aerosol, the volcanic aerosol is prescribed by the monthly zonal mean values of their optical properties - the extinction, single scattering albedo, and asymmetry factor - in 16 long wave and 14 short wave bands. During the simulation these monthly aerosol properties are interpolated linearly in time.
In the MPI-GE historical simulations the optical properties of the volcanic aerosol are prescribed with an updated version of the PADS data set (Stenchikov et al. (1998), Driscoll et al. (2012), Schmidt et al. (2013)). The Mt. Pinatubo eruption in June 1991 lies in the investigated time frame.

In the EVAens the setup of the MPI-GE historical simulations was kept, changing only the stratospheric aerosol representation. The respective forcing files were generated using the Easy Volcanic Aerosol (EVA) forcing generator (Toohey et al., 2016). Six 100 member ensembles were created: A control run with zero sulfur emission only using the EVA background aerosol and five volcanic eruption runs (2.5 Tg S, 5 Tg S, 10 Tg S, 20 Tg S, 40 Tg S) with both the EVA background aerosol and a volcanic eruptions occurring in June 1991 at the equator, each with 100 ensemble members. Every ensemble member was started from one of the different and independent runs of the MPI-GE historical simulations in 1991 (Maher et al. (2019)). Beside the volcanic aerosol, the forcing files include an aerosol background for the industrialized period supplied by EVA.

The aerosol optical depths (AOD) for the five different eruption strengths of the EVA forcing along with the PADS Mt. Pinatubo forcing are shown in Fig. 43 for the 550 nm waveband. All EVA aerosol distributions have very similar patterns, but differ in magnitude and duration of elevated AOD levels. Whereas the 2.5 Tg S run

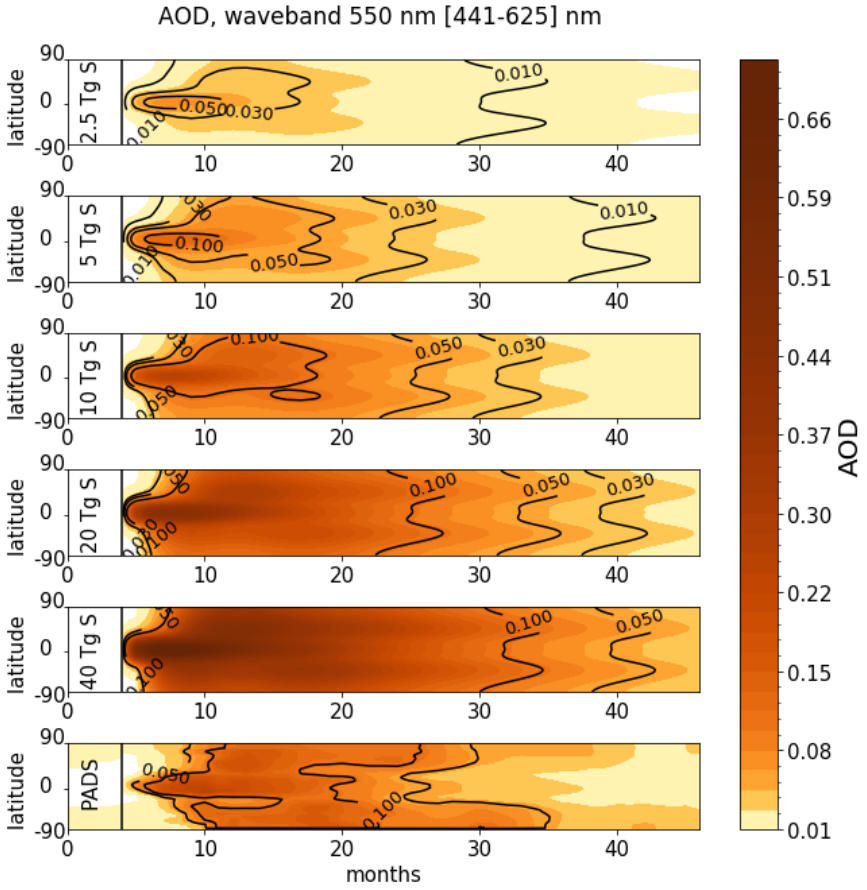

Figure 13: Time evolution of the aerosol optical depth (AOD) for the five volcanically perturbed EVAens runs (2.5 Tg S, 5 Tg S, 10 Tg S, 20 Tg S and 40 Tg S) and the PADS Mt. Pinatubo compilation. The zonal average AOD is shown for all latitudes considering the 550 nm waveband (441 nm - 625 nm).)

returns close to background conditions within 3.5 years after the eruption, the 40 Tg S run only declines to the peak values of the 2.5 Tg S run within this time.

The PADS data set has a higher background AOD level than the EVA data sets in the months before the eruption. With a sulfur amount of (7.5 $\pm$ 2.5) Tg (Timmreck et al., 2018) the Mt. Pinatubo AOD should be comparable to the 5 Tg and 10 Tg EVA data set (compare Table 4). Generally, the AOD in the PADS data set does not spread as fast to higher latitudes after the eruption. Additionally, the AOD values tend to be slightly higher than the values for the 10 Tg EVA data set and persist longer at elevated levels.

As we merely prescribe the aerosol, only the indirect volcanic pathway, which includes cold point warming and overshooting convection, and not the direct injection or aerosol chemistry is simulated in the EVAens.
In the following work all anomalies will be defined as the value difference between the volcanically perturbed (P) and unperturbed 0 Tg S (U) ensemble means (P-U).

Table 4: List of tropical volcanic eruptions with location, eruption date, and estimated amount of emitted sulfur. The sulfur amounts in parentheses represent the best estimates.

Mt Agung	8 °S, 115 °E	17 Mar 1963	2.5-5 (3.5)	Timmreck et al., 2018 and therein
El Chichón	17 °N, 93 °W	4 Apr 1982	2.5-5 (3.5)	Timmreck et al., 2018 and therein
Mt Pinatubo	15 °N, 120 °E	15 Jun 1991	5-10 (7)	Timmreck et al., 2018 and therein
Tambora	8 °S, 117 °E	April 1815	15-40 (30)	Marshall et al., 2018 and therein

A.2.2 *Stratospherically adjusted clear sky forcing calculations*

The stratospherically adjusted clear sky radiative forcing, as defined by Hansen et al. (2005), originating from the increase of stratospheric water vapour due to the indirect volcanic pathway (i.e. via tropopause warming by the aerosol layer), is calculated using the 1D radiative convective equilibrium (RCE) model konrad (Kluft et al., 2019, Dacie et al. (2019)). Konrad is designed to represent the tropical atmosphere. It uses the Rapid Radiative Transfer Model for GCMs (RRTMG) and a simple convective adjustment that fixes tropospheric temperatures up to the convective top according to a moist adiabat, whereas the temperatures in the higher atmospheric levels are determined by radiative-dynamical equilibrium. Being a 1D model, konrad employs a highly parameterized "circulation", i.e. an upwelling term constant in time which only causes adiabatic cooling. As the temperature above the convective top can adjust, this does not mean that the dynamical heating is fixed (compare Fels et al. (1980)).
In order to calculate the stratospherically adjusted SWV forcing, the following procedure is employed: For each eruption strength, including the 0 Tg S eruption, the ensemble mean of the clear sky humidity profile in the tropical region [-5,5]° latitude is determined from the EVAens output. In order to compute the adjusted radiative forcing due to the increased SWV, the difference between the fluxes in an equilibrated atmosphere with and without the additional SWV must be calculated. To determine the equilibrated reference without additional SWV, konrad is run to equilibrium with the humidity profile and chemical composition of the atmosphere fixed to the values from the 0 Tg S runs. The final surface temperature lies between [298-301] K. Starting from this equilibrium state, only the SWV profile is replaced by the volcanically perturbed EVAens humidity profile and a new equilibrium is calculated while keeping the surface temperature fixed, but allowing for the temperature above the convective top to adjust. Using both equilibrium states, the adjusted SWV forcing is determined from the flux differences at the top of the atmosphere. The corresponding instantaneous forcing as defined by Hansen et al. (2005) is calculated as the difference of tropopause fluxes obtained without running the perturbed atmosphere into equilibrium.

For the all sky case the contribution of clouds is investigated by additionally taking a 20 % fraction of high level clouds between 200 hPa and 300 hPa into consideration, while low levels clouds are considered in the albedo settings.

In order to relate the SWV forcing to the aerosol forcing, the instantaneous aerosol forcing is calculated using a double radiation call in the MPI-ESM. For the double radiation call fluxes are calculated for each time step once using the atmospheric conditions with and without aerosol. The stratospheric background aerosol is corrected for by additionally calculating the forcing for the corresponding 0 Tg S run and subtracting it.

A.3 RESULTS

A.3.1 *Effects on the time evolution of TOA radiative imbalance and surface temperature*

In order to relate the amount of emitted sulfur to its impact on the energy budget of the system, we analyze the top of the atmosphere (TOA) radiative imbalance after the volcanic eruptions as well as changes in surface temperature. The time span of negative global radiative TOA imbalance after the volcanic eruptions, during which more energy leaves the earth-atmosphere system than is taken up lasts between 17 and 28 months (Fig. 14). For the lower emissions (2.5 Tg S - 5 Tg S) the standard error of the negative TOA imbalance permanently overlaps with zero imbalance. Consequently single ensemble members of the 0 Tg S can produce similar signals to these lower emission runs due to internal variability. Overall the TOA imbalance exhibits a roughly linear relationship with respect to the emitted sulfur mass (see Fig. A.6). As a consequence of the negative TOA imbalance the surface temperatures in the volcanically perturbed runs decrease. The range of ensemble mean maximum global temperature decrease for the EVAens is -[0.09, 1.30] K (Fig. 14). As the surface temperature follows the TOA imbalance, the change in surface temperature is also roughly linear with respect to the emitted S mass (Fig. A.6).

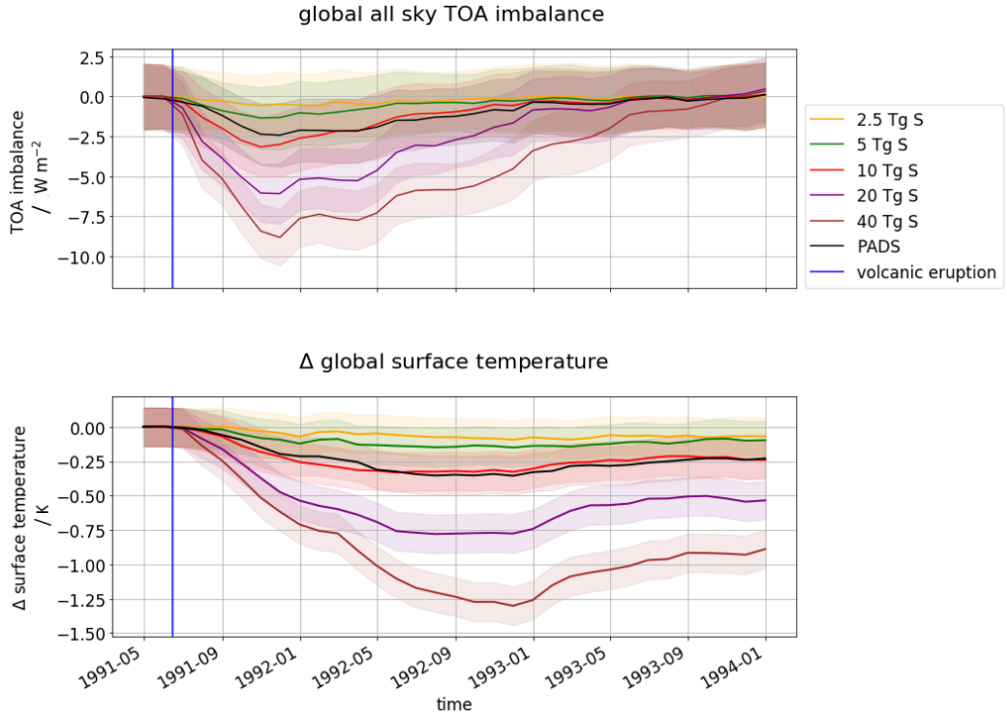

Figure 14: Global top of the atmosphere (TOA) radiative imbalance and anomaly of surface temperature in the five volcanically perturbed EVAens runs (2.5 Tg S, 5 Tg S, 10 Tg S, 20 Tg S and 40 Tg S). For each run the standard errors of the mean are shown as shading. The vertical blue line marks the eruption time. The plots also show the values for the MPI-GE historical simulations (PADS).

In addition to the EVAens results, the TOA imbalance and global surface temperature changes for the historical Mt Pinatubo eruption are shown in black in Figure 14. The global TOA imbalance, peaking at -2.4 W m^{-2}, compares favourably with the

approximately -3 W m^{-2} from Earth Radiation Budget Satellite observations (Soden et al., 2002) when considering the standard deviations of our ensemble. The average surface cooling between June 1991 and December 1993 is -0.26 K with a maximum cooling of -0.36 K in our simulations, whereas the cooling documented by satellite measurements from the microwave sounding unit (MSU) was -0.3 K between June 1991 and December 1995 after ENSO removal and reached a peak cooling of -0.5 K (Soden et al., 2002).

A.3.2 *Effects on the cold point temperature*

In the following analysis the cold point is estimated as the lowest temperature in the TTL lying on full pressure levels of model output remapped to a vertical spacing of 10 hPa in the tropical tropopause region. The associated errors in average cold point temperature lie below $\pm$ 1.1 K.
The effect of the volcanic forcing on the inner tropical temperature profile is visualized in Fig. 15 showing the EVAens ensemble mean of the temperature profiles three months after the eruption. The month of September was chosen as an example since it lies in the season of relatively large water vapour entry into the stratosphere due to a maximum cold point temperature in boreal autumn and winter. Due to the location of the aerosol peak above the cold point the largest temperature changes occur in the lower stratosphere, with increases up to 24 K in the 40 Tg S ensemble. The cold point warming reaches maximum values of 8 K in the case of the 40 Tg S run. Also visible in the figure is the downwards shift of the cold point with increasing sulfur burden caused by the stratospheric warming. This effect is amplified by tropospheric cooling (compare surface cooling in Fig. 14) due to the back scattering of solar radiation through the volcanic aerosol.

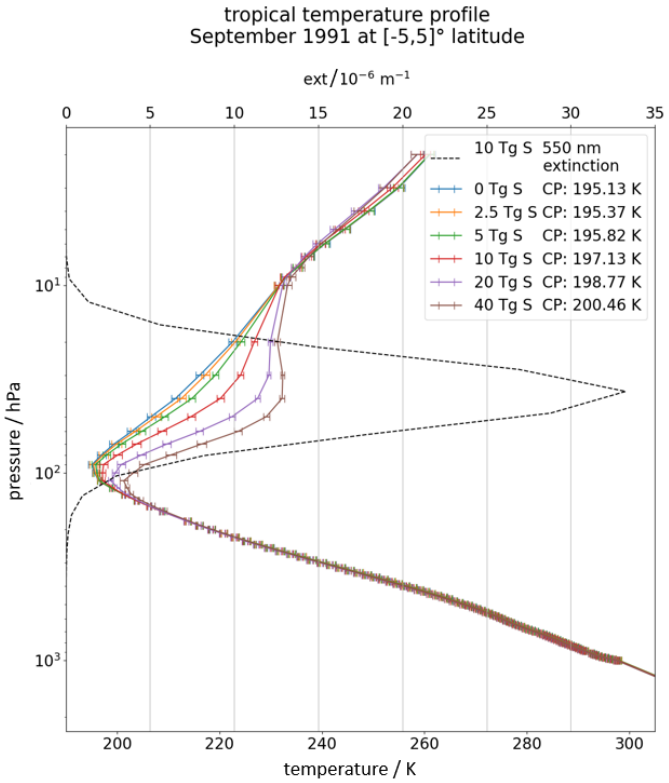

Figure 15: Inner tropical average of the temperature profiles for the five volcanically perturbed EVAens runs (2.5 Tg S, 5 Tg S, 10 Tg S, 20 Tg S and 40 Tg S) in September 1991 (three months after the eruption). The temperature of the respective cold point (CP) is indicated in the legend. The solid line represents the ensemble mean, the error bars symbolize the ensemble standard deviations. The 550 nm extinction values for the 10 Tg S aerosol profile are shown with a dashed black line.

Figure 16 shows the temporal evolution of the surface temperature (a), cold point temperature (b), and 70 hPa water vapour (c) as the difference to to the zero emission run in the inner tropics. Whereas the surface temperature decreases due to the scattering of incoming shortwave radiation by the volcanic aerosol, the cold point temperature increases due to warming of the tropopause layer by absorption of terrestrial long wave and solar near-IR radiation by the aerosol layer.

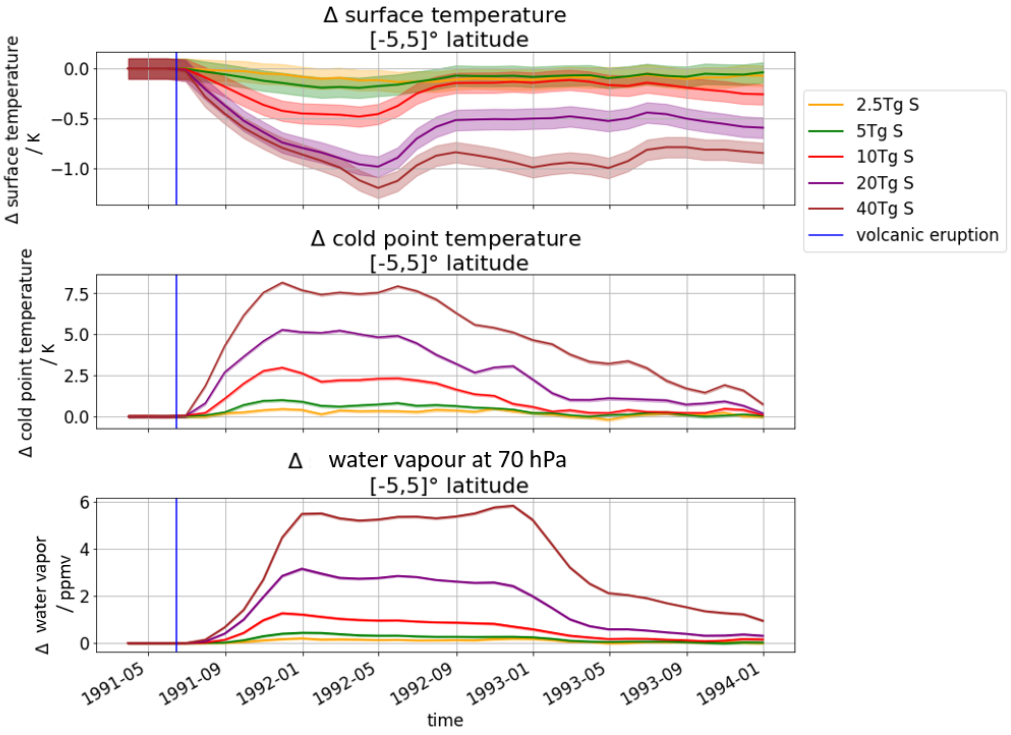

Figure 16: Temporal evolution of the inner tropical mean anomaly in surface temperature, cold point temperature, and stratospheric water vapour between volcanically perturbed and unperturbed ensemble runs. The ensemble means are shown with their standard errors. The time of the volcanic eruption is indicated by a vertical blue line.

When considering the ensemble mean and its standard error even the temperature changes of the low emission runs (2.5 Tg S and 5 Tg S) are significantly different from the control run for short periods of time. With a maximum value of 0.99 K the ensemble mean for the cold point temperature of the 5 Tg S is the lowest sulfur emission to reach a mean warming above the control run standard deviations, which are ten times larger than the standard error for our 100 member ensemble and reach maximum values of 0.73 K. Cold point values below the standard deviation range could be found for single control run ensemble members due to internal variability. The higher emission scenarios (20 Tg S and 40 Tg S) have longer periods with cold point temperature changes above the normally observed internal variability. In addition the 40 Tg S emission group shows a second amplification peak of the yearly cycle of the cold point temperatures between May and September 1992.

The monthly changes in cold point temperature are not linear, neither with respect to emitted sulfur mass nor to AOD in the prominent IR waveband (compare Fig. 30, 31). Additionally the transient behaviour of the volcanic forcing - the build up phase in 1991, the approximately constant forcing in 1992, and the declining phase in 1993, which also differ between the individual eruption sizes - leads to a hysteretic behaviour. Nevertheless, when partitioning the cold point warmings into these individual phases, the dependence of the cold point warming on IR-AOD can be described

with a power function of form $aAOD^b + c$ for the years 1991, 1992 and 1993 (Fig. 17).

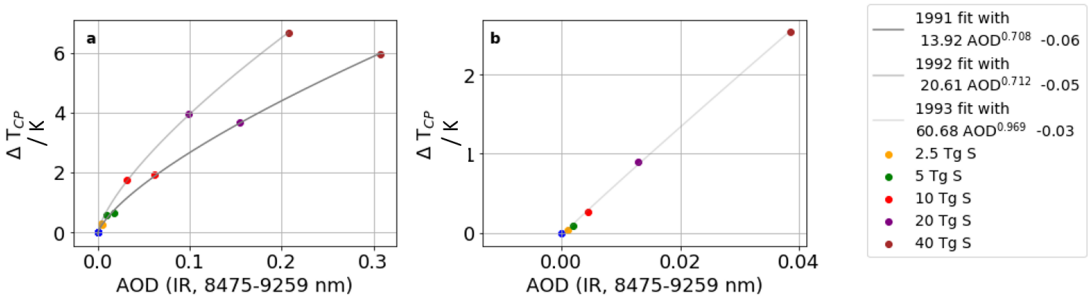

Figure 17: Yearly averages of adjusted tropical cold point temperature increases as a function of tropical AOD (IR, 8475-9259 nm) for the three examined years (1991-1993). A power function fit of form $aAOD^b + c$ for each year with corresponding equation is shown.

The found cold point temperature increases are accompanied by an increase in the saturation water vapour pressure, reducing the "freeze trap" drying in the cold point region. The increased saturation water vapour pressure enables more water vapour to enter the lower stratosphere as shown in Fig. 16 (c). Consequently, the evolution of the additional stratospheric water vapour closely follows the evolution of the cold point temperature changes.

A.3.3 *Effects on the tape recorder signal*

The manifestation of the annual cycle of the tropical SWV as seen in the vertical profile is often described as the tape recorder signal (Mote et al., 1996): The variations of the tropical cold point temperatures controlling the water vapour entry into the stratosphere via the saturation water vapour pressure is imprinted on the stratospheric water vapour as music is imprinted on a tape. This leads to an annual cycle of bands of high and low water vapour content propagating upwards in the stratosphere with the BDC.
As the heating by the volcanic aerosol will lead to increased tropical cold point temperatures, an increase of stratospheric water vapour is expected after volcanic eruptions with stratospheric aerosol. As shown in Sect. A.3.2 the water vapour shows an enhancement which does not stay constant and then declines but has an annual cycle like the tape recorder. In the following section we will investigate the seasonal cycle more closely.
Figure 18 and 19 show absolute SWV and the differences in the SWV content above 140 hPa with respect to the control run for all five eruption strengths. The maximum increases are found in the eruption year itself ranging from 0.1 ppmv for the 2.5 Tg S eruption to more than 5 ppmv for the 40 Tg S eruption. This corresponds to 5 %, respectively 160 %, of the unperturbed SWV values (see Fig. 34). The larger the eruption, the earlier the increase becomes visible and is significant. The additional SWV also follows the annual cycle of the tape recorder (Mote et al., 1996), showing maxima in the SWV enhancement around September which then propagate upwards. This seasonal variation is also apparent in the behaviour of the tropopause and cold

point heights: for scenarios with at least 10 Tg S onward the tropopause pressures and cold point pressures are higher in the northern hemispheric autumn; whereas in the 20 Tg S and 40 Tg S runs the volcanic forcing leads to higher pressure levels of the cold point from September 1991 until the end of 1992 accompanied by a seasonal signal in the SWV anomalies. Allowing for more water vapour to transit to the lower stratosphere.
In the 40 Tg S ensemble mean the second seasonal cycle is associated with an upward propagation of the SWV increases above 4 ppmv to even lower atmospheric pressures than in the preceding year. This behaviour can be attributed to the persistence of the high levels of aerosol in combination with the already enhanced SWV levels due to the presence of the aerosol in the previous year, the additional warming caused by the SWV and the lower lying cold point.
Shortly after the eruption a decrease in water vapour content above 50 hPa is visible. At these altitudes SWV increases with height due to its production by methane oxidation, which is parameterized in the MPI-ESM (Schmidt et al., 2013). Heating in the aerosol layer below leads to lofting of air parcels, bringing lower humidity air upwards to higher altitudes, where it causes a net reduction in humidity. However, this effect never exceeds 0.8 ppmv and is offset as soon as the lifted air becomes more moist due to enhanced SWV entry through the tropopause region.

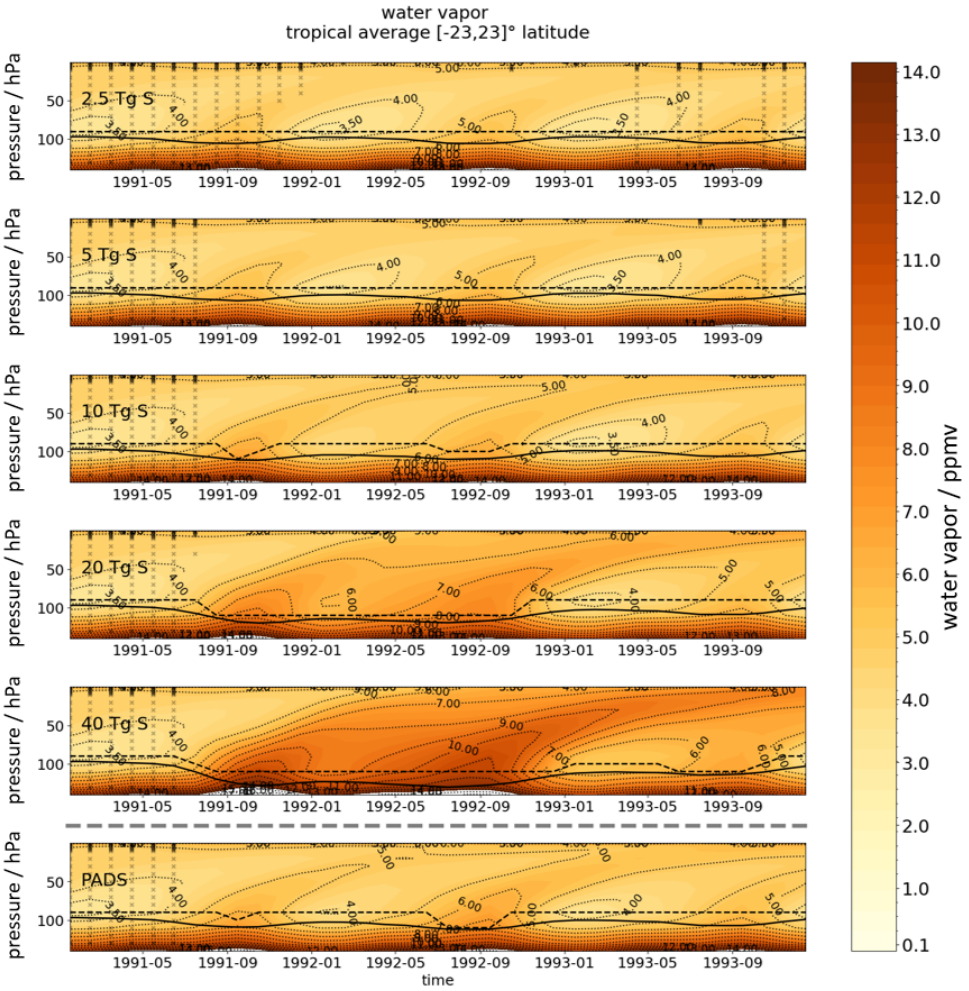

Figure 18: Tropical average in [-23,23]° latitude of WV above 140 hPa for sulfur injections of 2.5 Tg S, 5 Tg S, 10 Tg S, 20 Tg S and 40 Tg S as well as the PADS dataset. The WMO-tropopause pressure is indicated by a black line and the cold point pressure is shown as black dashed line. Absolute values are shown. In regions not covered by black crosses statistical significant difference between water vapour values of the perturbed and unperturbed runs (t-test at p=0.05) were found.

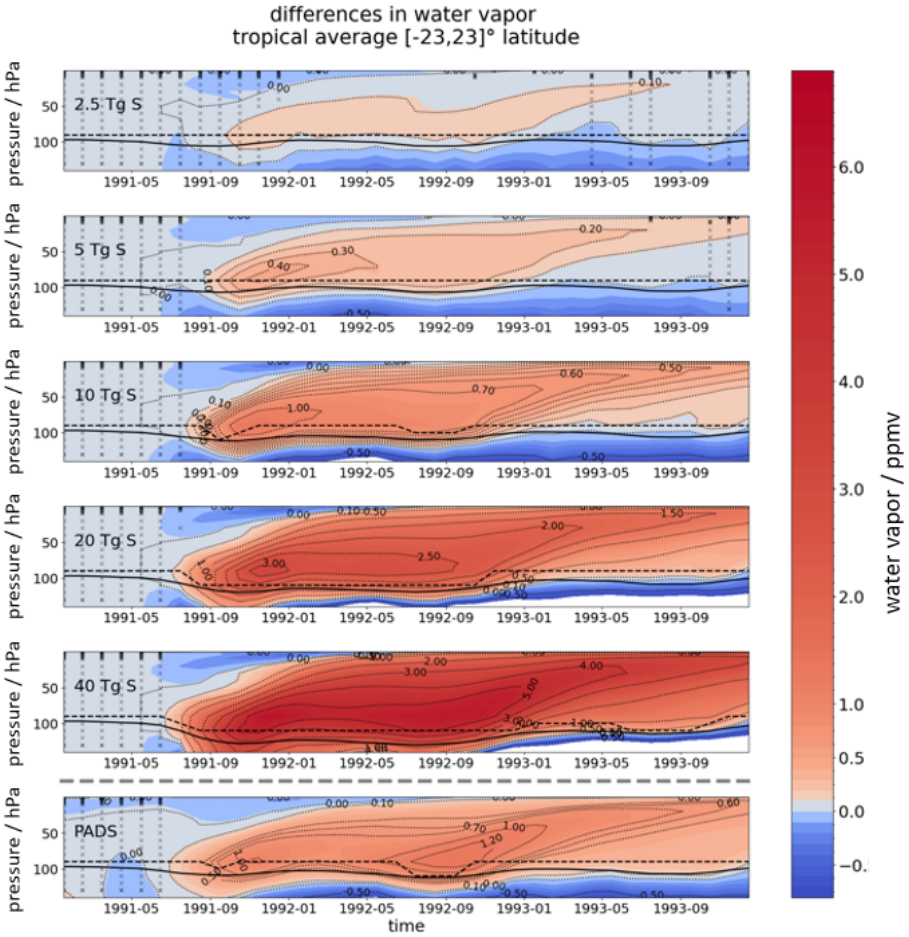

Figure 19: Tropical average in [-23,23]° latitude of WV anomalies above 140 hPa for the sulfur injections of 2.5 Tg S, 5 Tg S, 10 Tg S, 20 Tg S and 40 Tg S as well as the PADS dataset. The lowermost panel shows the MPI-GE historical simulations for Mt. Pinatubo using the PADS forcing data set discussed in Sect. A.3.5. The WMO-tropopause pressure is indicated by a black line and the cold point pressure is shown as black dashed line. Differences with respect to the 0 Tg S control run are shown. In regions not covered by black crosses statistical significant difference between water vapour values of the perturbed and unperturbed runs (t-test at p=0.05) were found.

A.3.4 *Intra-ensemble variability*

The investigation of single ensemble members is of interest because - unlike for the ensemble mean - their physical characteristics would actually be "observable". Figure 20 shows seasonal averages of the water vapour at the cold point as a function of cold point temperature for the inner tropical average in 1991 and 1992. The season SON was chosen, as it follows the period where the entry value of stratospheric water vapor is highest, leading to the highest SWV in the tropical lower stratosphere. Each point in Fig. 20 symbolizes one single ensemble member. Orange crosses show the theoretically possible maximum water vapour curve calculated as the saturation humidity for water vapour over ice at the average cold point temperature, using the corresponding exact solution for the Clausius Clapeyron equation by Murphy and Koop (2005)[1]. An approximation for the Clausius Clapeyron Equation at this temperature range with a 12 % increase of water vapour per K is shown with a dashed grey line. This approximation is based on the assumption that the atmosphere around the cold point is saturated in the 0 Tg S run. The single ensemble members follow the slopes and values of the calculated water vapour amount at saturation in the inner tropics ([-5,5]° latitude). In addition to water vapour, sublimated lofted ice can also contribute to the SWV leading to higher values than expected based on the saturation water vapour alone. Overshooting events are considered in our convective parametrization (Möbis and Stevens, 2012). However, at the location of the cold point, this lofted ice would still be in the ice state and not accounted for in the water vapour term.

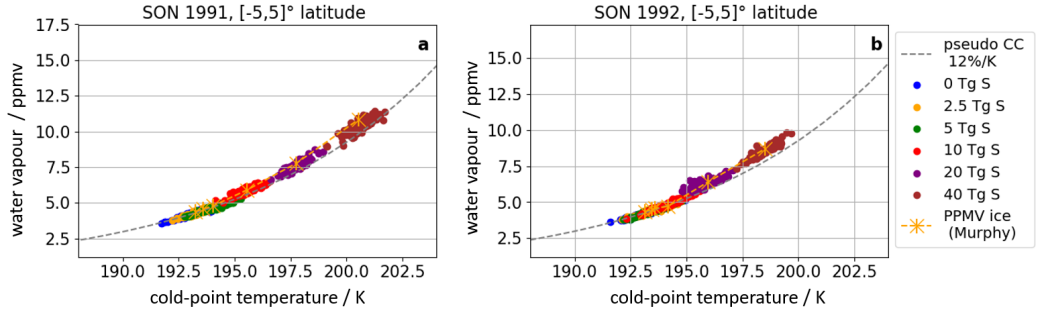

Figure 20: Seasonal averages of water vapour at the cold point as a function of cold point temperature for SON 1991 (a) and 1992 (b). Values for each individual ensemble member are shown as dots for the inner tropics. An approximation (see text) for the Clausius Clapeyron equation at this temperature range with an 12 % increase of water vapour per K is shown with a dashed grey line. The exact solution for the Clausius Clapeyron Equation over ice by Murphy and Koop (2005) is calculated for the average ensemble cold point temperatures and pressure and shown in orange.

1 Formula (7) giving the saturation water vapour pressure above ice p_{ice} as $p_{ice} = \exp(9.550426 - 5723.265/T + 3.53068\ln(T) - 0.00728332T)$ is used. This formula is valid for temperatures above 110 K. With the knowledge of p_{ice} and the respective total pressure a calculation of the water vapour is possible.

In the inner tropics the simulated water vapour values agree nicely with those from the Clausius Clapeyron equation and its approximated WV dependency of a 12 % increase of SWV per Kelvin. Considering the simplification of taking the average cold point temperatures between [-5,5]° latitude instead of the minimum cold point temperatures this agreement is surprisingly good. Oman et al., 2008, for example, only found good agreement when considering the minimum cold point temperatures in the tropics. As they were analyzing a band between [-10,10]° latitude, a factor contributing to the difference to our result could be that the main contribution to dehydration of air parcels during their horizontal motion in the vertical ascent takes place in the inner tropics (Schoeberl and Dessler, 2011), the region to which our study is restricted. Consistent with this analysis is the stronger discrepancy of approximately 1.6 ppmv between the SWV values predicted using the Clausius Clapeyron equation and the SWV output by the model when averaging over the entire tropics (compare Fig. 35).

In the first SON after the eruption in 1991 the SWV values and cold point temperatures are larger than in 1992. Additionally the separation by sulfur content is more pronounced in 1991. Table 5 lists the number of individual ensemble members lying within two standard deviations of the temperature or humidity value spread of the control run. In 1991 several individual group members up to the 5 Tg S run overlap with the control run spread as far as changes in cold point temperature and humidity values are concerned. The 10 Tg S run marks the emission strength at which single ensemble members start to be significantly different from the control run as only one ensemble member can not be distinguished from the control run using only the temperature values. The 20 Tg S run is the first emission strength with no control run overlap and for which all individual ensemble members show significant increase of SWV content and cold point temperatures in 1991 and even in 1992 where the lower emission runs start to show an increasing number of ensemble members overlapping with the control run values again. This analysis shows the difficulty to register the SWV increases in observational data which collect data for a single realisations of a volcanic eruption. Although signals similar to those of individual eruptions can be produced by internal variability of an unperturbed scenario, our larger ensemble size allows to extract a robust signal which may be obscured in one single observational record.

A.3.5 *Comparison to the MPI-GE historical simulations (Mt. Pinatubo)*

The importance of the aerosol profile shape and particularly the extinction at the cold point for the SWV entry becomes apparent when comparing the results of the EVAens members to the Mt. Pinatubo period in the MPI-GE historical simulations. In terms of the amount of emitted sulfur the EVAens simulations for 5 Tg S and 10 Tg S can be seen as bounds of recent estimates of the sulfur emission of the Mt. Pinatubo eruption of (7.5 ± 2.5) Tg S (Timmreck et al., 2018). As the PADS data set describing the Mt. Pinatubo eruption is based on observational evidence rather than simulation results, as is the case for the EVA data sets, only a range and not a set amount of emitted sulfur is given.

Table 5: Number of ensemble members lying within the two standard deviations of the corresponding control run values with respect to temperature (T) or water vapour (Q) or their union ($Q \cup T$) in 1991 and 1992.

Case	2.5 Tg S	5 Tg S	10 Tg S	20 Tg S	40 Tg S
Q_{1991}	93	76	0	0	0
T_{1991}	92	79	1	0	0
$(Q \cup T)_{1991}$	93	82	1	0	0
Q_{1992}	97	89	52	0	0
T_{1992}	98	90	65	0	0
$(Q \cup T)_{1992}$	99	90	65	0	0

In Fig. 14, which shows the global mean TOA radiative imbalance for the MPI-GE historical simulations along with the EVAens simulations, the values for the Mt. Pinatubo eruption in the MPI-GE historical simulations lie between the 5 Tg S and the 10 Tg S imbalances in 1991. In 1992 the mean MPI-GE TOA imbalance is slightly more negative than the ensemble mean of the 10 Tg S run, but overall the deviations between the 10 Tg S run and Mt. Pinatubo run in the MPI-GE historical simulations are small compared to the standard error of the ensemble means.

However, the tropical 1992 SWV anomalies in the historical simulations show a stronger increase than in the 10 Tg S EVAens simulations (absolute values are shown in Fig. 19, for percental changes see Fig. 34). In particular, the SWV increases show a seasonality enhancing the tape recorder amplitude in the historical simulations which is not present to that extent in the EVAens simulations. Notable is also a stronger SWV increase of 1.2 ppmv in the Mt. Pinatubo simulations of 1992 exceeding the 1.0 ppmv of 1991. The heights the corresponding SWV increases reach also differ: the 0.7 ppmv signal propagates upwards to 20 hPa in the historical run, whereas in the 10 Tg S run the 0.7 ppmv signal only reaches pressure levels of up to 50 hPa.

The higher SWV values are caused by a stronger heating of the atmospheric region around the cold point, controlling the indirect volcanic SWV entry. Fig. 21 shows cold point temperatures for the example of SON 1992. Mt. Pinatubo in the MPI-GE historical simulations reaches values lying between those of the 10 Tg S and 20 Tg S run. This can be understood when comparing the aerosol extinction profiles of EVA and PADS as proxy for the heating generated by the aerosol layer (Fig. 22).

Although the PADS data set Mt. Pinatubo forcing has a peak value lying between the 5 Tg S and 10 Tg S EVA extinctions, the extinction at the tropopause and cold point pressure is slightly higher than the 10 Tg S extinction in September 1991 (Fig. 22a and 22c). In September 1992 the PADS data set reaches values of the 20 Tg S EVA in the cold point region and a peak extinction comparable to the 10 Tg S profile (Fig. 22b and 22d). A similar behaviour is apparent in the solar extinction bands (s. Appendix 37). As the warming of the cold point determines the SWV entry anomaly, the extinction values at this point will have a significant impact.
In 1991 the 10 Tg S EVA extinction values at the cold point are only slightly weaker than the extinction values of the PADS forcing set. The SWV values in the MPI-GE

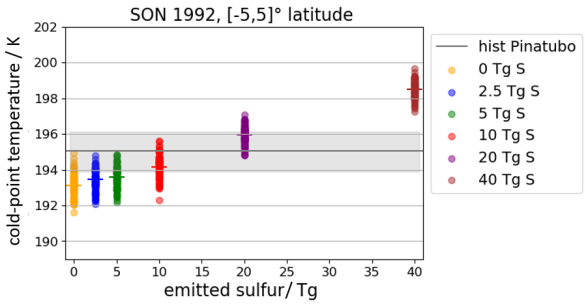

Figure 21: Average cold point temperature in the inner tropical region [-5,5]° latitude as a function of emitted sulfur for all EVAens members in SON 1992. Each point symbolizes one ensemble member, the horizontal lines denote the ensemble mean. The average cold point temperature range for the historical Mt Pinatubo eruptions (PADS) is shown as a grey line, the shaded region shows the extent between corresponding maximum and minimum cold point temperature.

historical simulations are nearer to, but not equal, to those in the 10 Tg S as the peak extinction values in the 10 Tg S are more than two times larger than the PADS extinction values and partially compensate the lower values at the cold point. In 1992 the situation changes and the MPI-GE shows higher SWV values than the 10 Tg S ensemble. The amplification of the SWV entry in the second SON after the eruption can be attributed to three phenomena. First, the heating was only building up in the northern hemisphere summer of 1991 and had not yet reached its maximum value, as can be seen in the plot for the cold point temperatures (Figure 16). Second, the peak extinction values of the PADS data set start to exceed the 10 Tg S values in 1992, which may lead to higher SWV-entry values (Figure 23a). Third, the LW-extinction at the cold point reaches a second, larger maximum around the northern summer of 1992 with values comparable to the 20 Tg S. This second maximum is not represented in the EVA-forcing (Figure 23b) and goes along with a decrease in the peak forcing difference in the EVAens, which lead to higher SWV entry values in the EVAens in 1991. The larger difference between peak extinction and extinction at the cold point compensated for the very similar extinction values at the cold point in 1991.

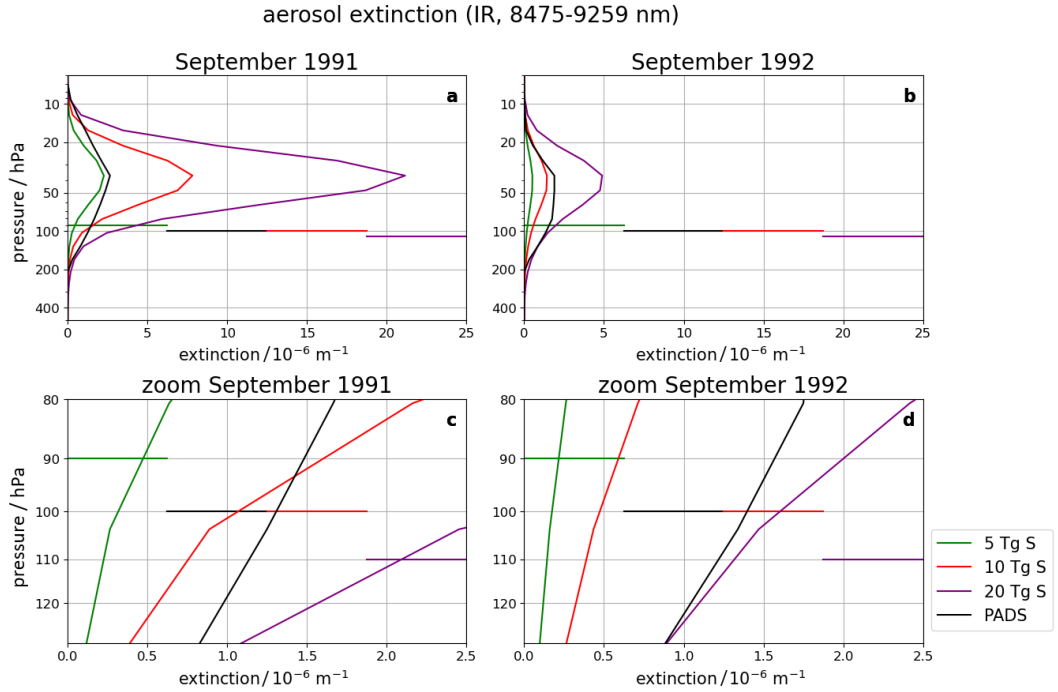

Figure 22: Average tropical aerosol extinction in the 8475-9259 nm infrared waveband from EVA for 5 Tg S, 10 Tg S, and 20 Tg S emissions as well as from PADS in September 1991 and 1992. The horizontal lines indicate the pressure levels of the cold point in the region between [-5,5]° latitude for each eruption strength. (a) and (b) show the entire profile. (c) and (d) are zooms on the cold point region.

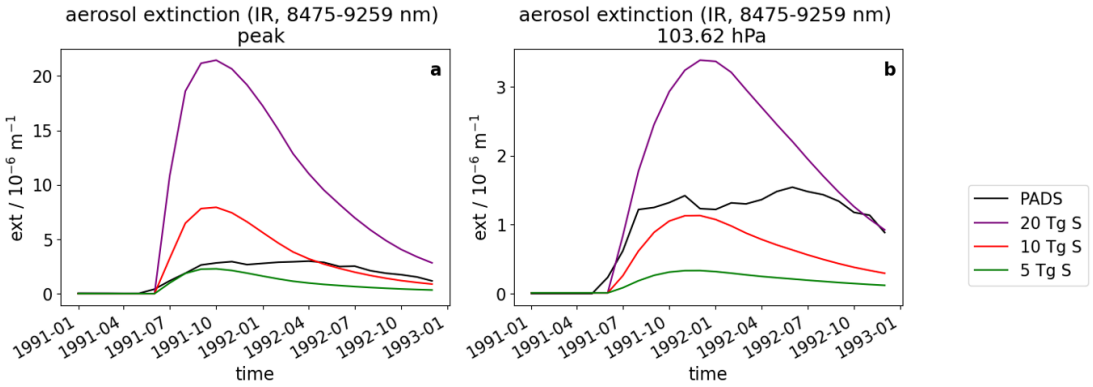

Figure 23: Temporal evolution of the aerosol extinction at the profile peak (a) and the cold point region (b) for the 8475-9259 nm IR-waveband.

A.3.6 *Adjusted forcing caused by the SWV increases*

In the following the adjusted SWV forcing is investigated using the one-dimensional model konrad, as described in Sect. A.2.2. Fig. 24a shows flux anomalies between an unperturbed run and a run perturbed with the increased SWV levels of the 40 Tg S run but without the volcanic aerosol. Although SWV levels are increased within the complete stratospheric column, the main flux changes occur in the tropopause region where the enhancement is largest, the atmosphere denser, and the effect of stratospheric water vapour on the radiative forcing strongest (Solomon et al., 2010). In this region, the incoming solar radiation (SWd) is reduced by absorption, while at lower altitudes there is no difference in the shortwave flux. This is caused by the SWV absorbing part of the solar spectrum which, amongst others, tropospheric water vapour completely absorbs at lower altitudes in the unperturbed run. The reflected solar radiation (SWu) at the surface is only changed negligibly since Δ SWd at the surface is also negligible.

Consequently, the SW contribution (SWd-SWu) to the adjusted forcing at the TOA is very small and negative - accounting for a slightly increased scattering due to the SWV.
The emitted long wave radiation (LWu) near the surface is unchanged. This is due to our setup: As the surface temperature is fixed in the perturbed run, the surface LWu is fixed as well. The SWV leads to an increase in the tropopause temperatures, following this increase the emitted long wave radiation at the main SWV levels is also increased, as can be seen in the increased downward long wave radiation (LWd). The outgoing long wave radiation (LWu) above the tropopause region is substantially reduced as the SWV acts as a greenhouse gas and traps part of the outgoing radiation. This leads to the characteristic net positive forcing of the greenhouse gas at the TOA.

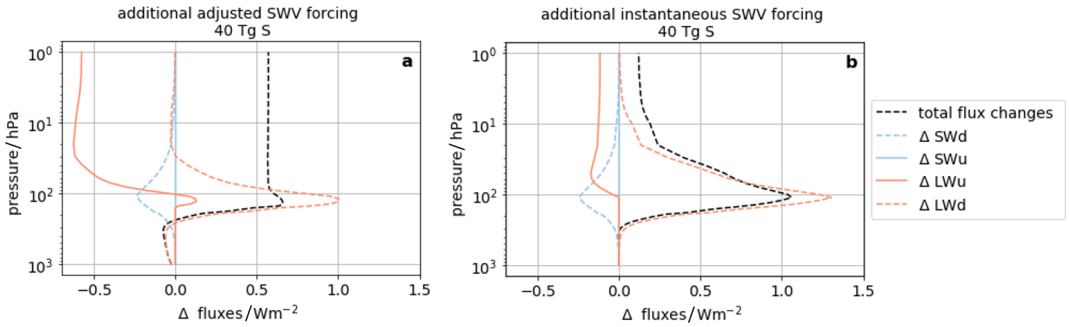

Figure 24: SW and LW contributions to the total adjusted SWV radiative forcing in the tropical stratosphere [-5,5]° latitude for November 1992 of the 40Tg S eruption. The upward fluxes are in solid lines and positive upward, the downward fluxes are in dashed lines and positive downward. The difference between the perturbed and unperturbed equilibrium state are shown. (a) adjusted forcing (b) instantaneous forcing.

A comparison to the instantaneous forcing (Fig. 24b) shows that the temperature adaptations in the stratosphere significantly amplify the SWV forcing. Whereas the atmospheric levels with increased SWV are warmed, stratospheric cooling is found

in higher atmospheric levels, reducing the LWu. This effect has to build up though and consequently is more pronounced in the adjusted SWV forcing. If addition to the stratosphere also the troposphere were allowed to adjust, part of this effect may be counterbalanced (Huang et al., 2020).

The temporal evolution of the adjusted inner tropical SWV forcing is shown for all five eruptions strengths in Fig. 25. The adjusted forcing caused by the SWV, corresponding to the 2.5 Tg S to 10 Tg S run, is below the maximum fluctuations caused by internal variability denoted by the grey line in Fig. 25. The forcing found for these runs could be found for one ensemble member in the 0 Tg case as well, although the time span in which it would occur would most probably be shorter. The adjusted SWV forcing for the 40 Tg S run reaches values of up to 0.65 W m^{-2}.
The signal evolution, especially in the 20 Tg S and 40 Tg S cases, matches the evolution already observed for the SWV increases in the tropical region, with two seasonal peaks. However, since also SWV at pressures lower than 100 hPa contribute to the total forcing - although to a smaller extent - and the transport out of the tropical region with the BDC is slow, the first peak forcing times are longer than the peak water vapour values at 100 hPa in Fig. 16.
When considering clouds the stratospherically adjusted forcing caused by the additional SWV is slightly increased by 0.1 W m^{-2} at most (compare Appendix Fig. 38). As the clouds reflect part of the down coming SW radiation, some of the SW bands, which could be completely absorbed while traveling through the complete stratosphere and troposphere, are not absorbed entirely. The additional SWV in the stratosphere increases the absorption in these bands and reduces the outgoing SW radiation. This leads to an increase of the forcing.

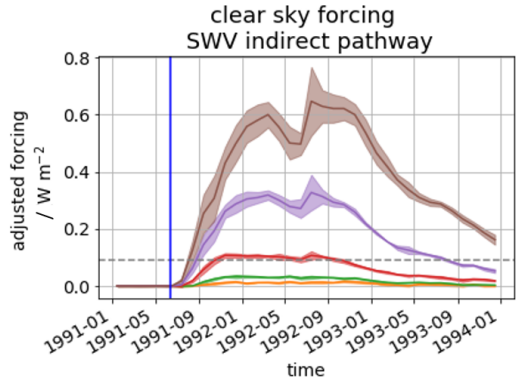

Figure 25: Time evolution of the TOA adjusted clear sky forcing in the tropical region [-5,5]° latitude for the ensemble mean SWV increases caused by all eruption strengths. The blue line marks the eruptions time, the dashed grey line shows the threshold up to which deviations in radiative fluxes can be caused by internal variability. Shaded areas indicate the flux anomaly range originating from the standard deviations of the SWV profiles are plotted to visualize the signal range.

The monthly SWV forcing does not exhibit a linear behaviour with respect to the mass of emitted sulfur or main IR AOD waveband (Fig. 32, 33) as was to be expected since the monthly cold point temperatures also did not change in a linear manner

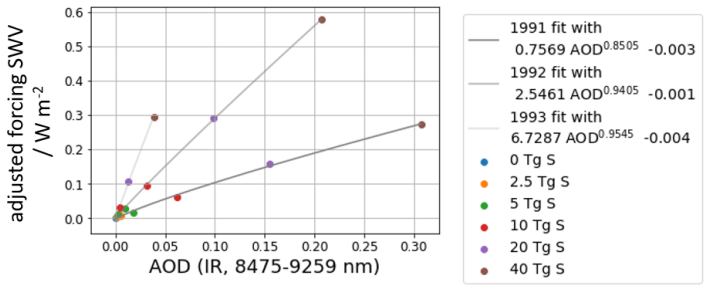

Figure 26: Yearly averages of adjusted forcing due to the additional SWV as a function of AOD (IR, 8475-9259 nm) for the three examined years (1991-1993). A power function fit for each year with corresponding equation is shown.

with respect to the emitted sulfur mass and the temperature increases showed a hysteretic behaviour. However again, when averaging out the seasonal dependencies and partitioning the time after the eruption in the signal build up phase (1991, after the eruption), the phase of approximately constant forcing (1992) and the phase of declining signal (1993), the relationship can be fitted to a power function of form $aAOD^b + c$ in the region of interest. Compared to the cold point - AOD relation the signal build up and relaxation back to the ground state is damped as the transport of the SWV into the stratosphere and out of the tropical region takes place over longer timescales than the cold point warming or cooling respectively.

As the SWV forcing counteracts the volcanic forcing, its relation to the aerosol forcing is of interest. Fig. 27a shows the tropical aerosol forcing as calculated using the double radiation call in the MPI-ESM. For the evaluation of the forcing in the double radiation call different conventions exists as far as the evaluation at the TOA or the tropopause are concerned (e.g. compare Forster et al. (2016)). As the double radiation call is used to determine an instantaneous forcing, the readout at the tropopause level would be following the standard convention as defined by Hansen et al. (2005) or in the IPCC. However, we present both values for the entire and inner tropics to allow for an easy comparison to other studies. The relative magnitude of the SWV adjusted forcing with respect to the aerosol forcing increases approximately linearly until September 1992 and then reaches a constant values of around 2.5 % for the readout at the tropopause and 4 % percent for the readout at the TOA (Fig. 27b).

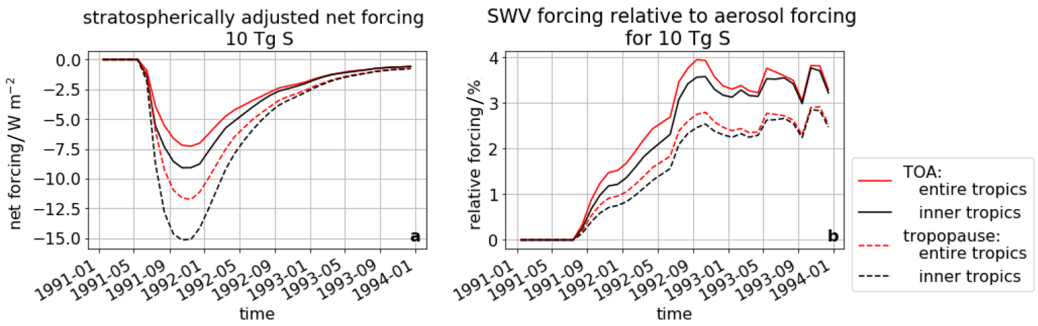

Figure 27: (a) Time evolution of the tropical aerosol forcing for the 10 Tg S run as calculated using the double radiation call in the MPI-ESM. The forcing is evaluated for the inner and entire tropics at the tropopause and the TOA. (b) Time evolution of the percentage of aerosol forcing counterbalanced by the SWV forcing in the inner and entire tropics .

A.4 DISCUSSION

A.4.1 *Magnitude of SWV increases due to indirect volcanic mechanism*

In general, the annual cycle of the tropical tropopause temperatures accounts for a variation of the SWV content of ± 1.4 ppmv around the mean background at 110 hPa in SAGE II data of the early 1990s (Mote et al., 1996) and ± 1.0-1.3 ppmv based on the SPARC Data Initiative multi-instrument mean (SDI MIM) at 100 hPa in 2005-2010 (Davis et al., 2017). In the MPI-GE the variation in the SWV tape recorder signal at the same height reaches up to ± 1.1 ppmv. This is in accordance with the SDI MIM and only slightly lower than the SAGE II data. The slightly higher values reported for early 1990 fall into the era of the Mt. Pinatubo eruption, however, and may be increased compared to the multiyear mean due to an amplification of the seasonal signal by the presence of the aerosol layer. This effect led to maximum deviations of up to ± 1.6 ppmv in the 10 Tg S scenario of the EVAens simulations.
In the case of volcanic perturbations, the alterations in SWV content caused by the indirect temperature controlled entry mechanism via tropopause warming after volcanic eruptions can surpass the SWV variations due to the annual cycle. In our simulations deviations of more than ± 1.1 ppmv are produced in the simulations for emissions equal to or larger than 10 Tg S eruption, which is an upper bound of the emission estimate for the Mt. Pinatubo eruption (Timmreck et al., 2018). The SWV anomaly caused by the 2.5 Tg S eruption is comparable to changes caused by the Quasi Biennial Oscillation (QBO), which are [0.16-0.32] ppmv according to the regression analysis by Dessler et al. (2013), whereas the 10 Tg S has an impact stronger than the changes in the BDC (maximum 0.65 ppmv).
In climate change studies, the stratospheric water vapour is also affected by doubled CO_2 concentrations. The SST increase leads to a consequent atmospheric humidity increase, amounting up to 6-10 % in the stratosphere, with values exceeding 10 % in the lower stratosphere (Wang et al. (2020)). These changes of SWV due to increased CO_2 levels are comparable to increases caused by the smaller eruptions of 2.5 Tg S and 5 Tg S. However, the SWV changes due to volcanic eruptions are only temporary.

A.4.2 *Comparison to studies based on observations and reanalysis data*

While our model study has the advantage that the large ensemble size allows determining the statistical significance of SWV increases, and the spread of responses to a volcanic eruption due to internal variability of the earth system, a model study is always limited by the ability of the model to represent the earth system realistically. Individual models may differ in the parameterization of convection, the entry of water vapour into the stratosphere and tropopause height. The aerosol profiles used in this study are artificial in case of the EVAens and will include uncertainties of the retrieval in case of the PADS data set. As our results are therefore at first only representative for the model used in our study, a comparison to results based on or derived from observational evidence of SWV changes after volcanic eruptions is desirable.

During the Mt. Pinatubo period, observations of SWV are scarce, especially as solar occultation measurements by HALOE and SAGE II suffered from aerosol interference in this time period. Therefore, the data usage is discouraged (e.g. Fueglistaler et al. (2013)). Although Fueglistaler et al. (2013) mention "anomalously large anomalies" of SWV values shortly after the Mt. Pinatubo eruption in SAGE II data, they also warn that the measurements may be biased by aerosol artifacts since the SWV signal is not present in the HALOE data. However, in the Boulder balloon data a 1-2 ppmv increase of SWV at 24-26 km and 18-20 km levels is registered for 1992 (Oltmans et al., 2000). Most likely due to additional contribution from e.g. methane oxidation or ENSO signals, the maximum increase is slightly larger than the 1.0-1.2 ppmv shown for the tropical region in Figure 19 or the value of approximately 0.5 ppmv at 70 hPa at corresponding latitude (compare Appendix 39). Santer et al. (2003) discuss a global warming of the lower stratosphere caused by the eruption of Mt Pinatubo amounting to 0.75-1.5 K as measured by MSU. Angell (1997) reports the stratospheric warming due the eruption of Mt. Pinatubo based on radiosonde data. The warmest seasonal anomaly in the 100-50 hPa layer at the equator reached (2.0±0.8) K, where we find 1.8 K for the 5 Tg S and 5.2 K for the 10 Tg S scenario in OND 1991. The corresponding SWV increase at background levels of 4.5-5 ppmv can be estimated to be 1.13-1.3 ppmv based on a 12 % increase of SWV per Kelvin. These values are consistent with our findings (Figure 19).
As more regression analyses exist based on reanalysis data, we now compare our results not directly to observations but to the outcome of two regression analysis studies of SWV entry fed by the reanalysis input by Dessler et al. (2014) and Tao et al. (2019). Dessler et al. (2014) studied the different contributors to SWV entry at 82 hPa slightly above the tropical tropopause in their model by using a regression analysis on data output from a trajectory model fed by MERRA reanalysis input (Rienecker et al., 2011). They found a maximum increase of 0.34 ppmv in the residual, which partially overlapped the AOD increase caused by the Mt. Pinatubo eruption. This value is lower than our finding of up to (0.8-1.1) ppmv increase in the first and second post eruption year. Our higher value may be explained by the different quantification approaches: whereas Dessler et al. (2014) indirectly quantified the SWV increase due to Mt. Pinatubo in the residuals after subtracting contributing terms like the BDC, we directly quantified the additional SWV entry by taking the differ-

ence between the MPI-GE historical ensemble with volcanic aerosol and the EVAens control run. This allowed us to avoid the subtraction of SWV entry caused by the volcanic eruption but attributed to other sources. For example, in the Dessler et al. (2014) study, the BDC term is described by the heating in the 82 hPa region, but part of this may be caused by the presence of the volcanic aerosol layer. Our method also eliminates other sources of SWV that may have caused the SWV increase prior to the Mt. Pinatubo eruption in the residual of Dessler et al. (2014). Additionally, the tropopause in our historical simulation is located at pressures larger than 100 hPa. Dessler et al. (2014) report that 82 hPa is slightly above the tropopause. Their possibly higher lying tropopause may also explain part of the difference.
Tao et al. (2019) use MERRA-2 (Gelaro et al., 2017), JRA-55 (Kobayashi et al., 2015) and ERAinterim (Dee et al., 2011) reanalysis data for the Mt. Pinatubo eruption in their trajectory model. The SWV increase attributed to the volcanic eruption ranges between 0.4 ppmv (ERAinterim) and 0.8 ppmv (MERRA-2 and JRA-55). Only MERRA-2 explicitly accounts for the volcanic aerosol (Fujiwara et al. (2017)): their corresponding 0.8 ppmv SWV increase is in good agreement with the SWV increases found in the first post eruption year in our historical simulations, although our SWV increase in the second post eruption year of 1.1 ppmv is larger. As analyzed in Sect. A.3.5, this higher increase is mainly caused by the height of the aerosol layer with respect to the cold point. Since the aerosol profiles are imported on fixed pressure levels, without prescribing the distance between the tropopause and the aerosol layer, and the tropopause heights differ amongst various models, the comparison between different studies and models would be facilitated if not only the total volcanic forcing but also the heating in the region were reported when quantifying and comparing volcanically induced SWV increases. A tropopause located at larger pressure in the second post eruption summer in the reanalysis data could explain the differences between the maximum values of 0.8 ppmv by Tao et al. (2019) using the MERRA-2 reanalysis and our results amounting up to 1.1 ppmv in the second post eruption summer, as it would lead to a lower heating rate in the cold point region and consequently a reduced water vapour entry compared to the control years. Additionally, our model does not include interactive chemistry - H_2O sinks could reduce the amount of water vapour and especially the build up in the second post eruption summer. However, Löffler et al. (2016) also found a stronger SWV increase in the second post eruption summer when investigating the perturbations of stratospheric water vapour using nudged chemistry-climate model simulations with prescribed aerosol for the Mt. Pinatubo eruption. The SWV increases for the Mt. Pinatubo eruption reach values of up to 35 % compared to the unperturbed run in the inner tropical average. Thus, our finding of an increase of 25 % above the unperturbed levels for the historical simulations (compare Fig. 34) lies between the estimates from reanalysis data by Tao et al. (2019) and the chemistry climate studies by Löffler et al. (2016).
In the EVAens, where the temporal evolution of the extinction profile does not lead to as drastic changes in the vertical shape as in the PADS forcing data set, the temporal evolution of the increase in SWV is similar to the evolution found by **Tao.2019**, with only one prominent maximum. Maximum values of SWV increase are in the range of 0.3 ppmv and 1.1 ppmv for the 5 Tg S and 10 Tg S EVAens runs - covering the estimated sulfur emission range of Mt. Pinatubo and in agreement with **Tao.2019**.

A.4.3 *SWV contributions due to the indirect volcanic and direct volcanic injection*

Unlike the direct volcanic mechanism the indirect volcanic pathway is active for the entire life time of the volcanic aerosol in the lower stratosphere, whereas the direct volcanic injection is a singular event. There is no study known to us comparing the SWV entry due to both events within one framework. Although up to 80 % of the eruption volume can be water vapour (Coffey (1996)), rapid condensation can remove 80-90 % of this humidity on the way to the stratosphere (Glaze et al. (1997)). There are only a few cases of direct volcanic injections reported, which cover relatively small eruption events. The water vapour within the eruption column reaching the stratosphere did not lead to elevated SWV above background for more than a week locally in the few cases reported, i.e the eruption of Kasatochi (2008) with maximum SWV content of 9 ppmv (Schwartz et al., 2013) lasting for around 1 day, the eruption of Calbuco (2015) with 10 ppmv values for approximately a week (Sioris et al. (2016a)), and the eruption of Mt. Saint Helens with (64 ± 4) ppmv (Murcray et al. (1981)) detectable above background for around a week, but only on local and not global scale. In the case of the Mt. Pinatubo eruption the model estimates for the direct volcanic injection tended to have a larger range and maximum values than the estimates based on observational data (Joshi and Jones, 2009). In contrast, the indirect volcanic pathway allows for slower, but more continuous, raised stratospheric water vapour levels ultimately spreading throughout the globe but with lower peak values. These enhanced SWV levels are detectable in our ensemble mean even years after the actual volcanic eruption if the emitted sulfur amount is larger than 10 Tg S. Depending on the explosivity of the volcano, the relative contributions of the direct and indirect volcanic injection mechanisms to SWV increases should change: for small eruptions the direct volcanic injection will lead to a relatively high increase in SWV, which is short lived and spatially confined. For the larger eruptions this short lived SWV enhancement is followed by a relatively stable increase of SWV which spreads throughout the entire globe, dominating the SWV increase due to the volcanic eruption.

A.4.4 *SWV Forcing*

In our simulations the stratospherically adjusted forcing caused by the increase of SWV in the tropical region amounts to maximally 2.5 to 4 percent of the tropical aerosol forcing over the time frame for the 10 Tg S eruption. However, although a decline of the tropical forcing within the three year time-frame is found, the forcing around the complete globe will last longer than the impact of the volcanic aerosol. The decline in tropical stratospheric water vapour is caused by its transport to the poles by the BDC, leading to a regional shift of the location of the SWV forcing (see Fig. 39). Forster and Shine (2002) found the polar SWV forcing to be 2.5 times stronger than the tropical forcing: Since in the polar region the tropopause height is lower and the water vapour content is generally lower, SWV increases of the same magnitude have a much larger impact there than in the tropical region. Based on the factor of 2.5, the 40 Tg S run 1993 values would cause an adjusted forcing of up to 0.5 W m^{-2} in the polar region, whereas the aerosol forcing is back to the levels of the 2.5 Tg S run by 1993. This shift in relative magnitude is one of the factors contributing

to the positive TOA imbalance at the end of 1993 (for 20 Tg S and 40 Tg S in Fig. 14).

For the eruption of Mt. Pinatubo, with (7.5 ± 2.5) Tg S emitted, earlier estimates of SWV forcing exist. Joshi and Shine (2003) calculated the global SWV forcing to be 0.1 W m^{-2}. Our 10 Tg S adjusted forcing results of up to 0.11 W m^{-2} are nearer to the estimate by Joshi and Shine (2003) than our 5 Tg S results of up to 0.03 W m^{-2}. In 1992, the adjusted forcing in the inner tropics lies between [0.02 - 0.03] W m^{-2} for the 5 Tg S and [0.06 - 0.11] W m^{-2} for the 10 Tg S scenarios. The better agreement of our 10 Tg S adjusted SWV forcing with Joshi and Shine (2003) value for the Mt. Pinatubo SWV forcing can be attributed to two points: First, the form and location of the forcing profile with respect to the cold point is crucial when comparing model results of increased SWV levels and the consequent changes in SWV forcing (s. Sect. A.3.5). This may contribute to differences between our values and the ones in the Joshi and Shine (2003) analysis. Second, the polar forcing will be stronger than the tropical forcing which was calculated with konrad. Using the ratio of polar forcing to tropical forcing by Forster and Shine (2002), the polar estimate would be [0.05 - 0.08] W m^{-2} for 5 Tg S and [0.15 - 0.28] W m^{-2} for 10 Tg S.

In their study on direct volcanic SWV entry for the Krakatau eruption Joshi and Jones (2009) found a LW-forcing of +(0.33 ± 0.09) W m^{-2} for a direct volcanic entry above 100 hPa of 1.5 ppmv using the downward TOA heat flux, climate feedback parameter, and near surface temperature changes. They chose a relatively high estimate of SWV increase, which would approximately correspond to the SWV increases in our 20 Tg S eruption run. As the TOA-SW contribution to our forcing is negligible (s. Fig. 24) a comparison to our total forcing is possible. The corresponding value of [0.21 - 0.33] W m^{-2} is in the lower part of the range found by Joshi and Jones (2009), which is likely caused mainly by the restriction of our study to the tropical region.

Krishnamohan et al., 2019 also mentioned the contribution of aerosol induced SWV changes to the flux changes at the TOA in a geoengineering study, however they did not explicitly calculate it. The amount of short wave forcing they attribute to additional SWV is much higher than our value and also positive. Presumably these differences are caused by the forcing including tropospheric adjustments and using a 2 x CO_2 reference frame and thus can not be compared to our study.

In order to put the adjusted radiative SWV forcing due to the indirect volcanic pathway into a broader context we compare it with SWV forcing due to anthropogenic CO_2 and methane releases: the rate of radiative forcing increase due to CO_2 in the 2000s[2] reached values of almost 0.03 W m^{-2} $year^{-1}$ and a total of (1.82 ± 0.19) W m^{-2} for the 1750 to 2011 time frame, whereas the additional radiative forcing due to methane in the same time frame is (0.48 ± 0.05) W m^{-2} (Myhre et al., 2013)[3]. The forcing caused by the SWV entering the stratosphere via the indirect volcanic entry mechanism exceeds the yearly increase of forcing due to CO_2 in the 2000s starting with the 5 Tg S run. The peak adjusted tropical SWV forcing for the 40 Tg S scenario amounts to one third of the total CO_2 forcing (due to the accumulated emissions

2 Atmospheric CO_2 concentration increased from (278 ± 2) ppmm to (390.5 ± 0.2) ppmm.
3 Methane concentration increased from (722 ± 25) ppb to (1803 ± 2) ppb.

from 1750 to 2011) and is larger than the forcing due to methane emissions for the same period.

A.4.5 *Predictability of responses*

The increase in cold point temperature and SWV are delayed events. Time is required for it to build up the signals as the aerosol warms the cold point region allowing more water vapour transit into the stratosphere. An approximately stable phase with fluctuations due to the seasonal cycle is attained a couple of months after eruption. The cold point warming has stabilized. The SWV forcing is mainly determined by the additional SWV entering the stratosphere each month as the tropopause region is the region in which WV has the strongest radiative effect. The corresponding build up of tropical SWV forcing due to an accumulation of SWV in the stratosphere is therefore counteracted by the transport to higher altitudes and to the polar region by the BDC.
Due to the transient character of the processes - the build up of the forcing and the consequent decline as well as the time shift between effect and response - our analysis showed that a linear relationship between AOD and cold point warming, or SWV, can not be determined for the entire era after the volcanic eruption. Time phases have to be considered as well to account for the resulting hysteresis. Other parameters additionally constrain the cold point warming and SWV response. The season during which the eruption occurs will influence the impact of the aerosol: The CP warming will be most effective during the peak times of the tape recorder signal around September. Each volcanic eruption is different and parameters like the eruption location, amount of emitted sulfur, and specifically the location of the aerosol layer will have a massive influence both on cold point warming and SWV entry/forcing. Feedbacks like the SWV forcing in the TTL will enhance the CP warming and lead to higher SWV forcing at same AODs eventually before the aerosol falls out.
Nevertheless, approximately a power function relationship of form $aAOD^b + c$ can be found in our simulations for CP warming and SWV forcing with respect to IR-AOD after the volcanic eruptions when taking yearly averages. These results however must be interpreted with care and the derived formulas are only applicable for tropical eruptions occurring in June and reaching to similar heights in the stratosphere.
Generally, the knowledge - both of the respective CP warming in the inner tropics for a specific volcanic eruption and the respective background SWV in the cold point region - allows for a relatively accurate prediction of the inner tropical increases in SWV levels when using a 12 % SWV increase per Kelvin warming in the mean CP values.

A.5 CONCLUSION AND OUTLOOK

Our study of EVAens and the historical simulations led us to draw the following conclusions:

1. The analysis of the ensemble runs showed the difficulty to extract the volcanic signal in the SWV if only individual observations are available as internal variability of SWV in the control run could produce SWV values as large as the

variation found for some of the 10 Tg S ensemble members in our simulations. Ensemble mean SWV increases are already significant (T-test with p=0.05) in the 2.5 Tg S eruption.

2. The increase in stratospheric water vapour does not remain constant throughout year, but can vary with the seasons. An amplification of the seasonal cycle could be observed, especially in the 20 Tg S and 40 Tg S scenarios.

3. The average WV at the cold point entering the stratosphere after volcanic eruptions can be approximated with only minor errors using the mean saturation water vapour pressure over ice at the respective average tropical cold point temperature for all investigated aerosol profiles of the EVAens. When given a base value of an unperturbed atmospheric state, a 12 % SWV increase per K increase in cold point temperature is a good first estimate for eruption strengths up to 40 Tg S.

4. The comparison of the idealized EVAens simulations and MPI-GE historical simulations of Mt. Pinatubo show that neither the simulated TOA radiative imbalance nor the estimated amount of emitted stratospheric sulfur suffice to constrain the SWV increases. However, the aerosol layer shape and height with respect to the tropopause play a crucial and dominating role when estimating the SWV increases.

5. The adjusted tropical forcing caused by the additional SWV last longer than the forcing caused by the aerosol layer itself and its contribution to the total volcanic forcing grows with time as the aerosol falls out. For the 20 Tg and the 40 Tg scenarios the TOA radiative imbalance shows a positive value by the end of the simulation. Part of this positive TOA radiative imbalance can be attributed to the forcing by the additional SWV.

6. When considering also the time dependence a power function relationship of form $aAOD^b + c$ between yearly averaged tropical cold point warming/adjusted SWV forcing and IR-AOD can be deduced. This relationship however only holds for comparable eruptions occurring at the same time of the year in the tropics. Additionally, the final eruption height and aerosol profile shape has to match the one used within our framework.

Based on our study follow up questions for future investigations arise. Our study only focuses on the indirect temperature controlled injection and, although other studies focus on the direct injection, no study known to us combines both effects allowing for a direct comparison within one single framework. Using integrated plume models for a combined study would allow the quantification of the entire SWV changes and for an estimation of their relative importance. As we use no interactive chemistry, the H_2O value determined by us might be overestimating the SWV from the indirect volcanic injection remaining in the stratosphere. A study using interactive chemistry would allow the assessment of the impact of H_2O sinks on the volcanically induced SWV increase and ozone chemistry. Of particular interest are the impact of the additional H_2O on the oxidation process of SO_2, as well as on sulfate particle formation and growth. A follow up study on this topic could give a lower boundary estimate for the SWV increases and the changed aerosol lifetime

(compare Case et al., 2015, Kilian et al., 2020). Additionally, the mechanism of the indirect volcanic injection has implications beyond that of a volcanic eruption: As geoengineering scenarios also apply sulfur derivatives in the stratosphere, an investigation of the long term SWV signal within these scenarios may be of interest as well (e.g. Boucher et al. (2017)).

Code and data availability. Primary data and scripts used in the analysis that may be useful in reproducing the author's work are archived by the Max Planck Institute for Meteorology and can be obtained via https://pure.mpg.de/pubman/faces/ViewItemOverviewPage.jsp?itemId=item_3270686.
A more comprehensive description of the EVAens is provided by Azoulay et al., submitted to JGR (2020). Further information was archived by the Max Planck Institute for Meteorology under http://hdl.handle.net/21.11116/0000-0007-8B38-E.
The 1D RCE model konrad is available online under https://github.com/atmtools/konrad.

A.6 APPENDIX A: SCALING OF DIFFERENT PHYSICAL PARAMETERS ALTERED BY THE PRESENCE OF VOLCANIC AEROSOL

Following the discussion in Sect. A.3.1, A.3.2 and A.3.6 the graphs for TOA imbalance (Fig. 28), surface temperature (Fig. 29), cold point temperature changes (Fig. 30) and SWV forcing (Figure 32) are shown. Each ensemble mean is divided by the mass of emitted sulfur. In case of the cold point temperature changes and the SWV forcing the dependence of monthly mean values of cold point temperature change and SWV forcing are shown as a function of AOD in the IR waveband of [8475,9259] nm in Fig. 31 and 33.

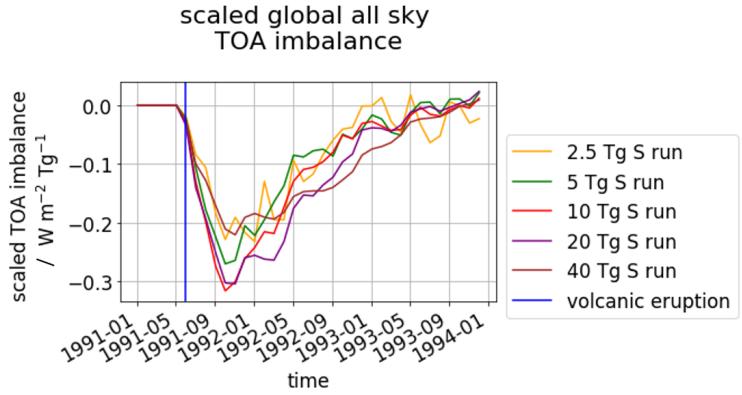

Figure 28: Scaled global all sky TOA imbalance for the five volcanically perturbed EVAens runs (2.5 Tg S, 5 Tg S, 10 Tg S, 20 Tg S and 40 Tg S). The ensemble means are shown. The vertical blue line marks the eruption time. All surface temperatures are divided by the mass of emitted sulfur.

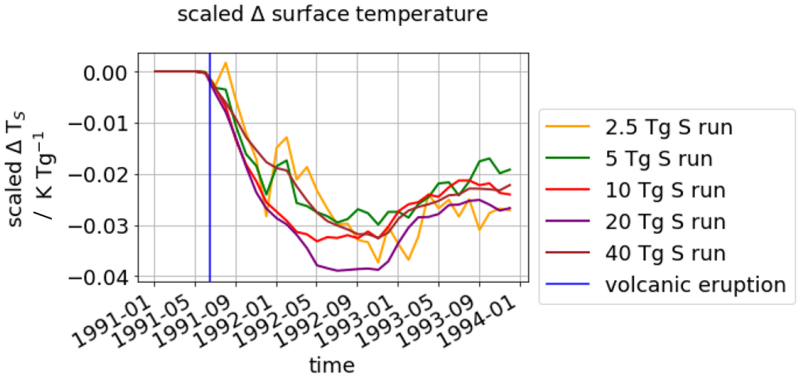

Figure 29: Scaled surface temperature for the five volcanically perturbed EVAens runs (2.5 Tg S, 5 Tg S, 10 Tg S, 20 Tg S and 40 Tg S). The ensemble means are shown. The vertical blue line marks the eruption time. All surface temperatures are divided by the mass of emitted sulfur.

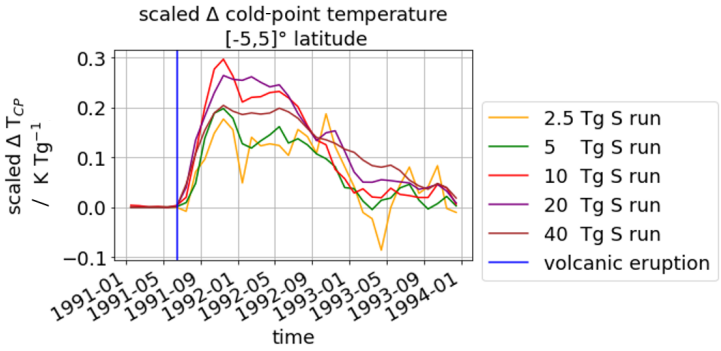

Figure 30: Scaled temporal evolution of the mean CP temperature anomaly. The time of the volcanic eruption is indicated by a vertical blue line. All changes in cold point temperature are divided by the mass of emitted sulfur.

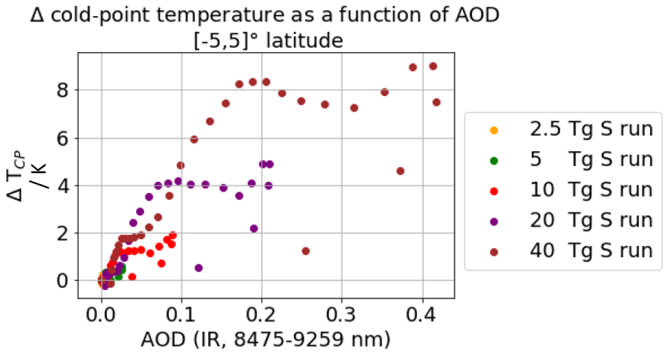

Figure 31: Scatter plot of AOD in the IR waveband (8475-9250 nm) and CP temperature anomaly for all time steps in the first 2.5 years after the eruption.

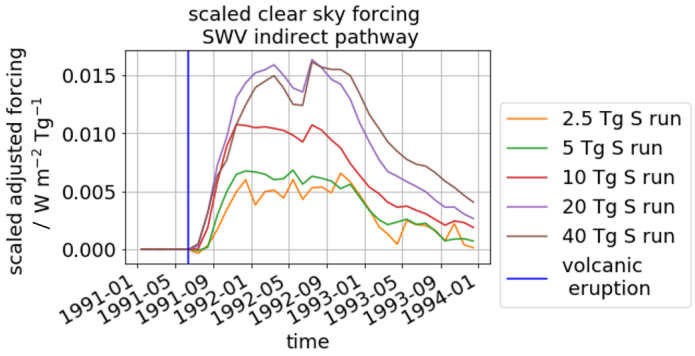

Figure 32: Scaled time evolution of the adjusted clear sky SW-forcing in the tropical region [-5,5]° latitude for all eruption strengths. The blue line marks the eruptions time. All clear sky forcings are divided by the mass of emitted sulfur. Incoming fluxes are defined positive, outgoing fluxes are defined negative.

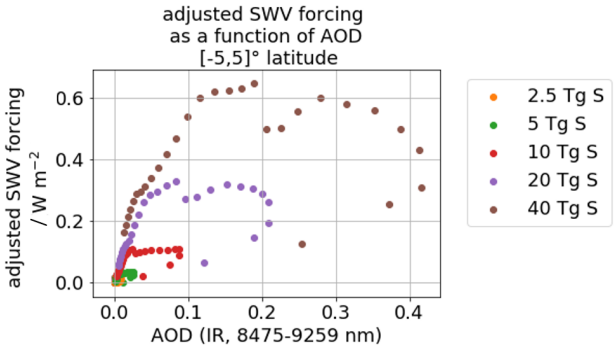

Figure 33: Scatter plot of AOD in the IR waveband (8475-9250 nm) and the clear sky SWV forcing for all time steps in the first 2.5 years after the eruption.

A.7 APPENDIX B: PERCENTAL CHANGES IN THE TAPE RECORDER SIGNAL

Complementary to the plot in Sect. A.3.3 we show the differences in water vapour between perturbed and unperturbed state with respect to the unperturbed state in percent.

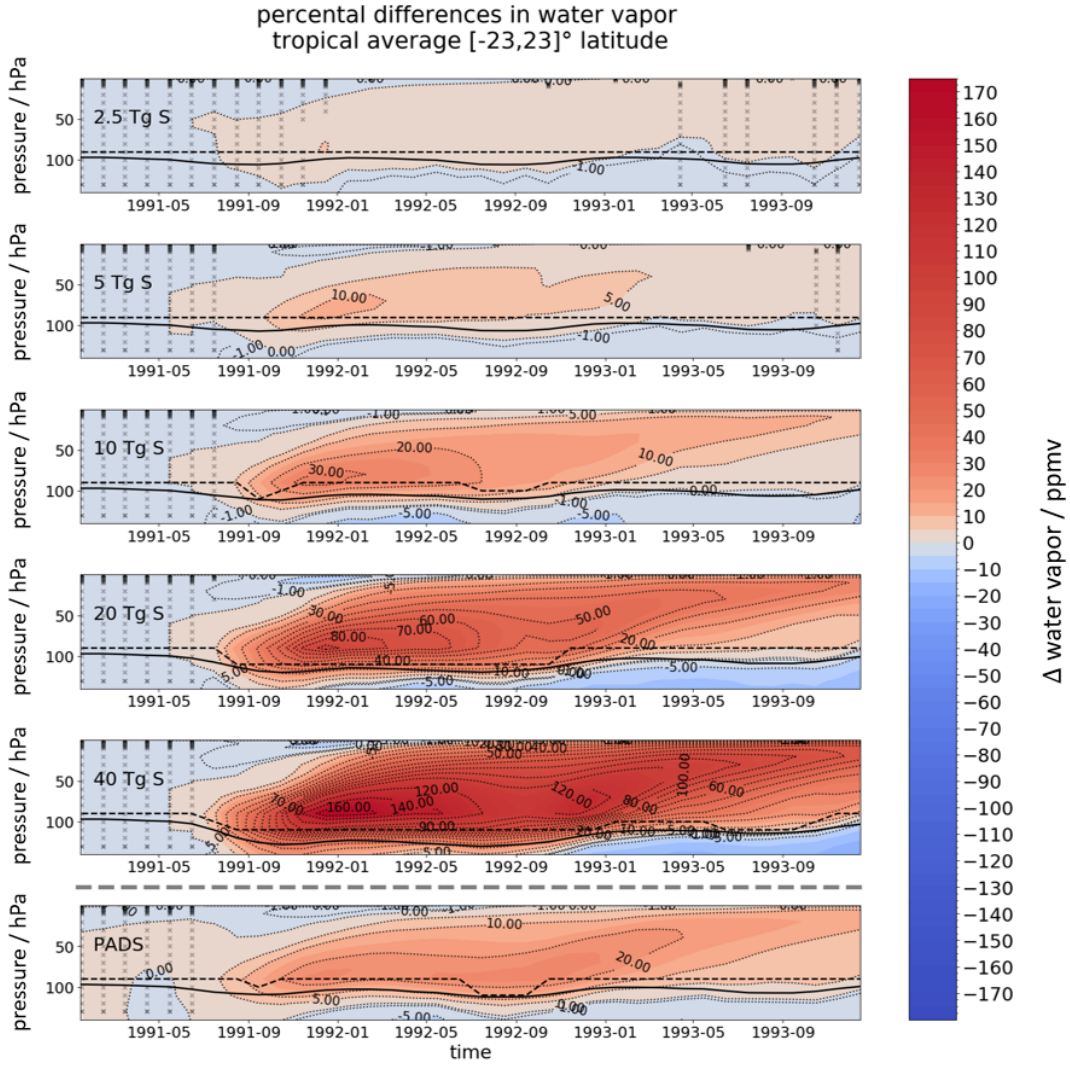

Figure 34: Percental difference in water vapour above 140 hPa in the tropical average over [-23,23]° latitude for the pure sulfur injections of the EVAens (2.5 Tg S, 5 Tg S, 10 Tg S, 20 Tg S and 40 Tg S). The lowermost panel shows the MPI-GE historical simulations for Mt. Pinatubo using the PADS forcing data set. The height of the WMO-tropopause is indicated by a black line, the cold point pressure is shown as black dashed line. In regions not covered by black crosses statistical significant difference between stratospheric water vapour values of the perturbed and unperturbed runs (t-test at p=0.05) were found.

A.8 APPENDIX C: INTRA-ENSEMBLE VARIABILITY IN THE ENTIRE TROPICS

Here we show the complementary plots to those in Sect. A.3.4 for the intra-ensemble variability in the entire tropics [-23,23]° latitude.

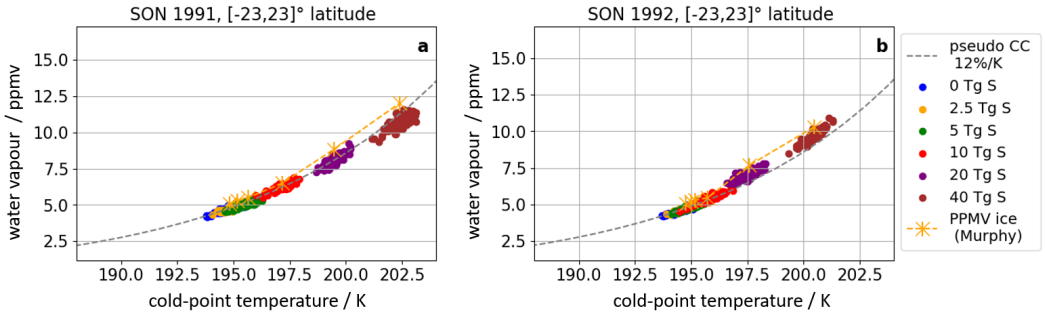

Figure 35: Seasonal averages of water vapour at cold point as a function of cold point temperature for SON 1991 (a) and 1992 (b) accounting for the entire tropics. Values for each individual ensemble member are shown as dots for the entire tropics. An approximation (see text) for the Clausius Clapeyron equation at this temperature range with an 12 % increase of water vapour per K is shown with a dashed grey line. The exact solution for the Clausius Clapeyron Equation over ice by **Murphy.2005** is calculated for the average ensemble cold point temperatures and pressure and shown in orange.

A.9 APPENDIX D: AEROSOL EXTINCTION PROFILES - 550 NM SOLAR WAVEBAND

Complementary to the discussion on the infrared extinction profiles in Sect. A.3.5 the 550 nm solar waveband is shown in the following plots.

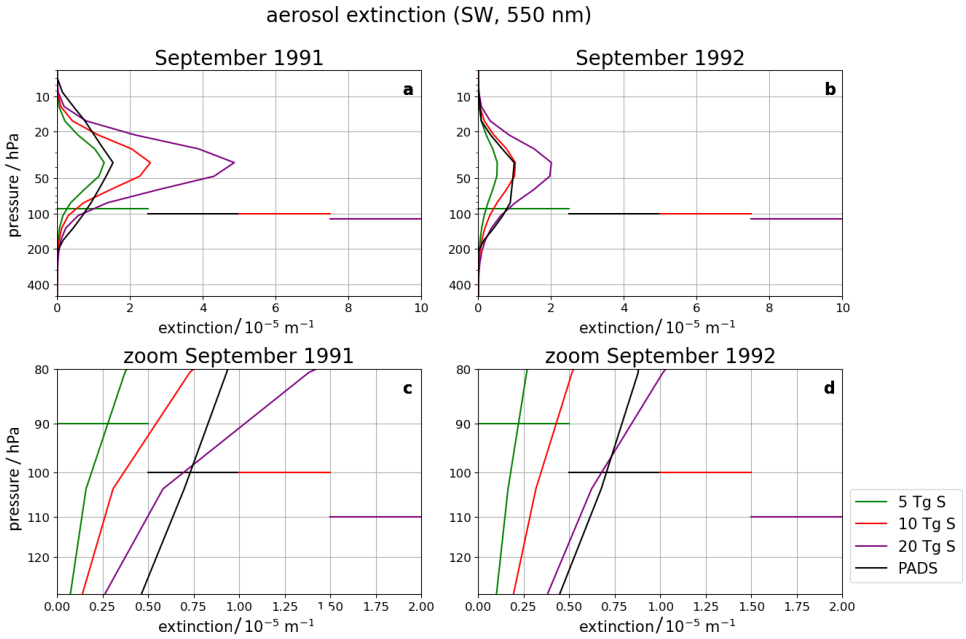

Figure 36: Tropical average of the aerosol extinction profile in the 550 nm solar waveband for the EVA forcing corresponding to 5 Tg S, 10 Tg S and 20 Tg S as well as the PADS forcing for the Mt. Pinatubo eruption.

A.10 APPENDIX E: SWV FORCING - SW COMPONENT

Fig. 37 shows the very small contribution of the SW component to the total adjusted SWV forcing presented in Sect. A.3.6. The total forcing and its SW component for the cloudy sky case as discussed in Sect. A.3.6 is shown in Fig. 38.

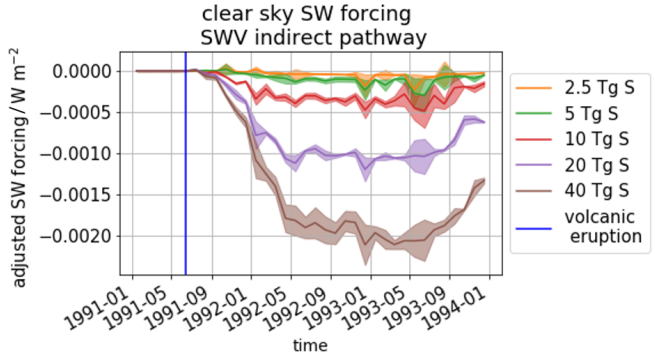

Figure 37: Time evolution of the SW-component to the adjusted clear sky forcing in the tropical region [-5,5]° latitude for the ensemble mean SWV increases caused by all eruption strengths. The blue line marks the eruptions time. The flux range originating from the standard deviations of the SWV profiles are plotted to visualize the signal range.

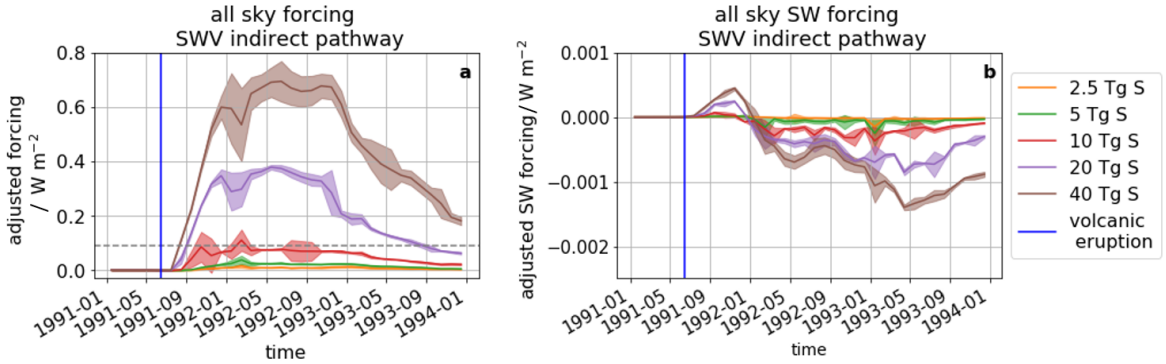

Figure 38: Time evolution of the (a) total (b) SW-component to the adjusted all sky forcing in the tropical region [-5,5]° latitude for the ensemble mean SWV increases caused by all eruption strengths. The blue line marks the eruptions time. The flux range originating from the standard deviations of the SWV profiles are plotted to visualize the signal range.

A.11 APPENDIX F: GLOBAL SPREAD OF THE STRATOSPHERIC WATER VAPOUR

Figure 39 shows the spread of the additional SWV around the globe as mentioned in the Discussion Sect. A.4.4.

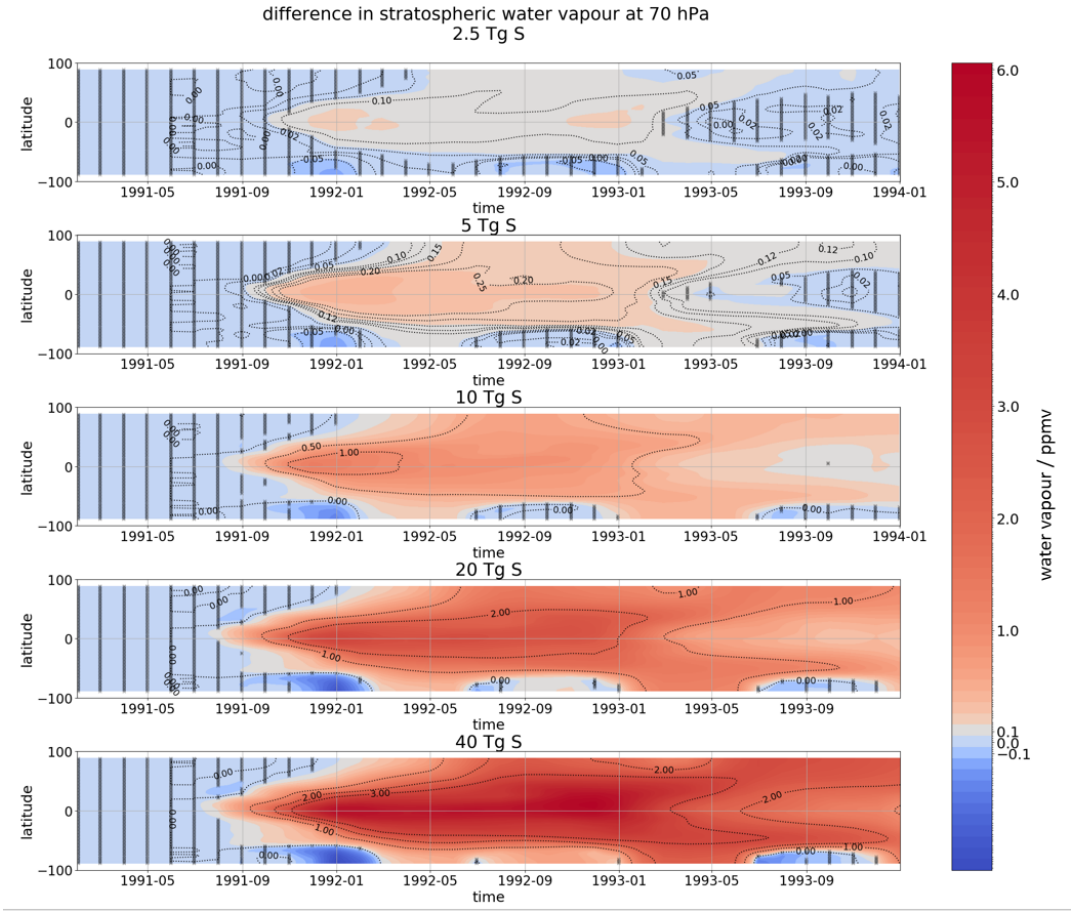

Figure 39: Difference in stratospheric water vapour content at 70 hPa as a function of time and latitude. Black crosses mark the regions of statistical significance of the data (Mann Whitney U Test at p=0.05).

Author contributions. CK, CT and HS designed the study. CK conducted the analysis/investigation and wrote the paper. SD contributed to the development of the methodology to calculate the SWV forcing with konrad and the interpretation of the corresponding result. AA set up the EVAens simulations. CT, SD and HS contributed to the writing of the paper.

Competing interests. The authors declare that they have no conflict of interest.

Acknowledgements. This research has been supported by the Deutsche Forschungsgemeinschaft (DFG) Research Unit VolImpact (FOR2820) within the projects VolDyn (TO 967/2-1) and VolClim (TI 344/2-1). SD and CK were/are members of the International Max Planck Research School (IMPRS). The data was processed using CDO (https://code.mpimet.mpg.de/projects/cdo/embedded/cdo.pdf) and using the computing facilities at the Deutsche Klimarechenzentrum (DKRZ). We thank Lukas Kluft for advising us on the usage of the 1D RCE model konrad.

B

THE SENSITIVITY OF MOISTURE FLUX PARTITIONING IN THE COLD-POINT TROPOPAUSE TO EXTERNAL FORCING

The work in this appendix has been submitted as:

Kroll, C. A., Fueglistaler, S., Schmidt, H., Kornblueh, L., Timmreck, C.: The sensitivity of moisture flux partitioning in the1 cold-point tropopause to external forcing, submitted to GRL, 2022

The sensitivity of moisture flux partitioning in the cold-point tropopause to external forcing

Clarissa Alicia Kroll[1,2], Stephan Fueglistaler[3], Hauke Schmidt[1], Luis Kornblueh[1], Claudia Timmreck[1]

[1]Max Planck Institute for Meteorology, Hamburg, Germany
[2]International Max Planck Research School on Earth System Modelling (IMPRS-ESM), Hamburg, Germany
[3]Program in Atmospheric and Oceanic Sciences, Princeton University, Princeton, NJ, USA

ABSTRACT

The dryness of the stratosphere is the result of air entering it through the cold tropical tropopause layer (TTL). However, our understanding of the moisture flux partitioning into water vapor and frozen hydrometeors is incomplete. This raises concerns regarding the ability of General Circulation Models (GCM) to accurately predict changes in stratospheric water vapour following perturbations in the radiative budget due to volcanic aerosol or stratospheric geoengineering. We present the first results using a global convection-resolving model to investigate the sensitivity of moisture fluxes within the TTL to an additional heating source. We address the question how the partitioning of moisture fluxes into water vapour and frozen hydrometeors changes under perturbations. The analysis reveals an exceptional resilience of the TTL, keeping the flux partitioning constant even at an average cold-point warming exceeding 8 K. In both simulations, water vapour contributes around 80 % of the moisture entering the stratosphere.

PLAIN LANGUAGE SUMMARY

The stratosphere is an extremely dry region since all moisture entering it from below has to pass the cold-point, a temperature minimum between troposphere and stratosphere. The very low temperatures lead to ice formation and sedimentation of moisture. Frozen water forming within convective clouds can pass this temperature barrier and be injected into the stratosphere, where temperatures increase again, promoting the melting and sublimation of ice crystals. However, little is known about the sensitivity of the split of moisture entering the stratosphere in frozen and non-frozen states of matter, especially under external influences, like heating by volcanic aerosol or stratospheric geoengineering efforts. Conventional simulations with General Circulation Models (GCMs) heavily rely on parameterizations and tuning, which leads to biases in their representation of convection. The emerging cloud-resolving simulations, which explicitly resolve the physical processes, offer the unique possibility to study moisture fluxes under external forcing while circumventing the downsides of parameterizations and tuning. In this work, the sensitivity of the partitioning of moisture fluxes into non-frozen and frozen components to external forcing in the form of an additional heating source is studied for the first time in global cloud-resolving simulations. The analysis reveals an unaltered flux partitioning even at an

average cold-point warming exceeding 8 K due to the additional heating source. In both, the control and perturbed simulations, water vapour contributes around 80 % of the moisture entering the stratosphere from below.

KEY POINTS:

- Slowly ascending water vapour dominates the stratospheric water vapour budget with a contribution of around 80 % in global convection-resolving simulations.
- The partitioning of stratospheric moisture fluxes into vapour and frozen hydrometeors remains stable even under large perturbations of the temperature profile.

B.1 INTRODUCTION

Stratospheric water vapour is important both as greenhouse gas (Forster and Shine, 2002, Solomon et al., 2010) as well as a reactant in stratospheric ozone chemistry (Ko et al., 2013). Volcanic eruptions or geoengineering interventions using sulfate aerosol perturb the stratospheric moisture budget. The model intercomparison projects for volcanoes and geoengineering, VolMIP (Zanchettin et al., 2016) and GeoMIP (Kravitz et al., 2015), both rely on GCM simulations. It is unclear how reliable their moisture budgets in the stratosphere are, particularly with respect to the frozen moisture content as they do not resolve deep convection. Consequently, the partitioning of moisture fluxes into water vapour and frozen hydrometeors and possible changes in the partitioning under corresponding perturbations are unclear. In this study we analyse how the phase partitioning of moisture fluxes into the stratosphere is changed under a strong perturbation of the tropical tropopause layer (TTL).
The stratosphere is extremely dry because virtually all moisture entering it from below has to pass the cold-point tropopause. This temperature minimum between the troposphere and stratosphere causes freeze drying of air on its upwards journey, restricting the vapour content entering the stratosphere (Brewer, 1949). The correlation between specific humidity entering the stratosphere and cold-point temperatures is also evident in the well known "atmospheric tape recorder" signal (Mote et al., 1996) formed by alternating bands of lower and higher specific humidity which are dictated by seasonal variations of the cold-point temperature. This correlation of cold-point temperature and specific humidity however, does not give information on the partitioning of moisture fluxes into large-scale upwelling water vapour and small-scale processes such as overshooting convection, in-cloud upwelling, and turbulent mixing. This adds uncertainty to estimates of the stratospheric water vapour budget as these small-scale processes have been recognized as a non negligible source of moisture (i.e. Fueglistaler et al., 2013, Dessler et al., 2016). Efforts to quantify the contribution of frozen hydrometeors often rely on an indirect quantification of the contribution of frozen moisture with the help of trajectory models. Corresponding estimates for the frozen contribution to the moisture flux can have a low bias if coarse scale wind fields are used. Reported values include Schoeberl et al., 2018 with 2 %, Ueyama et al., 2015 with 14 %, Ueyama et al., 2018 with 15 % and Smith et al., 2022

with 26 - 32 %.
The large spread of estimates demonstrates the difficulties in representing small-scale processes, especially in GCM model simulations. The situation is complicated by the fact that the convective parameterizations used in the current generation of GCMs do not reproduce all essential features of convection (i.e. Arakawa, 2004, Jones and Randall, 2011, Sherwood et al., 2014). For a description of the stratospheric water vapour budget an accurate representation of thin cirrus clouds and overshooting convection is essential however. Additionally some shortcomings of parametrization schemes are not immediately apparent as errors in process representation often compensate for each other (Hardiman et al., 2015).
Since computational resources are becoming more readily available and convection-resolving simulations are emerging, this problem can finally be alleviated by employing high resolution simulations which do not depend on convective parametrizations (i.e. Stevens et al., 2020). Based on the analysis of a single storm Dauhut et al., 2015 estimate a frozen moisture contribution of 18 %. Dauhut and Hohenegger, 2022 report a frozen moisture contribution of 11 %, which is the only estimate based on direct quantification using a global convection-resolving simulation. Additionally, Bolot and Fueglistaler, 2021 presented the first results based on observational data with a frozen contribution of around 18 %.
Apart from unperturbed scenarios, the explicitly resolved convection offers the possibility to predict the sensitivity of the TTL moisture fluxes to external forcing more reliably. The TTL sensitivity will be of special interest in a future where the TTL is affected by climate change and the potential employment of solar radiation management methods relying on sulfate aerosol in the lower stratosphere. We use this unprecedented opportunity and investigate the question how the moisture flux partitioning changes under perturbation. To address the question we set up a simulation pair consisting of a control and perturbed simulation in which the TTL is disturbed by introduction of a large heating source. This simulation pair allows us to address the question how the moisture fluxes into the stratosphere are partitioned between water vapour and frozen hydrometeors within one single framework. Additionally, the sensitivity experiment will shed light into changes of the flux partitioning at the cold-point tropopause under external perturbation. In order to get a clear signal we deliberately choose a strong forcing even if it may not be encountered in nature in this form.
In the following Section B.2 the model experiments and the analysis methods are described. Section B.3 summarizes the results of the study: first a quantification of the perturbation, followed by a description of the dependence of the water vapour content on the large-scale temperature field, and a discussion of the flux partitioning under perturbations. The results are discussed in Section B.4.

B.2 METHODS

B.2.1 *Model simulations*

B.2.1.1 *Model setup*

We use the atmosphere model of the Icosahedral Nonhydrostatic Weather and Climate Model (ICON) (Crueger et al., 2018; Giorgetta et al., 2018) and an approximately isotropic horizontal grid of 10 km. At this resolution the model can explicitly resolve deep convection and no convective parametrization is employed (Hohenegger et al., 2020,Vergara-Temprado et al., 2020). The model encompasses ninety vertical levels up to the model top at 75 km. The sponge layer reaches down to 44 km with continuously decreasing impact. We use the sapphire physics setup (Hohenegger et al., 2022) with the PSrad radiation parametrization (Pincus and Stevens, 2013) and the one moment "three category ice scheme" (an updated version of Baldauf et al., 2011), which considers six water categories: water vapour, cloud water, rain, cloud ice, graupel and snow.

B.2.1.2 *Experiments*

Two experiments are investigated: an unperturbed run (CTL) and a run perturbed by the introduction of an additional heating source in the TTL and lower stratosphere (PTB) with SSTs fixed to those of the control run. Both CTL and PTB run in perpetual January 1^{st} 2020 mode. In PTB, the additional heating source is realized by adding sulfate aerosol represented by two dimensional fields of zonal and monthly mean optical properties for all radiation bands of the model. The corresponding forcing fields were generated offline with the Easy Volcanic Aerosol (EVA) forcing generator (Toohey et al., 2016). EVA simulations were performed for an idealized equatorial volcanic eruption with 20 Tg S corresponding to twice the Mt. Pinatubo eruption. With the objective to generate a large tropopause perturbation the month with the highest near IR extinction was selected and set constant throughout the simulations. Our analysis is based on a 60 day average after 150 days of spin-up.

B.2.2 *Budget calculations*

In order to investigate the different contributions to the fluxes in the TTL a budget analysis of the states of matter relevant for the TTL, $i \in$ {water vapour, cloud ice, graupel, snow}, is performed. The changes in specific moisture content are described by the continuity equation

$$\frac{\partial \rho q_i}{\partial t} = \left(\frac{\partial \rho q_i u}{\partial x} + \frac{\partial \rho q_i v}{\partial y} + \frac{\partial \rho q_i w}{\partial z}\right) - \left(\frac{\partial \rho q_i w_{sedi,i}}{\partial z}\right) + \nabla(D \nabla \rho q_i) + \sigma_i, \quad (1)$$

where the first three terms on the right hand side of the equation describe the advective transport of the specific moisture q_i through the atmosphere of density ρ, the fourth term the flux due to the sedimentation velocity $w_{sedi,i}$, the fifth term the parameterized component of turbulent mixing with diffusion constant D, and σ_i accounts for the sources and sinks of moisture due to microphysical conversion

processes between water vapour, cloud ice, graupel and snow. We consider the respective vertical fluxes for all four tendencies. In order to evaluate the contribution of frozen hydrometeors to the total the fluxes of cloud ice, graupel, and snow are combined into one class hereafter.

Special care is taken to ensure mass conservation within the analysis. We circumvent issues arising from the mixing of variables calculated in different subsequent calculation steps, by adding advection and sedimentation fluxes, as well as the microphysical tendencies, as output streams to ICON allowing for a direct online calculation. The quality of our analysis also depends on the handling of the Courant-Friedrichs-Lewy criterion (Courant, 1928) and the choice of model surface on which the analysis is performed. Possible damping by the CFL criterion is reduced by using a quarter of the time step recommended for the used resolution. All calculations are performed on the native grid to ensure a closed budget.
ICON was used by Dauhut and Hohenegger, 2022 as well. Our 20 % contribution of frozen moisture (see Section B.3.3) lies between their estimates of 11 %, when only considering the deepest convection, and 29 %, when considering all hydrometeors. The calculations are not directly comparable though as they relied on a slightly different physics package and based their analysis on tendencies calculated offline and indirectly inferring the frozen moisture contribution, rather than directly calculating fluxes online as in our study.

B.2.3 *Choice of reference height*

The moisture budget calculation is carried out at the reference level of the cold-point tropopause. The latter is defined here as the lowest temperature between troposphere and stratosphere on height levels of around 500 m - 700 m spacing in the TTL. Any reference to the tropopause in the text hereafter consequently refers to the average cold-point tropopause.

B.3 RESULTS

B.3.1 *Quantifying the perturbation*

Figure 40 shows the inner tropical (potential) temperature and lapse rate profiles of the Control (CTL, blue) and Perturbed (PTB, red) simulations. The effects of the heating start to take effect at a height of around 12.5 km, but are most prominent in the TTL and lower stratosphere. Table 6 summarizes the changes in the physical parameters of CTL and PTB relevant for this study: The cold-point tropopause height is shifted downwards by 1.1 km and the mean cold-point tropopause temperature rises by 8.9 K. The increases in saturation specific humidity caused by the elevated cold-point temperatures enhance the specific humidity values at the cold-point by more than 200 %. To put these values in context, both the changes in cold-point temperature and specific humidity, are between three and four times larger than the amplitudes of their seasonal variations at the cold-point tropopause (i.e. Seidel et al., 2001).

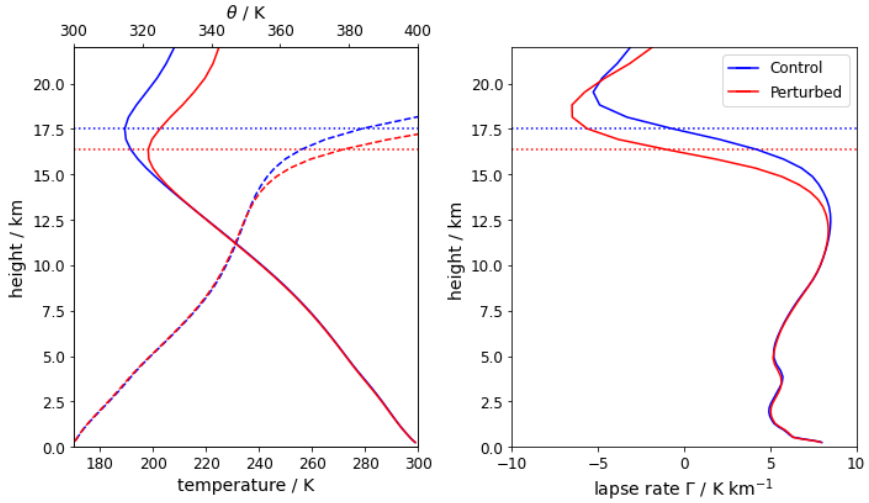

Figure 40: Left panel: temperature (solid line) and potential temperature profile (θ, dashed line). Right panel: lapse rate profile for temperature. An average over the inner tropical region between [-5,5]°N is taken for both plots. Control is shown in blue, Perturbed in red. The dotted line indicates the height of the cold-point tropopause.

Table 6: Two-monthly average [-5,5]°N tropical cold-point tropopause height, temperature, 10^{th} percentile temperature and specific humidity in the control and perturbed simulations.

	CTL	PTB	Δ (PTB - CTL)
tropopause height [km]	17.5	16.4	-1.1
tropopause temperature [K]	189.3	198.2	+8.9
10^{th} percentile of tropopause temperature [K]	186.8	195.9	+9.2
tropopause water vapour [ppmv]	2.1	6.7	+4.6 (+ 219 %)

B.3.2 *Water vapour distribution at the cold-point tropopause*

Figure 41 visualizes the average water vapour at the cold-point for CTL (blue) and PTB (red) in relation to the temperature dependent saturation water vapour mixing ratio as implemented in ICON (Doms and Förstner, 2021). In PTB the average water vapour is circa three times higher than in CTL due to the cold-point warming. Nevertheless, the large-scale picture of the dependence of the average water vapour on the cold-point temperature remains unchanged. In line with previous studies, the model results show that the vapour at the cold point scales well with an equivalent frost point temperature. The water vapour at the cold point is dictated by the lowest temperatures in the inner tropics (Fueglistaler and Haynes, 2005). Here the 10^{th} percentile of cold-point temperatures in the region between [-5,5]°N describe the vapour values for CTL and PTB. For PTB, the estimate using the 10^{th} percentile of cold-point temperatures slightly exceeds (about 2.5 %) the model's water vapour mixing ratio. This discrepancy may be explained by an increase in the horizontal velocities at the cold-point tropopause (+14 %) and enhanced variability of the cold-point temperatures (± 4 %). Nevertheless, the correlation between saturation water

vapour mixing ratio and the 10^{th} percentile of cold-point temperatures remains a good indicator to estimate the average water vapour at the cold-point, also for the perturbed case. It is only shifted according to the 9 K ΔT of cold-point warming (compare Table 6). The 10^{th} percentile of cold-point temperatures in Control and Perturbed can consequently be seen as the equivalent frost point temperature of the TTL in this simulation.

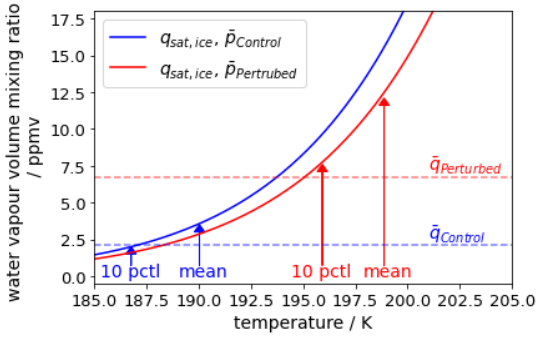

Figure 41: Two-months average water vapour mixing ratio at the mean cold-point height for CTL (blue) and PTB (red) in the inner tropics between [-5,5]°N, marked by horizontal dashed lines. The average water vapour values are compared against the expected saturation water vapour mixing ratio at the mean cold-point temperature and the 10^{th} percentile of cold-point temperatures for CTL and PTB, marked with arrows. The saturation mixing ratio above ice as function of temperature at the cold-point pressure as implemented in ICON (COSMO, Doms and Förstner, 2021) is plotted for CTL and PTB.

B.3.3 *Change in flux partitioning*

Figure 42 shows the contribution from water vapour and frozen hydrometeors to the total flux for CTL (blue) and PTB (red)[1]. A first inspection of the CTL data reveals that frozen moisture flux of 0.0006 kg m^{-2} $year^{-1}$ contributes with around 20 %, a value which is well within the value spread reported in previous studies. The leading order term however is the water vapour flux of 0.0021 kg m^{-2} $year^{-1}$ contributing around 80 % to the total flux. The computed water vapour and water vapour flux at the cold point is also consistent observations in January (Fueglistaler et al., 2009, Sioris et al., 2016a). In PTB the water vapour flux is enhanced to 0.0081 kg m^{-2} $year^{-1}$ by a factor of four. However, the flux of frozen hydrometeors is increased by almost the same factor to 0.0023 kg m^{-2} $year^{-1}$. This means that the partitioning into fluxes of water vapour and frozen hydrometeors remains virtually unchanged despite the strong perturbation of the TTL in the PTB experiment.

B.4 DISCUSSION

We used ICON, a convection-resolving global model, to study the sensitivity of the moisture flux partitioning in the TTL to external forcing. The base simulation is in

1 The plot shows unrounded values, the calculated percentage changes therefore deviate slightly from those calculated based on the values reported in the text.

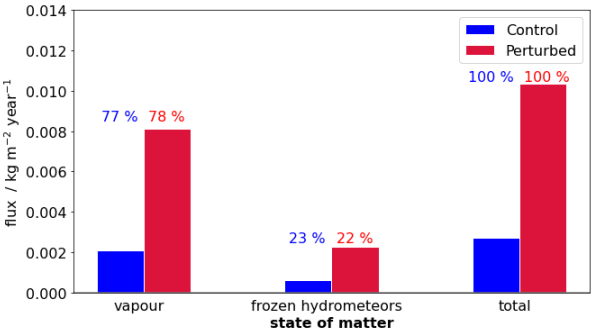

Figure 42: Two-month average of the moisture fluxes at the average cold-point tropopause in the region between [-30,30]°N. The contribution of water vapour and frozen hydrometeors is shown along with the total. The control simulation is shown in blue, the perturbed simulations in red. Above the bars the corresponding percentage share to the total moisture flux is shown.

line with previously published data on moisture flux partitioning in non-frozen and frozen contributions. The analysis shows that in response to the strong tropopause perturbation, the moisture flux partitioning remains almost constant - even for a very strong perturbation with a change of cold-point temperatures by over 8 K. The constant share of frozen moisture to the total moisture entering the stratosphere underlines the character of the TTL as a region which is set based by a balance between radiative-dynamically induced temperature changes in the higher lying regions and temperature changes due to convective-radiative-dynamical process from below (Fueglistaler et al., 2009).

The result of roughly constant partitioning may surprise at first, but is consistent with a trajectory model based climate change study (Smith et al., 2022), where ice content was explicitly tracked. Studies analyzing the annual cycle (Liu et al., 2010, Fueglistaler et al., 2013) also found a constant frozen hydrometeor contribution, which they calculated from the offset between observed and modelled water vapour values. Here the frozen moisture flux is calculated directly. The agreement on the constant partitioning despite the different analysis method indicates that the robustness of the moisture flux partitioning in the TTL is not exclusive to a perturbation in form of an heating layer, as in our volcanic or geoengineering scenarios, but has also holds for other disturbances such as seasonal variations and climate change. The constant partitioning of moisture fluxes into frozen and non-frozen states of matter demonstrates that the large-scale temperature field determines both moisture fluxes entering the stratosphere for these various perturbations. Frozen and non-frozen moisture follows the Clausius Clapeyron scaling. Consequently, the total flux can be thought of as a water vapour flux controlled by an equivalent frost point temperature, whereas the flux of frozen hydrometeors is given by an additional constant temperature offset ΔT. Based on a 12 % increase of specific humidity per Kelvin in the cold-point region (Kroll et al., 2021), this offset gives an estimate of the constant relative contribution of frozen moisture to the total budget.
The contribution of frozen moisture to the total stratospheric moisture budget is still largly uncertain, especially in the current generation of GCMs. The agreement on the constant partitioning between our direct quantification in a convection-resolving

framework and the indirect quantification in a framework relying on convective parametrization (Smith et al., 2022) is therefore encouraging. Provided that GCMs can correctly represent (changes in) the cold-point temperature, the ΔT offset would also offer the possibility to improve currently used parametrization schemes. As the current generation of CMIP6 models (Garfinkel et al., 2021) still show a cold-point temperature spread of around 10 K, this approach would require improvements in the parametrizations of some models. If the underlying problem is found to be capturing the influence of convective heating in the TTL, the usage of convection-resolving models might be inevitable.

In summary, the result of the analysis shows that the moisture flux partitioning at the cold-point tropopause is robust, even under large perturbations. The explicitly resolved convection in our numerical model increases the confidence that this result is not a model artifact. The actual numbers presented in this study may be model specific, further constraints of the percental contribution of frozen moisture to the total flux based on observations are needed.

OPEN RESEARCH

The ICON model is available to individuals (https://mpimet.mpg.de/en/science/modeling-with-icon/code-availability). Simulations were carried out with the code version in branch icon-aes-CaVE-test005. All data shown in the figures and scripts needed to generate the figures in this work available under https://hdl.handle.net/21.11116/0000-000B-5D17-4.

ACKNOWLEDGMENTS

This research has been supported by the Deutsche Forschungsgemeinschaft (DFG) Research Unit VolImpact (FOR2820, grant:.398006378) within the projects VolDyn and VolClim. CK is a member of the International Max Planck Research School (IMPRS). Her research stay at Princeton was supported by the Fueglistaler group. HS acknowledges support from the SOCTOC project of the BMBF research initiative ROMIC2. The data was processed using CDO (`https://code.mpimet.mpg.de/projects/cdo/embedded/cdo.pdf`) and the resources at the Deutsche Klimarechenzentrum (DKRZ) granted by its Scientific Steering Committee (WLA) under project ID bb1093. For parts of the analysis the open source libraries "easyd" by M. Roßmy (`https://github.com/matti-82/easyd`) and "netcdfd" by J. Colvin (`https://code.dlang.org/packages/netcdf`) were employed. We thank H. Franke, A. Schneidereit, U. Niemeier, J. Bao as well as L. Kluft for discussing different aspects of this work with the authors.

C

THE IMPACT OF VOLCANIC AEROSOL HEATING ON TURBULENT MIXING, IN-CLOUD UPWELLING AND CONVECTION IN THE TROPICAL TROPOPAUSE LAYER

In this appendix some additional figures for the analysis of a manuscript in preparation are shown:

Kroll, C. A., Fueglistaler, S., Schmidt, H., Kornblueh, L., Timmreck, C.: The impact of heating in the tropical tropopause layer on turbulent mixing, in-cloud upwelling, and convection, in preparation for ACP, 2023

The impact of heating in the TTL on turbulent mixing, in-cloud upwelling, and convection

Clarissa Alicia Kroll[1,2], Stephan Fueglistaler[3], Hauke Schmidt[1], Luis Kornblueh[1], Claudia Timmreck[1]

[1]Max Planck Institute for Meteorology, Hamburg, Germany
[2]International Max Planck Research School on Earth System Modelling (IMPRS-ESM), Hamburg, Germany
[3]Program in Atmospheric and Oceanic Sciences, Princeton University, Princeton, NJ, USA

In the following some figures and analysis results are presented which are part of the above manuscript in preparation and were not presented in Section 2.3.

C.1 MODEL SETUP

Figure 43 shows the distribution of volcanic aerosols. Table 7 gives information on the volcanic aerosol forcing.

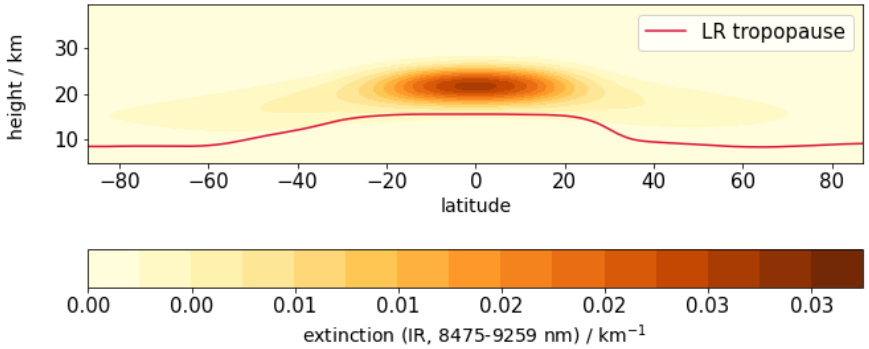

Figure 43: Zonal mean distribution of the volcanic aerosols in the volcanically perturbed simulations (Vol) visualized using the extinction values in the strongest IR waveband ([8475-9259] nm). Indication of the lapse rate tropopause height (LR tropopause) with a red line.

Table 7: Volcanic aerosol forcing as calculated using the double radiation call (DR call) for all sky and clear sky conditions as well as the estimates according to Marshall et al., 2020, and Hansen et al., 2005.

forcing	F_i DR call all sky	F_i DR call clear sky	F_i Marshall et al.	F_a Hansen et al.
forcing / Wm^{-2}	-9.15	-13.80	-12.88	-10.70

C.2 HEIGHT DEPENDENT MOISTURE DISTRIBUTION

Changes in moisture distribution and their dependence on the chosen vertical coordinate are visualized in Figure 44 and Figure 45.

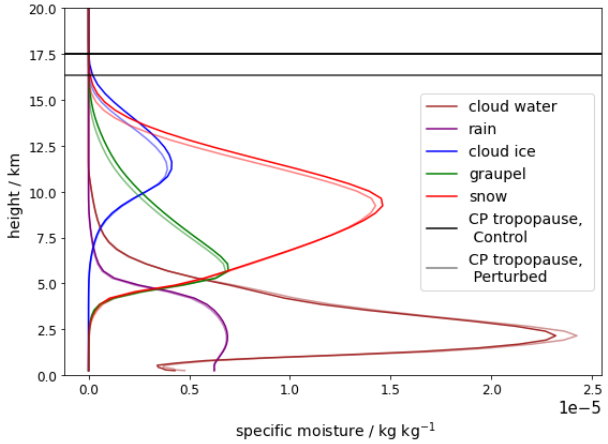

Figure 44: Two-months average of the atmospheric moisture as a function of height for all states of matter in the region between [-30,30]° N of Control and Perturbed. The height of the CP tropopause for Control is shown in black, for Perturbed in grey.

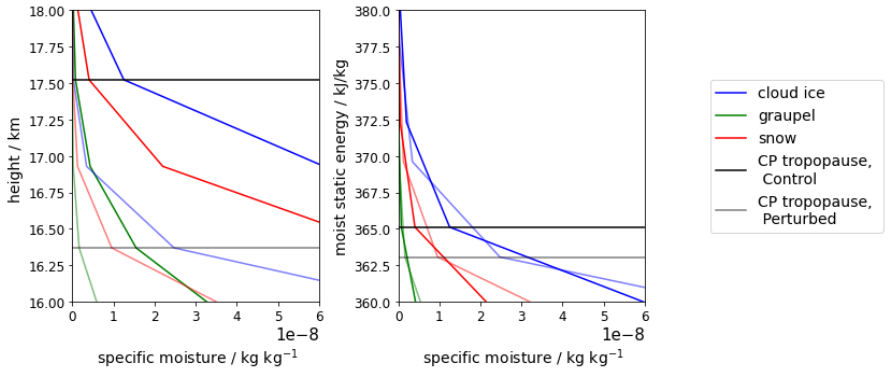

Figure 45: Two-months average of the atmospheric moisture fluxes as a function of height and moist static energy for all states of matter in the region between [-30,30]° N of Control and Perturbed. The height of the CP tropopause for Control is shown in black, for Perturbed in grey.

C.3 HEIGHT DEPENDENT MOISTURE FLUXES

The height dependent moisture fluxes for Control are shown in Figure 46, which also offers two close-ups into higher altitudes and the TTL. Figure 47 visualizes the moisture fluxes for all moisture forms relevant at the LR and CP tropopause for Control and Perturbed.

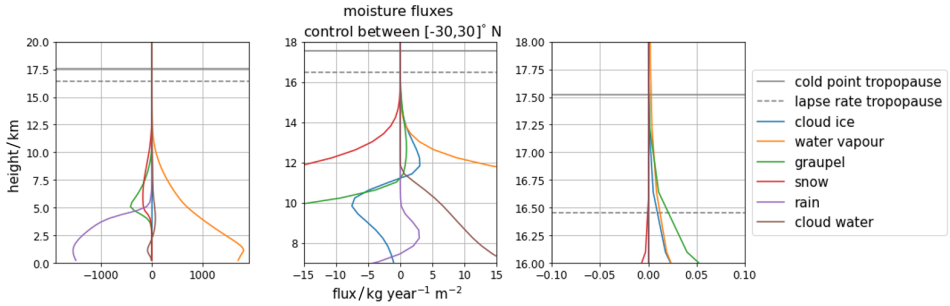

Figure 46: Two-months average of the atmospheric moisture fluxes as a function of height for all states of matter in the region between [-30,30]° N of Control. For each state of matter the contribution of advection is considered; for all states of matter, except for water vapour and cloud water, sedimentation is subtracted, and in the case of lightest contributors, cloud ice, cloud water and water vapour, turbulent mixing is taken into account in the budget. From left to right the zoom into the TTL is increased. The LR tropopause is indicated with a dashed, the CP tropopause with a solid, line. Positive fluxes are directed upwards, negative fluxes downwards.

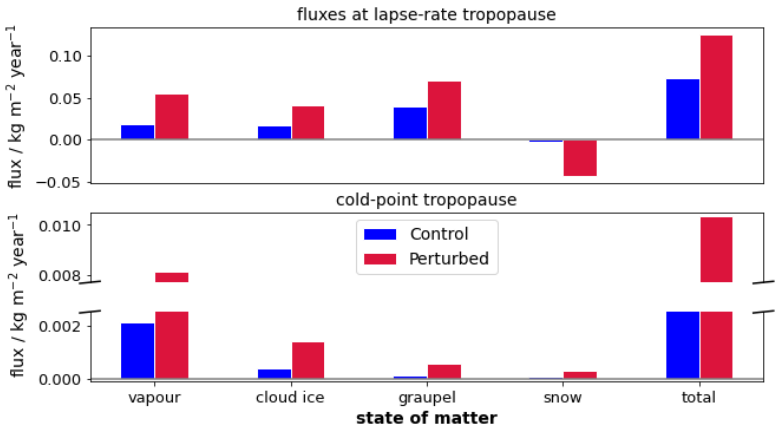

Figure 47: Average net moisture flux through the lapse-rate (upper panel) and cold-point tropopause (lower panel) due to the states of matter relevant for the TTL, as well as their total, between [-30,30]° N. Control is shown in blue, the corresponding fluxes for the perturbed simulation in red.

C.4 CONVECTION IN ICON

Fig. 48 and Fig. 49 give an overview over important characteristics of the convective cells selected during the LNB calculations described above. For all figures one specific convective event was selected without spatial or temporal averaging.

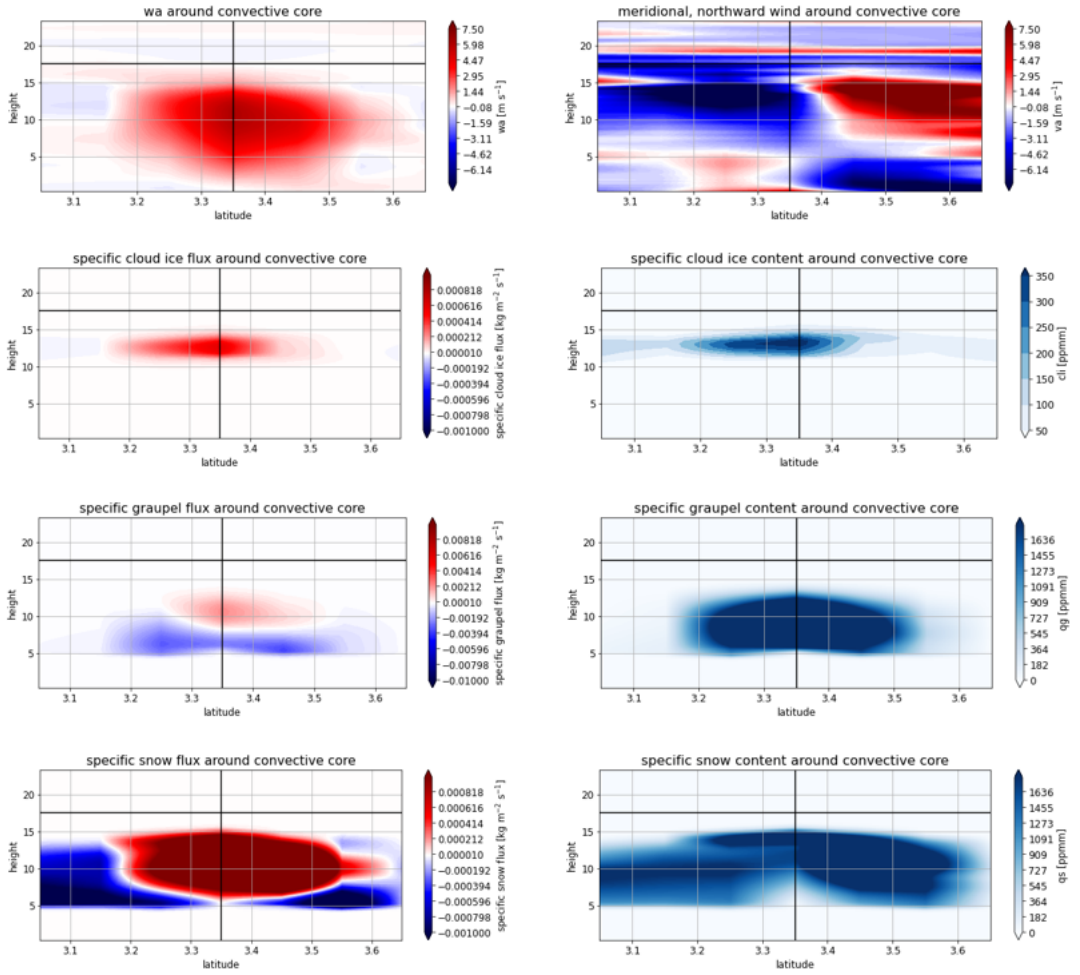

Figure 48: Example snapshot of one single specific convective cell. Display of the vertical wind, meridional northward wind, cloud ice flux, specific cloud ice, graupel flux, specific graupel, snow flux, and specific snow content in a single convective event. The cell which was used to detect the convective event is marked with a vertical black line, the cold point height is denoted with a black line.

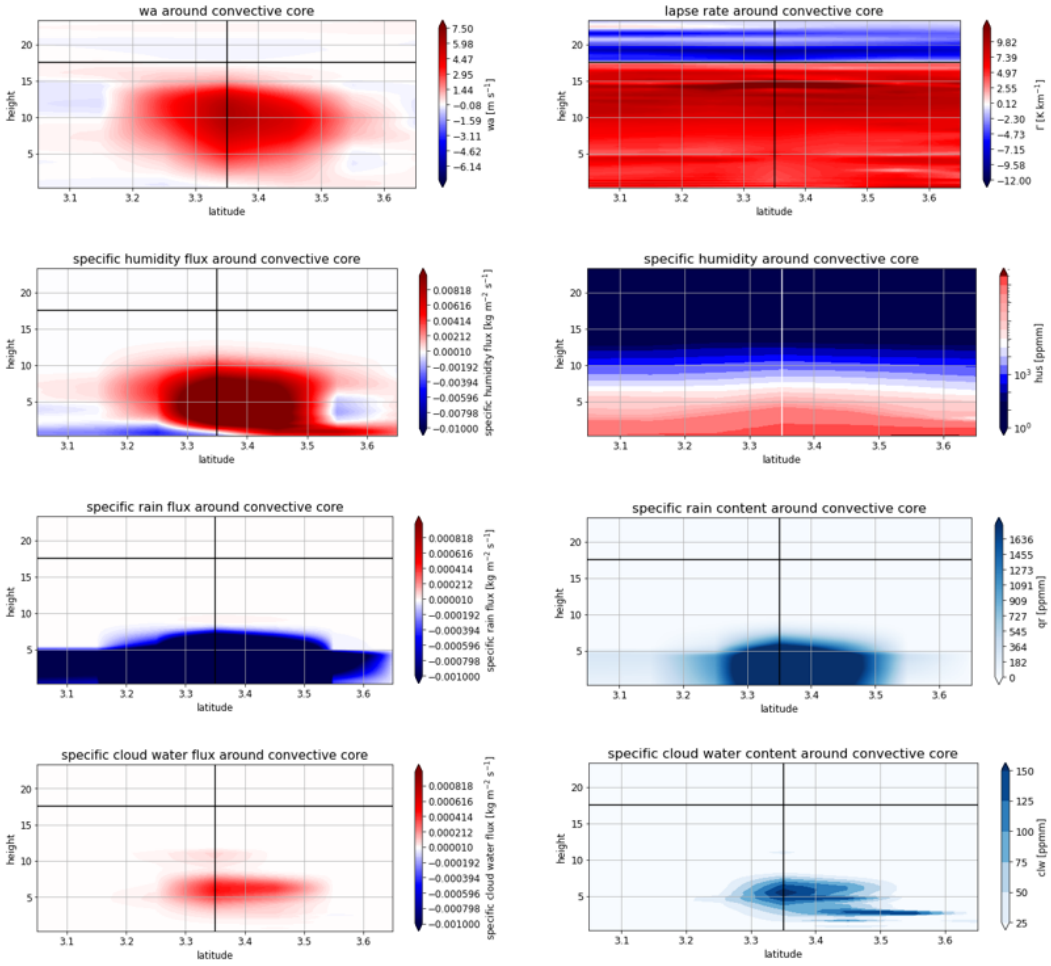

Figure 49: Example snapshot of one single specific convective cell. Display of the vertical wind, temperature lapse rate, water vapour flux, specific humidity, rain flux, specific rain, cloud water flux, and specific cloud water content in a single convective event. The cell which was used to detect the convective event is marked with a vertical black line, the cold point height is denoted with a black line.

C.5 SUBLIMATION ABOVE THE COLD POINT TROPOPAUSE

Table 8 lists the microphysical conversions integrated above the CP tropopause giving insight of sublimation and condensation processes above the CP.

Table 8: Two-monthly average of vertically integrated microphysical tendencies for the states of matter relevant for the TTL between [-30,30]°N evaluated one level above the average CP tropopause. Negative values denote loss of the corresponding state of matter, positive creation of the respective state of matter.

integrated pure microphysical tendency / 10^{-10} kg m^{-2} s^{-1}	Control	Perturbed
water vapour	0.0353	0.2580
cloud ice	-0.0214	-0.1916
graupel	-0.0053	-0.0186
snow	-0.0075	-0.0477

Angell, J. K. (1997). "Stratospheric warming due to Agung, El Chichón, and Pinatubo taking into account the quasi-biennial oscillation." In: *Journal of Geophysical Research: Atmospheres* 102.D8, pp. 9479–9485. DOI: https://doi.org/10.1029/96JD03588. URL: https://agupubs.onlinelibrary.wiley.com/doi/abs/10.1029/96JD03588.

Angevine, Wayne M., Hongli Jiang, and Thorsten Mauritsen (July 2010). "Performance of an Eddy Diffusivity–Mass Flux Scheme for Shallow Cumulus Boundary Layers." EN. In: *Monthly Weather Review* 138.7. Publisher: American Meteorological Society Section: Monthly Weather Review, pp. 2895–2912. ISSN: 1520-0493, 0027-0644. DOI: 10.1175/2010MWR3142.1. URL: https://journals.ametsoc.org/view/journals/mwre/138/7/2010mwr3142.1.xml (visited on 06/08/2021).

Arakawa, Akio (2004). "The Cumulus Parameterization Problem: Past, Present, and Future." In: *Journal of Climate* 17, pp. 2493–2525.

Atlas, R. and C. Bretherton (2022). "Aircraft observations of gravity wave activity and turbulence in the tropical tropopause layer: prevalence, influence on cirrus and comparison with global-storm resolving models." In: *Atmospheric Chemistry and Physics Discussions* 2022, pp. 1–30. DOI: 10.5194/acp-2022-491. URL: https://acp.copernicus.org/preprints/acp-2022-491/.

Azoulay, Alon, Hauke Schmidt, and Claudia Timmreck (2020). "The Arctic polar vortex response to volcanic forcing of different strengths." In: *J. Geophys. Res., submitted*.

Baldauf, Michael et al. (2011). "Operational Convective-Scale Numerical Weather Prediction with the COSMO Model: Description and Sensitivities." In: *Monthly Weather Review* 139.12. Place: Boston MA, USA Publisher: American Meteorological Society, pp. 3887 –3905. DOI: 10.1175/MWR-D-10-05013.1. URL: https://journals.ametsoc.org/view/journals/mwre/139/12/mwr-d-10-05013.1.xml.

Bardeen, C. G. et al. (2013). "Improved cirrus simulations in a general circulation model using CARMA sectional microphysics." en. In: *Journal of Geophysical Research: Atmospheres* 118.20, pp. 11,679–11,697. ISSN: 2169-8996. DOI: 10.1002/2013JD020193. URL: https://agupubs.onlinelibrary.wiley.com/doi/abs/10.1002/2013JD020193 (visited on 06/18/2021).

Bekki, S. (1995). "Oxidation of volcanic SO 2 : A sink for stratospheric OH and H 2 O." In: *Geophysical Research Letters* 22.8, pp. 913–916. ISSN: 00948276. DOI: 10.1029/95GL00534.

Bolot, Maximilien and Stephan Fueglistaler (2021). "Tropical Water Fluxes Dominated by Deep Convection Up to Near Tropopause Levels." en. In: *Geophysical Research Letters* 48.4, e2020GL091471. ISSN: 1944-8007. DOI: 10.1029/2020GL091471. URL: https://agupubs.onlinelibrary.wiley.com/doi/abs/10.1029/2020GL091471 (visited on 06/08/2021).

Boucher, Olivier, Christoph Kleinschmitt, and Gunnar Myhre (2017). "Quasi-Additivity of the Radiative Effects of Marine Cloud Brightening and Stratospheric Sulfate Aerosol Injection." In: *Geophysical Research Letters* 44.21, pp. 11,158–11,165. DOI:

https://doi.org/10.1002/2017GL074647. URL: https://agupubs.onlinelibrary.wiley.com/doi/abs/10.1002/2017GL074647.

Brewer, A. W. (1949). "Evidence for a world circulation provided by the measurements of helium and water vapour distribution in the stratosphere." In: *Quarterly Journal of the Royal Meteorological Society* 75.326, pp. 351–363. ISSN: 00359009. DOI: 10.1002/qj.49707532603.

Brinkop, Sabine and Erich Roeckner (1995). "Sensitivity of a general circulation model to parameterizations of cloud–turbulence interactions in the atmospheric boundary layer." en. In: *Tellus A* 47.2, pp. 197–220. ISSN: 1600-0870. DOI: 10.1034/j.1600-0870.1995.t01-1-00004.x. URL: https://onlinelibrary.wiley.com/doi/abs/10.1034/j.1600-0870.1995.t01-1-00004.x (visited on 06/08/2021).

Case, P. A., K. Tsigaridis, and A. N. LeGrande (2015). "The Effect of Stratospheric Water Vapor in Large Volcanic Eruptions on Climate and Atmospheric Composition." In: *AGU Fall Meeting, San Fracisco, California, 14-18 December 2015, A51N-0270*. Journal Abbreviation: AGU 2015, presented on Friday, 18 December 2015. AGU. URL: https://agu.confex.com/agu/fm15/meetingapp.cgi/Paper/79947.

Clyne, M. et al. (2021). "Model physics and chemistry causing intermodel disagreement within the VolMIP-Tambora Interactive Stratospheric Aerosol ensemble." In: *Atmospheric Chemistry and Physics* 21.5, pp. 3317–3343. DOI: 10.5194/acp-21-3317-2021. URL: https://acp.copernicus.org/articles/21/3317/2021/.

Coffey, M. T. (1996). "Observations of the impact of volcanic activity on stratospheric chemistry." In: *Journal of Geophysical Research: Atmospheres* 101.D3, pp. 6767–6780. ISSN: 01480227.

Considine, D. B., J. E. Rosenfield, and E. L. Fleming (2001). "An interactive model study of the influence of the Mount Pinatubo aerosol on stratospheric methane and water trends." In: *Journal of Geophysical Research: Atmospheres* 106.D21, pp. 27711–27727. ISSN: 01480227. DOI: 10.1029/2001JD000331.

Corti, Thierry et al. (July 2006). "The impact of cirrus clouds on tropical troposphere-to-stratosphere Transport." In: *Atmospheric Chemistry and Physics* 6. DOI: 10.5194/acp-6-2539-2006.

Courant K.; Lewy, H. R.; Friedrichs (1928). "Über die partiellen Differenzengleichungen der mathematischen Physik." In: 100, pp. 32–74. DOI: https://doi.org/10.1007/BF01448839.

Crueger, T. et al. (2018). "ICON-A, The Atmosphere Component of the ICON Earth System Model: II. Model Evaluation." In: *Journal of Advances in Modeling Earth Systems* 10.7, pp. 1638–1662. ISSN: 19422466. DOI: 10.1029/2017MS001233.

Dacie, Sally (2020). "Using simple models to understand changes in the tropical mean atmosphere under warming." PhD thesis. Hamburg: University of Hamburg. URL: http://hdl.handle.net/21.11116/0000-0006-B380-E.

Dacie, Sally et al. (2019). "A 1D RCE Study of Factors Affecting the Tropical Tropopause Layer and Surface Climate." In: *Journal of Climate* 32.20, pp. 6769–6782. ISSN: 0894-8755. DOI: 10.1175/JCLI-D-18-0778.1.

Dauhut, Thibaut and Cathy Hohenegger (2022). "The Contribution of Convection to the Stratospheric Water Vapor: The First Budget Using a Global Storm-Resolving Model." In: *Journal of Geophysical Research: Atmospheres* 127.5, e2021JD036295. DOI: https://doi.org/10.1029/2021JD036295. URL: https://agupubs.onlinelibrary.wiley.com/doi/abs/10.1029/2021JD036295.

Dauhut, Thibaut et al. (2015). "Large-eddy simulations of Hector the convector making the stratosphere wetter." In: *Atmospheric Science Letters* 16.2, pp. 135–140. ISSN: 1530261X. DOI: 10.1002/asl2.534.

Dauhut, Thibaut et al. (2018). "The Mechanisms Leading to a Stratospheric Hydration by Overshooting Convection." In: *Journal of the Atmospheric Sciences* 75.12. Place: Boston MA, USA Publisher: American Meteorological Society, pp. 4383–4398. DOI: 10.1175/JAS-D-18-0176.1. URL: https://journals.ametsoc.org/view/journals/atsc/75/12/jas-d-18-0176.1.xml.

Davis, S. M. et al. (2016). "The Stratospheric Water and Ozone Satellite Homogenized (SWOOSH) database: a long-term database for climate studies." In: *Earth System Science Data* 8.2, pp. 461–490. DOI: 10.5194/essd-8-461-2016. URL: https://essd.copernicus.org/articles/8/461/2016/.

Davis, Sean M. et al. (2017). "Assessment of upper tropospheric and stratospheric water vapor and ozone in reanalyses as part of S-RIP." In: *Atmospheric Chemistry and Physics* 17.20, pp. 12743–12778. DOI: 10.5194/acp-17-12743-2017.

Dee, D. P. et al. (2011). "The ERA-Interim reanalysis: configuration and performance of the data assimilation system." In: *Quarterly Journal of the Royal Meteorological Society* 137.656, pp. 553–597. ISSN: 00359009. DOI: 10.1002/qj.828.

Dessler, A. E. et al. (2013). "Stratospheric water vapor feedback." In: *Proceedings of the National Academy of Sciences of the United States of America* 110.45, pp. 18087–18091. DOI: 10.1073/pnas.1310344110.

Dessler, A. E. et al. (2014). "Variations of stratospheric water vapor over the past three decades." In: *Journal of Geophysical Research: Atmospheres* 119.22, pp. 12,588–12,598. ISSN: 01480227. DOI: 10.1002/2014JD021712.

Dessler, A.E. et al. (Mar. 2016). "Transport of ice into the stratosphere and the humidification of the stratosphere over the 21st century." In: *Geophysical research letters* 43.5, pp. 2323–2329. ISSN: 0094-8276. DOI: 10.1002/2016GL067991. URL: https://www.ncbi.nlm.nih.gov/pmc/articles/PMC5854491/ (visited on 06/09/2021).

Diallo, M. et al. (2017). "Significant Contributions of Volcanic Aerosols to Decadal Changes in the Stratospheric Circulation." In: *Geophysical Research Letters* 44.20, pp. 10,780–10,791. ISSN: 00948276. DOI: 10.1002/2017GL074662.

Dobson, Gordon Miller Bourne, A. W. Brewer, and B. M. Cwilong (1946). "Bakerian Lecture: Meteorology of the lower stratosphere." In: *Proceedings of the Royal Society of London. Series A. Mathematical and Physical Sciences* 185.1001. _eprint: https://royalsocietypublishing.org/doi/pdf/10.1098/rspa.1946.0010, pp. 144–175. DOI: 10.1098/rspa.1946.0010. URL: https://royalsocietypublishing.org/doi/abs/10.1098/rspa.1946.0010.

Domeisen, Daniela et al. (2020a). "The Role of the Stratosphere in Subseasonal to Seasonal Prediction: 1. Predictability of the Stratosphere." In: *Journal of Geophysical Research: Atmospheres* 125.2, e2019JD030920. DOI: https://doi.org/10.1029/2019JD030920. URL: https://agupubs.onlinelibrary.wiley.com/doi/abs/10.1029/2019JD030920.

— (2020b). "The Role of the Stratosphere in Subseasonal to Seasonal Prediction: 2. Predictability Arising From Stratosphere-Troposphere Coupling." In: *Journal of Geophysical Research: Atmospheres* 125.2, e2019JD030923. DOI: https://doi.org/10.1029/2019JD030923. URL: https://agupubs.onlinelibrary.wiley.com/doi/abs/10.1029/2019JD030923.

Doms, G and E.; Herzog H.-J.; Mironov D. Raschendorfer M. Reinhardt T.; Ritter B. Schroding R. Schulz J.P. Vogel G. Förstner J.; Heise (Sept. 2021). *A Description of the Nonhydrostatic Regional COSMO-Model Part II Physical Parameterizations*. Tech. rep. COSMO 6.00. Deutscher Wetterdienst. URL: http://www.cosmo-model.org/content/model/documentation/core/cosmo_physics_6.00.pdf (visited on 11/08/2022).

Driscoll, Simon et al. (2012). "Coupled Model Intercomparison Project 5 (CMIP5) simulations of climate following volcanic eruptions." In: *Journal of Geophysical Research: Atmospheres* 117.D17, n/a–n/a. ISSN: 01480227. DOI: 10.1029/2012JD017607.

Fels, S. B. et al. (1980). "Stratospheric Sensitivity to Perturbations in Ozone and Carbon Dioxide: Radiative and Dynamical Response." In: *Journal of Atmospheric Sciences* 37.10, pp. 2265–2297. DOI: 10.1175/1520-0469(1980)037<2265:SSTPIO>2.0.CO;2.

Forster, Piers M. et al. (2016). "Recommendations for diagnosing effective radiative forcing from climate models for CMIP6." In: *Journal of Geophysical Resarch: Atmosphere* 121.20, pp. 12460–12475. DOI: 10.1002/2016JD025320.

Forster, Piers M. de F. and K. P. Shine (2002). "Assessing the climate impact of trends in stratospheric water vapor." In: *Geophysical Research Letters* 29.6, pp. 10–1–10–4. ISSN: 00948276. DOI: 10.1029/2001GL013909.

Fueglistaler, S. (2012). "Stepwise changes in stratospheric water vapor?" In: *Journal of Geophysical Research: Atmospheres* 117.D13. DOI: https://doi.org/10.1029/2012JD017582. URL: https://agupubs.onlinelibrary.wiley.com/doi/abs/10.1029/2012JD017582.

Fueglistaler, S. and P. H. Haynes (2005). "Control of interannual and longer-term variability of stratospheric water vapor." In: *Journal of Geophysical Research: Atmospheres* 110.D24. DOI: https://doi.org/10.1029/2005JD006019. URL: https://agupubs.onlinelibrary.wiley.com/doi/abs/10.1029/2005JD006019.

Fueglistaler, S. et al. (2009). "Tropical tropopause layer." In: *Reviews of Geophysics* 47.1, p. 1606. ISSN: 87551209. DOI: 10.1029/2008RG000267.

Fueglistaler, S. et al. (2013). "The relation between atmospheric humidity and temperature trends for stratospheric water." In: *Journal of Geophysical Research: Atmospheres* 118.2, pp. 1052–1074. ISSN: 01480227. DOI: 10.1002/jgrd.50157.

Fujiwara, Masatomo et al. (2017). "Introduction to the SPARC Reanalysis Intercomparison Project (S-RIP) and overview of the reanalysis systems." In: *Atmospheric Chemistry and Physics* 17.2, pp. 1417–1452. DOI: 10.5194/acp-17-1417-2017.

Fujiwara, Masatomo et al. (2022). *SPARC Reanalysis Intercomparison Project (S-RIP) Final Report*. Tech. rep. 10. doi: 10.17874/800dee57d13. URL: www.sparc-climate.org/publications/sparc-reports.

Garcia, Rolando R., William J. Randel, and Douglas E. Kinnison (2011). "On the Determination of Age of Air Trends from Atmospheric Trace Species." In: *Journal of the Atmospheric Sciences* 68.1. Place: Boston MA, USA Publisher: American Meteorological Society, pp. 139 –154. DOI: 10.1175/2010JAS3527.1. URL: https://journals.ametsoc.org/view/journals/atsc/68/1/2010jas3527.1.xml.

Garfinkel, C. I. et al. (2017). "Time-varying changes in the simulated structure of the Brewer–Dobson Circulation." In: *Atmospheric Chemistry and Physics* 17.2, pp. 1313–1327. DOI: 10.5194/acp-17-1313-2017. URL: https://acp.copernicus.org/articles/17/1313/2017/.

Garfinkel, C. I. et al. (2021). "Influence of the El Niño–Southern Oscillation on entry stratospheric water vapor in coupled chemistry–ocean CCMI and CMIP6 models." In: *Atmospheric Chemistry and Physics* 21.5, pp. 3725–3740. DOI: 10.5194/acp-21-3725-2021. URL: https://acp.copernicus.org/articles/21/3725/2021/.

Gelaro, Ronald et al. (2017). "The Modern-Era Retrospective Analysis for Research and Applications, Version 2 (MERRA-2)." In: *Journal of Climate* Volume 30.Iss 13, pp. 5419–5454. ISSN: 0894-8755. DOI: 10.1175/JCLI-D-16-0758.1.

Geller, Marvin A., Xuelong Zhou, and Minghua Zhang (2002). "Simulations of the Interannual Variability of Stratospheric Water Vapor." In: *Journal of the Atmospheric Sciences* 59.6. Place: Boston MA, USA Publisher: American Meteorological Society, pp. 1076 –1085. DOI: 10.1175/1520-0469(2002)059<1076:SOTIVO>2.0.CO;2. URL: https://journals.ametsoc.org/view/journals/atsc/59/6/1520-0469_2002_059_1076_sotivo_2.0.co_2.xml.

Giorgetta, M. A. et al. (2018). "ICON-A, the Atmosphere Component of the ICON Earth System Model: I. Model Description." In: *Journal of Advances in Modeling Earth Systems* 10.7, pp. 1613–1637. ISSN: 19422466. DOI: 10.1029/2017MS001242.

Giorgetta, Marco A. et al. (2013). "Climate and carbon cycle changes from 1850 to 2100 in MPI-ESM simulations for the Coupled Model Intercomparison Project phase 5." In: *Journal of Advances in Modeling Earth Systems* 5.3, pp. 572–597. ISSN: 19422466. DOI: 10.1002/jame.20038.

Glaze, Lori S., Stephen M. Baloga, and Lionel Wilson (1997). "Transport of atmospheric water vapor by volcanic eruption columns." In: *Journal of Geophysical Research: Atmospheres* 102.D5, pp. 6099–6108. ISSN: 01480227. DOI: 10.1029/96JD03125.

Gowan, E. H. and Gordon Miller Bourne Dobson (1947). "Ozonosphere temperatures under radiation equilibrium." In: *Proceedings of the Royal Society of London. Series A. Mathematical and Physical Sciences* 190.1021, pp. 219–226. DOI: 10.1098/rspa.1947.0071. URL: https://royalsocietypublishing.org/doi/abs/10.1098/rspa.1947.0071.

Hall, Timothy M. and Darryn Waugh (1997). "Tracer transport in the tropical stratosphere due to vertical diffusion and horizontal mixing." In: *Geophysical Research Letters* 24.11, pp. 1383–1386. ISSN: 00948276. DOI: 10.1029/97GL01289.

Hansen, J. et al. (2005). "Efficacy of climate forcings." In: *Journal of Geophysical Research: Atmospheres* 110.D18. DOI: 10.1029/2005JD005776. URL: https://agupubs.onlinelibrary.wiley.com/doi/abs/10.1029/2005JD005776.

Hardiman, Steven C. et al. (2015). "Processes Controlling Tropical Tropopause Temperature and Stratospheric Water Vapor in Climate Models." In: *Journal of Climate* 28.16. Place: Boston MA, USA Publisher: American Meteorological Society, pp. 6516 –6535. DOI: 10.1175/JCLI-D-15-0075.1. URL: https://journals.ametsoc.org/view/journals/clim/28/16/jcli-d-15-0075.1.xml.

Hartmann, Dennis L. and Kristin Larson (2002). "An important constraint on tropical cloud - climate feedback." In: *Geophysical Research Letters* 29.20, pp. 12–1–12–4. DOI: https://doi.org/10.1029/2002GL015835. URL: https://agupubs.onlinelibrary.wiley.com/doi/abs/10.1029/2002GL015835.

Hegglin, M. I. et al. (Oct. 2014). "Vertical structure of stratospheric water vapour trends derived from merged satellite data." In: *Nature Geoscience* 7.10, pp. 768–776. ISSN: 1752-0908. DOI: 10.1038/ngeo2236. URL: https://doi.org/10.1038/ngeo2236.

Hohenegger, C. et al. (2022). "ICON-Sapphire: simulating the components of the Earth System and their interactions at kilometer and subkilometer scales." In: *Geoscientific Model Development Discussions* 2022, pp. 1–42. DOI: 10.5194/gmd-2022-171. URL: https://gmd.copernicus.org/preprints/gmd-2022-171/.

Hohenegger, Cathy et al. (2020). "Climate Statistics in Global Simulations of the Atmosphere, from 80 to 2.5 km Grid Spacing." In: *Journal of the Meteorological Society of Japan. Ser. II* 98.1, pp. 73–91. DOI: 10.2151/jmsj.2020-005.

Holloway, Christopher E. and J. David Neelin (2007). "The Convective Cold Top and Quasi Equilibrium." In: *Journal of the Atmospheric Sciences* 64.5. Place: Boston MA, USA Publisher: American Meteorological Society, pp. 1467 –1487. DOI: 10.1175/JAS3907.1. URL: https://journals.ametsoc.org/view/journals/atsc/64/5/jas3907.1.xml.

Holton, James R. and Andrew Gettelman (2001). "Horizontal transport and the dehydration of the stratosphere." In: *Geophysical Research Letters* 28.14, pp. 2799–2802. DOI: https://doi.org/10.1029/2001GL013148. URL: https://agupubs.onlinelibrary.wiley.com/doi/abs/10.1029/2001GL013148.

Hu, Zeyuan, Fayçal Lamraoui, and Zhiming Kuang (2021). "Influence of Upper-Troposphere Stratification and Cloud–Radiation Interaction on Convective Overshoots in the Tropical Tropopause Layer." In: *Journal of the Atmospheric Sciences* 78.8. Place: Boston MA, USA Publisher: American Meteorological Society, pp. 2493 –2509. DOI: 10.1175/JAS-D-20-0241.1. URL: https://journals.ametsoc.org/view/journals/atsc/78/8/JAS-D-20-0241.1.xml.

Huang, Yi, Yuwei Wang, and Han Huang (2020). "Stratospheric Water Vapor Feedback Disclosed by a Locking Experiment." In: *Geophysical Research Letters* 47.12, e2020GL087987. DOI: https://doi.org/10.1029/2020GL087987. URL: https://agupubs.onlinelibrary.wiley.com/doi/abs/10.1029/2020GL087987.

Ilyina, Tatiana et al. (2013). "Global ocean biogeochemistry model HAMOCC: Model architecture and performance as component of the MPI-Earth system model in different CMIP5 experimental realizations." In: *Journal of Advances in Modeling Earth Systems* 5.2, pp. 287–315. ISSN: 19422466. DOI: 10.1029/2012MS000178.

Johnson, Richad H. and Donald C. Kriete (1982). "Thermodynamic and Circulation Characteristics, of Winter Monsoon Tropical Mesoscale Convection." In: *Monthly Weather Review* 110.12. Place: Boston MA, USA Publisher: American Meteorological Society, pp. 1898 –1911. DOI: 10.1175/1520-0493(1982)110<1898:TACCOW>2.0.CO;2. URL: https://journals.ametsoc.org/view/journals/mwre/110/12/1520-0493_1982_110_1898_taccow_2_0_co_2.xml.

Jones, Todd R. and David A. Randall (2011). "Quantifying the limits of convective parameterizations." In: *Journal of Geophysical Research: Atmospheres* 116.D8. DOI: https://doi.org/10.1029/2010JD014913. URL: https://agupubs.onlinelibrary.wiley.com/doi/abs/10.1029/2010JD014913.

Joshi, M. M. and G. S. Jones (2009). "The climatic effects of the direct injection of water vapour into the stratosphere by large volcanic eruptions." In: *Atmospheric Chemistry and Physics* 9.16, pp. 6109–6118. DOI: 10.5194/acp-9-6109-2009.

Joshi, Manoj M. and Keith P. Shine (2003). "A GCM Study of Volcanic Eruptions as a Cause of Increased Stratospheric Water Vapor." In: *Journal of Climate* 16.21, pp. 3525–3534. ISSN: 0894-8755. DOI: 10.1175/1520-0442(2003)016\textless3525:AGSOVE\textgreater2.0.CO;2.

Jungclaus, J. H. et al. (2013). "Characteristics of the ocean simulations in the Max Planck Institute Ocean Model (MPIOM) the ocean component of the MPI-Earth system model." In: *Journal of Advances in Modeling Earth Systems* 5.2, pp. 422–446. ISSN: 19422466. DOI: 10.1002/jame.20023.

Khosrawi, F. et al. (2018). "The SPARC water vapour assessment II: comparison of stratospheric and lower mesospheric water vapour time series observed from satellites." In: *Atmospheric Measurement Techniques* 11.7, pp. 4435–4463. DOI: 10.5194/amt-11-4435-2018. URL: https://amt.copernicus.org/articles/11/4435/2018/.

Kilian, M., S. Brinkop, and P. Jöckel (2020). "Impact of the eruption of Mt Pinatubo on the chemical composition of the stratosphere." In: *Atmospheric Chemistry and Physics* 20.20, pp. 11697–11715. DOI: 10.5194/acp-20-11697-2020. URL: https://acp.copernicus.org/articles/20/11697/2020/.

Kim, Joowan, Kevin M. Grise, and Seok-Woo Son (2013). "Thermal characteristics of the cold-point tropopause region in CMIP5 models." In: *Journal of Geophysical Research: Atmospheres* 118.16, pp. 8827–8841. ISSN: 2169-897X. DOI: 10.1002/jgrd.50649. URL: https://doi.org/10.1002/jgrd.50649.

Kim, Joowan, William J. Randel, and Thomas Birner (2018). "Convectively Driven Tropopause-Level Cooling and Its Influences on Stratospheric Moisture." In: *Journal of Geophysical Research: Atmospheres* 123.1, pp. 590–606. DOI: https://doi.org/10.1002/2017JD027080. URL: https://agupubs.onlinelibrary.wiley.com/doi/abs/10.1002/2017JD027080.

Kluft, Lukas et al. (2019). "Re-Examining the First Climate Models: Climate Sensitivity of a Modern Radiative–Convective Equilibrium Model." In: *Journal of Climate* 32.23, pp. 8111–8125. ISSN: 0894-8755. DOI: 10.1175/JCLI-D-18-0774.1.

Ko, M. K. W. et al. (2013). *SPARC Report on Lifetimes of Stratospheric Ozone-Depleting Substances, Their Replacements, and Related Species*. Tech. rep. Backup Publisher: SPARC Publication Title: SPARC Report Volume: No. 6. SPARC Office, 256 pp. URL: http://www.sparc-climate.org/publications/sparc-reports/.

Kobayashi, S. et al. (2015). "The JRA-55 Reanalysis: General Specifications and Basic Characteristics." In: *Journal of the Meteorological Society of Japan. Ser. II* 93.1, pp. 5–48. ISSN: 0026-1165. DOI: 10.2151/jmsj.2015-001.

Kodera, K. et al. (2015). "The role of convective overshooting clouds in tropical stratosphere–troposphere dynamical coupling." In: *Atmospheric Chemistry and Physics* 15.12, pp. 6767–6774. DOI: 10.5194/acp-15-6767-2015. URL: https://acp.copernicus.org/articles/15/6767/2015/.

Konopka, P. et al. (June 2007). "Contribution of mixing to upward transport across the tropical tropopause layer (TTL)." en. In: *Atmospheric Chemistry and Physics* 7.12, pp. 3285–3308. ISSN: 1680-7324. DOI: 10.5194/acp-7-3285-2007. URL: https://acp.copernicus.org/articles/7/3285/2007/ (visited on 08/17/2021).

Kravitz, B. et al. (2015). "The Geoengineering Model Intercomparison Project Phase 6 (GeoMIP6): simulation design and preliminary results." In: *Geoscientific Model Development* 8.10, pp. 3379–3392. DOI: 10.5194/gmd-8-3379-2015. URL: https://gmd.copernicus.org/articles/8/3379/2015/.

Krishnamohan, Krishna-Pillai Sukumara-Pillai et al. (2019). "Climate system response to stratospheric sulfate aerosols: sensitivity to altitude of aerosol layer." In: *Earth*

System Dynamics 10.4, pp. 885–900. ISSN: 2190-4979. DOI: 10.5194/esd-10-885-2019.

Kroll, Clarissa Alicia et al. (May 2021). "The impact of volcanic eruptions of different magnitude on stratospheric water vapor in the tropics." English. In: *Atmospheric Chemistry and Physics* 21.8. Publisher: Copernicus GmbH, pp. 6565–6591. ISSN: 1680-7316. DOI: 10.5194/acp-21-6565-2021. URL: https://acp.copernicus.org/articles/21/6565/2021/ (visited on 06/08/2021).

Kuang, Zhiming and Christopher S. Bretherton (2004). "Convective Influence on the Heat Balance of the Tropical Tropopause Layer: A Cloud-Resolving Model Study." In: *Journal of the Atmospheric Sciences* 61.23. Place: Boston MA, USA Publisher: American Meteorological Society, pp. 2919 –2927. DOI: 10.1175/JAS-3306.1. URL: https://journals.ametsoc.org/view/journals/atsc/61/23/jas-3306.1.xml.

Kuebbeler, Miriam, Ulrike Lohmann, and Johann Feichter (2012). "Effects of stratospheric sulfate aerosol geo-engineering on cirrus clouds." In: *Geophysical Research Letters* 39.23, n/a–n/a. ISSN: 00948276. DOI: 10.1029/2012GL053797.

Lang, Theresa et al. (2022). *How model uncertainties influence tropical humidity in1 global storm-resolving simulations*. URL: https://pure.mpg.de/pubman/faces/ViewItemOverviewPage.jsp?itemId=item_3456081 (visited on 11/15/2022).

Le Texier, H., S. Solomon, and R. R. Garcia (1988). "The role of molecular hydrogen and methane oxidation in the water vapour budget of the stratosphere." In: *Quarterly Journal of the Royal Meteorological Society* 114.480, pp. 281–295. ISSN: 00359009. DOI: 10.1002/qj.49711448002.

LeGrande, Allegra N., Kostas Tsigaridis, and Susanne E. Bauer (2016). "Role of atmospheric chemistry in the climate impacts of stratospheric volcanic injections." In: *Nature Geoscience* 9, pp. 652–655. URL: https://doi.org/10.1038/ngeo2771.

Liu, Chuntao and Edward J. Zipser (Dec. 2005). "Global distribution of convection penetrating the tropical tropopause." en. In: *Journal of Geophysical Research: Atmospheres* 110.D23. Publisher: John Wiley & Sons, Ltd. ISSN: 2156-2202. URL: https://onlinelibrary.wiley.com/doi/abs/10.1029/2005JD006063 (visited on 11/03/2021).

Liu, Y. S., S. Fueglistaler, and P. H. Haynes (2010). "Advection-condensation paradigm for stratospheric water vapor." In: *Journal of Geophysical Research: Atmospheres* 115.D24. DOI: https://doi.org/10.1029/2010JD014352. URL: https://agupubs.onlinelibrary.wiley.com/doi/abs/10.1029/2010JD014352.

Livesey, N. J. et al. (2003). "The UARS Microwave Limb Sounder version 5 data set: Theory, characterization, and validation." In: *Journal of Geophysical Research: Atmospheres* 108.D13. DOI: https://doi.org/10.1029/2002JD002273. URL: https://agupubs.onlinelibrary.wiley.com/doi/abs/10.1029/2002JD002273.

Louis, Jean-François (Sept. 1979). "A parametric model of vertical eddy fluxes in the atmosphere." en. In: *Boundary-Layer Meteorology* 17.2, pp. 187–202. ISSN: 1573-1472. DOI: 10.1007/BF00117978. URL: https://doi.org/10.1007/BF00117978 (visited on 06/08/2021).

Löffler, Michael, Sabine Brinkop, and Patrick Jöckel (2016). "Impact of major volcanic eruptions on stratospheric water vapour." In: *Atmospheric Chemistry and Physics* 16.10, pp. 6547–6562. DOI: 10.5194/acp-16-6547-2016.

Maher, Nicola et al. (2019). "The Max Planck Institute Grand Ensemble: Enabling the Exploration of Climate System Variability." In: *Journal of Advances in Modeling Earth Systems* 11.7, pp. 2050–2069. ISSN: 19422466. DOI: 10.1029/2019MS001639.

Manabe, S. and F. Möller (1961). "ON THE RADIATIVE EQUILIBRIUM AND HEAT BALANCE OF THE ATMOSPHERE." In: *Monthly Weather Review* 89.12. Place: Boston MA, USA Publisher: American Meteorological Society, pp. 503 –532. DOI: 10.1175/1520-0493(1961)089<0503:OTREAH>2.0.CO;2. URL: https://journals.ametsoc.org/view/journals/mwre/89/12/1520-0493_1961_089_0503_otreah_2_0_co_2.xml.

Manabe, Syukuro and Richard T. Wetherald (1975). "The Effects of Doubling the CO2 Concentration on the climate of a General Circulation Model." In: *Journal of Atmospheric Sciences* 32.1. Place: Boston MA, USA Publisher: American Meteorological Society, pp. 3 –15. DOI: 10.1175/1520-0469(1975)032<0003:TEODTC>2.0.CO;2. URL: https://journals.ametsoc.org/view/journals/atsc/32/1/1520-0469_1975_032_0003_teodtc_2_0_co_2.xml.

Marshall, L. et al. (2018). "Multi-model comparison of the volcanic sulfate deposition from the 1815 eruption of Mt. Tambora." In: *Atmospheric Chemistry and Physics* 18.3, pp. 2307–2328. DOI: 10.5194/acp-18-2307-2018. URL: https://acp.copernicus.org/articles/18/2307/2018/.

Marshall, Lauren R. et al. (2020). "Large Variations in Volcanic Aerosol Forcing Efficiency Due to Eruption Source Parameters and Rapid Adjustments." en. In: *Geophysical Research Letters* 47.19, e2020GL090241. ISSN: 1944-8007. DOI: 10.1029/2020GL090241. URL: https://agupubs.onlinelibrary.wiley.com/doi/abs/10.1029/2020GL090241 (visited on 06/08/2021).

Marsland, S. J. et al. (2003). "The Max-Planck-Institute global ocean/sea ice model with orthogonal curvilinear coordinates." In: *Ocean Modelling* 5.2, pp. 91–127. ISSN: 14635003. DOI: 10.1016/S1463-5003(02)00015-X.

Mauritsen, Thorsten et al. (Nov. 2007). "A Total Turbulent Energy Closure Model for Neutrally and Stably Stratified Atmospheric Boundary Layers." EN. In: *Journal of the Atmospheric Sciences* 64.11. Publisher: American Meteorological Society Section: Journal of the Atmospheric Sciences, pp. 4113–4126. ISSN: 0022-4928, 1520-0469. DOI: 10.1175/2007JAS2294.1. URL: https://journals.ametsoc.org/view/journals/atsc/64/11/2007jas2294.1.xml (visited on 06/08/2021).

Mauritsen, Thorsten et al. (2019). "Developments in the MPI–M Earth System Model version 1.2 (MPI–ESM1.2) and Its Response to Increasing CO 2." In: *Journal of Advances in Modeling Earth Systems* 11.4, pp. 998–1038. ISSN: 19422466. DOI: 10.1029/2018MS001400.

Maycock, Amanda C. et al. (2013). "The Circulation Response to Idealized Changes in Stratospheric Water Vapor." In: *Journal of Climate* 26.2, pp. 545–561. ISSN: 0894-8755. DOI: 10.1175/JCLI-D-12-00155.1.

Michelsen, H. A. et al. (2000). "Features and trends in Atmospheric Trace Molecule Spectroscopy (ATMOS) version 3 stratospheric water vapor and methane measurements." In: *Journal of Geophysical Research: Atmospheres* 105.D18, pp. 22713–22724. DOI: https://doi.org/10.1029/2000JD900336. URL: https://agupubs.onlinelibrary.wiley.com/doi/abs/10.1029/2000JD900336.

Millán, L. et al. (2022). "The Hunga Tonga-Hunga Ha'apai Hydration of the Stratosphere." In: *Geophysical Research Letters* 49.13, e2022GL099381. DOI: https://doi.

org/10.1029/2022GL099381. URL: https://agupubs.onlinelibrary.wiley.com/doi/abs/10.1029/2022GL099381.

Mlawer, Eli J. et al. (1997). "Radiative transfer for inhomogeneous atmospheres: RRTM, a validated correlated-k model for the longwave." In: *Journal of Geophysical Research: Atmospheres* 102.D14, pp. 16663–16682. DOI: https://doi.org/10.1029/97JD00237. URL: https://agupubs.onlinelibrary.wiley.com/doi/abs/10.1029/97JD00237.

Mote, Philip W. et al. (1996). "An atmospheric tape recorder: The imprint of tropical tropopause temperatures on stratospheric water vapor." In: *Journal of Geophysical Research: Atmospheres* 101.D2, pp. 3989–4006. ISSN: 01480227. DOI: 10.1029/95JD03422.

Murcray, D. G. et al. (1981). "Changes in stratospheric water vapor associated with the mount st. Helens eruption." In: *Science (New York, N.Y.)* 211.4484, pp. 823–824. DOI: 10.1126/science.211.4484.823.

Murphy, D. M. and T. Koop (2005). "Review of the vapour pressures of ice and supercooled water for atmospheric applications." In: *Quarterly Journal of the Royal Meteorological Society* 131.608, pp. 1539–1565. ISSN: 00359009. DOI: 10.1256/qj.04.94.

Myhre et al. (2013). "Anthropogenic and Natural Radiative Forcing: Climate Change 2013: The Physical Science Basis." In: *Contribution of Working Group I to the Fiith Assessment Report of the Intergovernmental Panel of Climate Change*. URL: https://www.ipcc.ch/site/assets/uploads/2018/02/WG1AR5_Chapter08_FINAL.pdf.

Möbis, Benjamin and Bjorn Stevens (2012). "Factors controlling the position of the Intertropical Convergence Zone on an aquaplanet." In: *Journal of Advances in Modeling Earth Systems* 4.4. DOI: https://doi.org/10.1029/2012MS000199. URL: https://agupubs.onlinelibrary.wiley.com/doi/abs/10.1029/2012MS000199.

Müller, Rolf et al. (2016). "The need for accurate long-term measurements of water vapor in the upper troposphere and lower stratosphere with global coverage." In: *Earth's Future* 4.2, pp. 25–32. DOI: https://doi.org/10.1002/2015EF000321. URL: https://agupubs.onlinelibrary.wiley.com/doi/abs/10.1002/2015EF000321.

Newell, Reginald E. and Sharon Gould-Stewart (1981). "A Stratospheric Fountain?" In: *Journal of Atmospheric Sciences* 38.12. Place: Boston MA, USA Publisher: American Meteorological Society, pp. 2789 –2796. DOI: 10.1175/1520-0469(1981)038<2789:ASF>2.0.CO;2. URL: https://journals.ametsoc.org/view/journals/atsc/38/12/1520-0469_1981_038_2789_asf_2_0_co_2.xml.

Oltmans, S. et al. (2000). "Increase in stratospheric water vapor from balloon-borne, frostpoint hygrometer measurements at Washington, DC and Boulder, Colorado." In: *Geophysical Research Letters* 27.PreJuSER-44738.

Oman, Luke et al. (2008). "Understanding the Changes of Stratospheric Water Vapor in Coupled Chemistry Climate Model Simulations." In: *Journal of the Atmospheric Sciences* 65.10. Place: Boston MA, USA Publisher: American Meteorological Society, pp. 3278 –3291. DOI: 10.1175/2008JAS2696.1. URL: https://journals.ametsoc.org/view/journals/atsc/65/10/2008jas2696.1.xml.

Paulik, L. C. and T. Birner (2012). "Quantifying the deep convective temperature signal within the tropical tropopause layer (TTL)." In: *Atmospheric Chemistry and Physics* 12.24, pp. 12183–12195. DOI: 10.5194/acp-12-12183-2012. URL: https://acp.copernicus.org/articles/12/12183/2012/.

Pincus, Robert and Bjorn Stevens (2013). "Paths to accuracy for radiation parameterizations in atmospheric models." In: *Journal of Advances in Modeling Earth Systems* 5.2, pp. 225–233. DOI: https://doi.org/10.1002/jame.20027. URL: https://agupubs.onlinelibrary.wiley.com/doi/abs/10.1002/jame.20027.

Pithan, Felix (Aug. 2014). "Arctic boundary-layer processes and climate change." eng. PhD thesis. Universität Hamburg Hamburg. DOI: 10.17617/2.2049530. URL: https://pure.mpg.de/pubman/faces/ViewItemFullPage.jsp?itemId=item_2049530 (visited on 06/08/2021).

Podglajen, Aurélien et al. (Nov. 2017). "Small-Scale Wind Fluctuations in the Tropical Tropopause Layer from Aircraft Measurements: Occurrence, Nature, and Impact on Vertical Mixing." EN. In: *Journal of the Atmospheric Sciences* 74.11. Publisher: American Meteorological Society Section: Journal of the Atmospheric Sciences, pp. 3847–3869. ISSN: 0022-4928, 1520-0469. DOI: 10.1175/JAS-D-17-0010.1. URL: https://journals.ametsoc.org/view/journals/atsc/74/11/jas-d-17-0010.1.xml (visited on 06/18/2021).

Prasad, Abhnil A. et al. (2019). "Rapidly Evolving Cirrus Clouds Modulated by Convectively Generated Gravity Waves." In: *Journal of Geophysical Research: Atmospheres* 124.13, pp. 7327–7338. DOI: https://doi.org/10.1029/2019JD030538. URL: https://agupubs.onlinelibrary.wiley.com/doi/abs/10.1029/2019JD030538.

Randel, William J. et al. (2004). "Interannual Changes of Stratospheric Water Vapor and Correlations with Tropical Tropopause Temperatures." In: *Journal of the Atmospheric Sciences* 61.17, pp. 2133 –2148. DOI: 10.1175/1520-0469(2004)061<2133:ICOSWV>2.0.CO;2. URL: https://journals.ametsoc.org/view/journals/atsc/61/17/1520-0469_2004_061_2133_icoswv_2.0.co_2.xml.

Randel, William J. et al. (2006). "Decreases in stratospheric water vapor after 2001: Links to changes in the tropical tropopause and the Brewer-Dobson circulation." In: *Journal of Geophysical Research: Atmospheres* 111.D12. DOI: https://doi.org/10.1029/2005JD006744. URL: https://agupubs.onlinelibrary.wiley.com/doi/abs/10.1029/2005JD006744.

Reick, C. H. et al. (2013). "Representation of natural and anthropogenic land cover change in MPI-ESM." In: *Journal of Advances in Modeling Earth Systems* 5.3, pp. 459–482. ISSN: 19422466. DOI: 10.1002/jame.20022.

Rienecker, Michele M. et al. (2011). "MERRA: NASA's Modern-Era Retrospective Analysis for Research and Applications." In: *Journal of Climate* 24.14, pp. 3624–3648. ISSN: 0894-8755. DOI: 10.1175/JCLI-D-11-00015.1.

Riese, M. et al. (Aug. 2012). "Impact of uncertainties in atmospheric mixing on simulated UTLS composition and related radiative effects: IMPACT OF MIXING ON RADIATIVE EFFECTS." en. In: *Journal of Geophysical Research: Atmospheres* 117.D16, n/a–n/a. ISSN: 01480227. DOI: 10.1029/2012JD017751. URL: http://doi.wiley.com/10.1029/2012JD017751 (visited on 11/03/2021).

Robock, Alan (2000). "Volcanic eruptions and climate." In: *Reviews of Geophysics* 38.2, pp. 191–219. ISSN: 87551209. DOI: 10.1029/1998RG000054.

Robrecht, Sabine et al. (2019). "Mechanism of ozone loss under enhanced water vapour conditions in the mid-latitude lower stratosphere in summer." In: *Atmospheric Chemistry and Physics* 19.9, pp. 5805–5833. DOI: 10.5194/acp-19-5805-2019.

Rohs, S. et al. (2006). "Long-term changes of methane and hydrogen in the stratosphere in the period 1978–2003 and their impact on the abundance of stratospheric water vapor." In: *Journal of Geophysical Research: Atmospheres* 111.D14. DOI: https://doi.org/10.1029/2005JD006877. URL: https://agupubs.onlinelibrary.wiley.com/doi/abs/10.1029/2005JD006877.

Rosenlof, K. H. et al. (2001). "Stratospheric water vapor increases over the past half-century." In: *Geophysical Research Letters* 28.7, pp. 1195–1198. ISSN: 00948276. DOI: 10.1029/2000GL012502.

Rosenlof, Karen H. (2018). "Changes in water vapor and aerosols and their relation to stratospheric ozone." In: *Comptes Rendus Geoscience* 350.7, pp. 376–383. ISSN: 16310713. DOI: 10.1016/j.crte.2018.06.014.

Russell III, James M. et al. (1993). "The Halogen Occultation Experiment." In: *Journal of Geophysical Research: Atmospheres* 98.D6, pp. 10777–10797. DOI: https://doi.org/10.1029/93JD00799. URL: https://agupubs.onlinelibrary.wiley.com/doi/abs/10.1029/93JD00799.

Saint-Lu, Marion, Sandrine Bony, and Jean-Louis Dufresne (Oct. 2022). "Clear-sky control of anvils in response to increased CO2 or surface warming or volcanic eruptions." In: *npj Climate and Atmospheric Science* 5.1, p. 78. ISSN: 2397-3722. DOI: 10.1038/s41612-022-00304-z. URL: https://doi.org/10.1038/s41612-022-00304-z.

Santer, B. D. et al. (2003). "Behavior of tropopause height and atmospheric temperature in models, reanalyses, and observations: Decadal changes." In: *Journal of Geophysical Research: Atmospheres* 108.D1, ACL 1–1–ACL 1–22. DOI: 10.1029/2002JD002258. URL: https://agupubs.onlinelibrary.wiley.com/doi/abs/10.1029/2002JD002258.

Schmidt, H. et al. (2013). "Response of the middle atmosphere to anthropogenic and natural forcings in the CMIP5 simulations with the Max Planck Institute Earth system model." In: *Journal of Advances in Modeling Earth Systems* 5.1, pp. 98–116. ISSN: 19422466. DOI: 10.1002/jame.20014.

Schneck, Rainer, Christian H. Reick, and Thomas Raddatz (2013). "Land contribution to natural CO 2 variability on time scales of centuries." In: *Journal of Advances in Modeling Earth Systems* 5.2, pp. 354–365. ISSN: 19422466. DOI: 10.1002/jame.20029.

Schoeberl, M. R. and A. E. Dessler (2011). "Dehydration of the stratosphere." In: *Atmospheric Chemistry and Physics* 11.16, pp. 8433–8446. DOI: 10.5194/acp-11-8433-2011. URL: https://acp.copernicus.org/articles/11/8433/2011/.

Schoeberl, M. R. et al. (2022). "Analysis and Impact of the Hunga Tonga-Hunga Ha'apai Stratospheric Water Vapor Plume." In: *Geophysical Research Letters* 49.20, e2022GL100248. DOI: https://doi.org/10.1029/2022GL100248. URL: https://agupubs.onlinelibrary.wiley.com/doi/abs/10.1029/2022GL100248.

Schoeberl, Mark R. et al. (2018). "Convective Hydration of the Upper Troposphere and Lower Stratosphere." In: *Journal of Geophysical Research: Atmospheres* 123.9, pp. 4583–4593. DOI: https://doi.org/10.1029/2018JD028286. URL: https://agupubs.onlinelibrary.wiley.com/doi/abs/10.1029/2018JD028286.

Schulz, Hauke and Bjorn Stevens (2018). "Observing the Tropical Atmosphere in Moisture Space." In: *Journal of the Atmospheric Sciences* 75.10. Place: Boston MA, USA Publisher: American Meteorological Society, pp. 3313 –3330. DOI: 10.1175/

JAS-D-17-0375.1. URL: https://journals.ametsoc.org/view/journals/atsc/75/10/jas-d-17-0375.1.xml.

Schwartz, Michael J. et al. (2013). "Convectively injected water vapor in the North American summer lowermost stratosphere." In: *Geophysical Research Letters* 40.10, pp. 2316–2321. DOI: 10.1002/grl.50421.

Seidel, Dian J. et al. (2001). "Climatological characteristics of the tropical tropopause as revealed by radiosondes." In: *Journal of Geophysical Research: Atmospheres* 106.D8, pp. 7857–7878. DOI: https://doi.org/10.1029/2000JD900837. URL: https://agupubs.onlinelibrary.wiley.com/doi/abs/10.1029/2000JD900837.

Sherwood, Steven C. (1996). "Maintenance of the Free-Tropospheric Tropical Water Vapor Distribution. Part II: Simulation by Large-Scale Advection." In: *Journal of Climate* 9.11. Place: Boston MA, USA Publisher: American Meteorological Society, pp. 2919 –2934. DOI: 10.1175/1520-0442(1996)009<2919:MOTFTT>2.0.CO;2. URL: https://journals.ametsoc.org/view/journals/clim/9/11/1520-0442_1996_009_2919_motftt_2_0_co_2.xml.

Sherwood, Steven C., Sandrine Bony, and Jean-Louis Dufresne (Jan. 2014). "Spread in model climate sensitivity traced to atmospheric convective mixing." In: *Nature* 505.7481, pp. 37–42. ISSN: 1476-4687. DOI: 10.1038/nature12829. URL: https://doi.org/10.1038/nature12829.

Shindell, D. T. (2013). "GLACIAL CLIMATES | Volcanic and Solar Forcing." In: *Encyclopedia of Quaternary Science (Second Edition)*. Ed. by Scott A. Elias and Cary J. Mock. Second Edition. Amsterdam: Elsevier, pp. 748–753. ISBN: 978-0-444-53642-6. DOI: https://doi.org/10.1016/B978-0-444-53643-3.00021-2. URL: https://www.sciencedirect.com/science/article/pii/B9780444536433000212.

Sioris, Christopher E. et al. (2016a). "Direct injection of water vapor into the stratosphere by volcanic eruptions." In: *Geophysical Research Letters* 43.14, pp. 7694–7700. DOI: 10.1002/2016GL069918.

Sioris, Christopher E. et al. (2016b). "Upper tropospheric water vapour variability at high latitudes – Part 1: Influence of the annular modes." In: *Atmospheric Chemistry and Physics* 16.5, pp. 3265–3278. DOI: 10.5194/acp-16-3265-2016.

Smith, Jacob W. et al. (2022). "The Effect of Convective Injection of Ice on Stratospheric Water Vapor in a Changing Climate." In: *Geophysical Research Letters* 49.9, e2021GL097386. DOI: https://doi.org/10.1029/2021GL097386. URL: https://agupubs.onlinelibrary.wiley.com/doi/abs/10.1029/2021GL097386.

Soden, Brian J. et al. (2002). "Global cooling after the eruption of Mount Pinatubo: a test of climate feedback by water vapor." In: *Science (New York, N.Y.)* 296.5568, pp. 727–730. DOI: 10.1126/science.296.5568.727.

Solomon, Susan et al. (2010). "Contributions of stratospheric water vapor to decadal changes in the rate of global warming." In: *Science (New York, N.Y.)* 327.5970, pp. 1219–1223. DOI: 10.1126/science.1182488.

Stenchikov, Georgiy L. et al. (1998). "Radiative forcing from the 1991 Mount Pinatubo volcanic eruption." In: *Journal of Geophysical Research: Atmospheres* 103.D12, pp. 13837–13857. ISSN: 01480227. DOI: 10.1029/98JD00693.

Stevens, Bjorn et al. (2013). "Atmospheric component of the MPI-M Earth System Model: ECHAM6." In: *Journal of Advances in Modeling Earth Systems* 5.2, pp. 146–172. ISSN: 19422466. DOI: 10.1002/jame.20015.

Stevens, Bjorn et al. (Sept. 2019). "DYAMOND: the DYnamics of the Atmospheric general circulation Modeled On Non-hydrostatic Domains." In: *Progress in Earth and Planetary Science* 6.1, p. 61. ISSN: 2197-4284. DOI: 10.1186/s40645-019-0304-z. URL: https://doi.org/10.1186/s40645-019-0304-z.

Stevens, Bjorn et al. (2020). "The Added Value of Large-eddy and Storm-resolving Models for Simulating Clouds and Precipitation." In: *Journal of the Meteorological Society of Japan. Ser. II* 98.2, pp. 395–435. DOI: 10.2151/jmsj.2020-021.

Tao, Mengchu et al. (2019). "Multitimescale variations in modeled stratospheric water vapor derived from three modern reanalysis products." In: *Atmospheric Chemistry and Physics* 19.9, pp. 6509–6534. DOI: 10.5194/acp-19-6509-2019.

Thomason, Larry W. et al. (2004). "A revised water vapor product for the Stratospheric Aerosol and Gas Experiment (SAGE) II version 6.2 data set." In: *Journal of Geophysical Research: Atmospheres* 109.D6. DOI: https://doi.org/10.1029/2003JD004465. URL: https://agupubs.onlinelibrary.wiley.com/doi/abs/10.1029/2003JD004465.

Thuburn, John and George C. Craig (2002). "On the temperature structure of the tropical substratosphere." In: *Journal of Geophysical Research: Atmospheres* 107.D2, ACL 10–1–ACL 10–10. DOI: https://doi.org/10.1029/2001JD000448. URL: https://agupubs.onlinelibrary.wiley.com/doi/abs/10.1029/2001JD000448.

Tian, Wenshou, Martyn P. Chipperfield, and Daren Lü (2009). "Impact of increasing stratospheric water vapor on ozone depletion and temperature change." In: *Advances in Atmospheric Sciences* 26.3, pp. 423–437. ISSN: 0256-1530. DOI: 10.1007/s00376-009-0423-3.

Timmreck, Claudia et al. (2018). "The Interactive Stratospheric Aerosol Model Intercomparison Project (ISA-MIP): motivation and experimental design." In: *Geoscientific Model Development* 11.7, pp. 2581–2608. DOI: 10.5194/gmd-11-2581-2018.

Toohey, Matthew et al. (2016). "Easy Volcanic Aerosol (EVA v1.0): an idealized forcing generator for climate simulations." In: *Geoscientific Model Development* 9.11, pp. 4049–4070. DOI: 10.5194/gmd-9-4049-2016.

Ueyama, Rei, Eric J. Jensen, and Leonhard Pfister (2018). "Convective Influence on the Humidity and Clouds in the Tropical Tropopause Layer During Boreal Summer." In: *Journal of Geophysical Research: Atmospheres* 123.14, pp. 7576–7593. DOI: https://doi.org/10.1029/2018JD028674. URL: https://agupubs.onlinelibrary.wiley.com/doi/abs/10.1029/2018JD028674.

Ueyama, Rei et al. (2015). "Dynamical, convective, and microphysical control on wintertime distributions of water vapor and clouds in the tropical tropopause layer." In: *Journal of Geophysical Research: Atmospheres* 120.19, pp. 10,483–10,500. ISSN: 2169-897X. DOI: 10.1002/2015JD023318. URL: https://doi.org/10.1002/2015JD023318.

Vergara-Temprado, Jesús et al. (2020). "Climate Models Permit Convection at Much Coarser Resolutions Than Previously Considered." In: *Journal of Climate* 33.5. Place: Boston MA, USA Publisher: American Meteorological Society, pp. 1915–1933. DOI: 10.1175/JCLI-D-19-0286.1. URL: https://journals.ametsoc.org/view/journals/clim/33/5/jcli-d-19-0286.1.xml.

Visioni, D. et al. (2018). "Upper tropospheric ice sensitivity to sulfate geoengineering." In: *Atmospheric Chemistry and Physics* 18.20, pp. 14867–14887. DOI: 10.5194/

acp-18-14867-2018. URL: https://acp.copernicus.org/articles/18/14867/2018/.

Vömel, H. et al. (1995). "The evolution of the dehydration in the Antarctic stratospheric vortex." In: *Journal of Geophysical Research: Atmospheres* 100.D7. _eprint: https://agupubs.onlinelibrary.wiley.com/doi/pdf/10.1029/95JD01000, pp. 13919–13926. DOI: https://doi.org/10.1029/95JD01000. URL: https://agupubs.onlinelibrary.wiley.com/doi/abs/10.1029/95JD01000.

Vömel, Holger, Stephanie Evan, and Matt Tully (2022). "Water vapor injection into the stratosphere by Hunga Tonga-Hunga Ha’apai." In: *Science* 377.6613. _eprint: https://www.science.org/doi/pdf/10.1126/science.abq2299, pp. 1444–1447. DOI: 10.1126/science.abq2299. URL: https://www.science.org/doi/abs/10.1126/science.abq2299.

Wang, Tongmei et al. (2020). "Response of stratospheric water vapour to CO2 doubling in WACCM." In: *Climate Dynamics* 54.11-12, pp. 4877–4889. ISSN: 0930-7575. DOI: 10.1007/s00382-020-05260-z.

Wilson, R. (2004). "Turbulent diffusivity in the free atmosphere inferred from MST radar measurements: a review." In: *Annales Geophysicae* 22.11, pp. 3869–3887. DOI: 10.5194/angeo-22-3869-2004. URL: https://angeo.copernicus.org/articles/22/3869/2004/.

Wright, J. S. et al. (2011). "The influence of summertime convection over Southeast Asia on water vapor in the tropical stratosphere." In: *Journal of Geophysical Research: Atmospheres* 116.D12. DOI: https://doi.org/10.1029/2010JD015416. URL: https://agupubs.onlinelibrary.wiley.com/doi/abs/10.1029/2010JD015416.

Wu, Zheng and Thomas Reichler (2020). "Variations in the Frequency of Stratospheric Sudden Warmings in CMIP5 and CMIP6 and Possible Causes." In: *Journal of Climate* 33.23. Place: Boston MA, USA Publisher: American Meteorological Society, pp. 10305–10320. DOI: 10.1175/JCLI-D-20-0104.1. URL: https://journals.ametsoc.org/view/journals/clim/33/23/jcliD200104.xml.

Xu, Jingyuan et al. (2022). "Large Amounts of Water Vapor Were Injected into the Stratosphere by the Hunga Tonga–Hunga Ha’apai Volcano Eruption." In: *Atmosphere* 13.6. ISSN: 2073-4433. DOI: 10.3390/atmos13060912. URL: https://www.mdpi.com/2073-4433/13/6/912.

Zanchettin, D. et al. (2016). "The Model Intercomparison Project on the climatic response to Volcanic forcing (VolMIP): experimental design and forcing input data for CMIP6." In: *Geoscientific Model Development* 9.8, pp. 2701–2719. DOI: 10.5194/gmd-9-2701-2016. URL: https://gmd.copernicus.org/articles/9/2701/2016/.

Zhang, Guang J. et al. (Oct. 2016). "Estimation of convective entrainment properties from a cloud-resolving model simulation during TWP-ICE." In: *Climate Dynamics* 47.7, pp. 2177–2192. ISSN: 1432-0894. DOI: 10.1007/s00382-015-2957-7. URL: https://doi.org/10.1007/s00382-015-2957-7.

Zhu, Yunqian et al. (Oct. 2022). "Perturbations in stratospheric aerosol evolution due to the water-rich plume of the 2022 Hunga-Tonga eruption." In: *Communications Earth & Environment* 3.1, p. 248. ISSN: 2662-4435. DOI: 10.1038/s43247-022-00580-w. URL: https://doi.org/10.1038/s43247-022-00580-w.

Zilitinkevich, S. S. et al. (Nov. 2009). "Energy- and Flux-Budget Turbulence Closure Model for Stably Stratified Flows. Part II: The Role of Internal Gravity Waves." en. In: *Boundary-Layer Meteorology* 133.2, pp. 139–164. ISSN: 1573-1472. DOI: 10.

1007/s10546-009-9424-0. URL: https://doi.org/10.1007/s10546-009-9424-0 (visited on 06/08/2021).

Hinweis / Reference

Die gesamten Veröffentlichungen in der Publikationsreihe des MPI-M
„Berichte zur Erdsystemforschung / Reports on Earth System Science“,
ISSN 1614-1199

sind über die Internetseiten des Max-Planck-Instituts für Meteorologie erhältlich:
http://www.mpimet.mpg.de/wissenschaft/publikationen.html

All the publications in the series of the MPI -M
„Berichte zur Erdsystemforschung / Reports on Earth System Science“,
ISSN 1614-1199

are available on the website of the Max Planck Institute for Meteorology:
http://www.mpimet.mpg.de/wissenschaft/publikationen.html